Naval Command,
Control and Ocean
Surveillance Center RDT&E Division San Diego, CA
92152-5001

(4)

Technical Report 1360
August 1994

The Response of Bioluminescent Organisms to Fully Developed Pipe Flow

J. Rohr
J. Losee
G. Anderson

Technical Report 1360
August 1994

The Response of Bioluminescent Organisms to Fully Developed Pipe Flow

J. Rohr
J. Losee
G. Anderson

NAVAL COMMAND, CONTROL AND OCEAN SURVEILLANCE CENTER
RDT&E DIVISION
San Diego, California 92152–5001

K. E. EVANS, CAPT, USN
Commanding Officer

R. T. SHEARER
Executive Director

ADMINISTRATIVE INFORMATION

Members of the Applied Sciences Division (Code 574) and Environmental Sciences Division (Code 524) at the Naval Command, Control and Ocean Surveillance Center, RDT&E Division, San Diego, CA 92152–5001, conducted this research. Sponsorship was provided by the Office of Naval Research under the Independent Research Program.

Released by
E. W. Hendricks, Head
Fluid Mechanics and Energy
Research Branch

Under authority of
R. H. Moore, Head
Applied Sciences Division

ACKNOWLEDGMENTS

The authors are particularly indebted to Stewart Fallon for assisting in the experiments, Dr. Andre Huvard for providing a much needed biological perspective, Dr. Charles Hicks for his invaluable help in formalizing the role of the convective velocity (appendix 3), and Dr. Michael Latz for enumerable discussions and permission to reference his recent data. Special thanks are also in order for Eric Stromvall, Alex Doyle, and Robert Kolesar who helped in various ways throughout the previous years of experimentation. Support from the Naval Research and Development Center Independent Research Program through Dr. Alan Gordon is gratefully acknowledged.

PS

EXECUTIVE SUMMARY

OBJECTIVES

The principal objective of the present experiments is to study the response of luminescent organisms to hydrodynamic stimuli in a well characterized flow field. In particular, using fully developed pipe flow: (1) the bioluminescent response of freshly collected organisms are compared in laminar and turbulent flow, (2) threshold values of wall shear stress, τ_{wall}, are determined, and (3) the flash level of individual organisms as a function of τ_{wall} are examined.

RESULTS

Several trends describing the response of *in situ* bioluminescent organisms to fully developed, pipe flow stimuli are reported. These include the repeated observation that the bioluminescent organisms studied are stimulated in laminar flow at threshold levels of wall shear stress, τ_{wall}, of the order of a few (0.5–3) dynes/cm^2. It is argued that this level of threshold stimulus should provide antipreditation value. For the same value of τ_{wall}, it does not appear that turbulent flow is particularly more stimulatory than laminar flow on an individual cell basis (more cells may be excited in turbulent flow but peak values do not appear to be effected). Another general feature of these measurements is that with increasing τ_{wall} a conspicuous break in the rate of increase of average bioluminescence normally occurs between 10 to 20 dynes/cm^2 (laminar flow), with the greater increase occurring initially. This range of τ_{wall} is also where peak flash levels of individual organisms become, after initially exhibiting a graded response (increasing with τ_{wall} for τ_{wall} < 10–20 dynes/cm^2), approximately constant thereafter.

RECOMMENDATIONS

It is hoped that this work will lead to better predictive capabilities toward assessing bioluminescent stimulation in a variety of oceanic flow fields. Further work with a greater range of τ_{wall} and Re_{trans} values is necessary (preferably complimented by laboratory experiments with cultures of representative luminous dinoflagellates) to corroborate this initial study. Also the reaction of these luminescent organisms to varying shear stress (transitional flows) and acceleration (developing flows) needs to be investigated.

CONTENTS

SUMMARY 1

1.0 INTRODUCTION 1

2.0 MATERIALS AND METHODS 5

3.0 RESULTS 9

3.1 BIOLUMINESCENCE BEFORE (LAMINAR) AND AFTER (TURBULENT) TRANSITION 9

3.1a San Diego Bay Measurements 9

3.1b At–Sea Measurements Off San Clemente Island 10

3.2 BIOLUMINESCENCE IN LAMINAR FLOW 11

3.2a High Levels of Laminar Flow Stimulus, $\tau_{wall} > 15$ dynes/cm^2 11

3.2b Low Levels of Laminar Flow Stimulus, $\tau < 15$ dynes/cm^2 12

3.3 INDIVIDUAL FLASH LEVELS 12

4.0 DISCUSSION 15

4.1 COMPARISON WITH PREVIOUS EXPERIMENTS 15

4.1a Christianson and Sweeney (1972) 15

4.1b Anderson, Nosenchuck, Reynolds and Walton (1988) 15

4.1c Morita and Johnson (1974) 16

4.1d Latz, Case and Gran (1994) 16

4.1e Rohr, Losee and Hoyt (1990) 16

4.2 RESPONSE OF BIOLUMINESCENT ORGANISMS IN LAMINAR FLOW 18

4.3 RESPONSE OF BIOLUMINESCENT ORGANISMS IN TURBULENT FLOW 19

5.0 CONCLUSIONS 21

REFERENCES 43

APPENDIX 1: VIDEO CALIBRATION AND LIGHT ESTIMATES FOR PROJECT BONS (Bioluminescence for Ocean Night Surveillance) 1-1

1.1 INTRODUCTION 1-1

APPENDIX 2: PROPERTIES OF FULLY DEVELOPED PIPE FLOW 2-1

2.1 FULLY DEVELOPED FLOW 2-1

2.2 LAMINAR FLOW 2-1

2.3 TURBULENT FLOW 2-2

2.4 LENGTH SCALES OF TURBULENT EDDIES 2-4

2.5 CAVEATS 2-5

APPENDIX 3: INTERPRETING PMT MEASUREMENTS IN FULLY DEVELOPED PIPE FLOW – THE ROLE OF THE MEAN VELOCITY 3-1

FIGURES

1. Photograph of bioluminescence. The marine bioluminescent dinoflagellate, *Gonyaulax polyedra* (culture of $\sim 10^6$ cells per liter), are stimulated as they are poured over a 17.5 cm model of a dolphin. 23

2. Computer enhanced photographs of *in situ*, flow induced bioluminescence obtained via a low-light video camera. Objects can be identified 3–5 meters beneath the sea surface as a result of stimulated bioluminescence. At these depths it is likely that one or more species of dinoflagellates are responsible for the emitted light. 25

3. Diagrammatic illustration of the primary pipe flow apparatus. 26

4. Representative seawater friction factor *vs* Reynolds number data. Most of the measurements show good agreement with theoretical (laminar flow – solid line) and empirically derived (turbulent flow – dashed line) values. Laminar flow measurements taken in the 0.635-cm i.d. pipe (●, ◆, △) for Re > 2000, however, begin to diverge from theoretical values because the pipe's dimensionless entrance length (L_e/D) is not long enough to support fully developed flow. Measurements obtained in the 0.305-cm i.d. pipe (▼), with its much longer entrance length, exhibit better agreement. 27

5. Downstream flash termination location of bioluminescent organisms stimulated at the pipe inlet as a function of Reynolds number. A response time of 100 ms is assumed, followed by flash durations of 100 ms (short dash) and 200 ms (long dash). PMT positions are indicated by solid lines. Pipe i.d. = 0.635 cm; 69°F (ν = 0.0104 cm^2/sec). 28

6a. Representative San Diego Bay PMT levels *vs* Reynolds number. The PMT is located 67 cm from the inlet of the 0.635-cm i.d. pipe. Each data point represents an average of 2.2 l of sea water. Open symbols (Run 1; □, △) refer to measurements taken from the bottom half of the 75–l tank, where the flow sequence is monotonically decreasing. Solid symbols (Run 2; ■, ▲) refer to measurements taken from the remaining half of the tank, where the flow sequence is monotonically increasing. Transition (dotted line) from laminar to turbulent flow occurs at $Re_{trans} \approx 6000$, where a change in the PMT *vs* Re dependence is evident. 29

6b. PMT levels *vs* wall shear stress. San Diego Bay data, collected 67 cm from the 0.635-cm i.d. pipe inlet, are represented by symbols and composed both of 2.2–l (□, △; same PMT data as in figure 6a) and 100-s (◆, ○, ■) averages. Sea of Cortez data, collected 65 cm from the 0.635-cm i.d. pipe inlet, are represented by crosses and composed of 2.2–l averages. Transition (dotted line) from laminar to turbulent flow, for all the experiments, occurs around a Reynolds number of 6000. 30

7a. Representative San Clemente Island PMT levels *vs* Reynolds number. Each data point represents a 100-s average of two PMTs, located 22 and 67 cm from the inlet

of the 0.635-cm i.d. pipe. Transition from laminar to turbulent flow varies due to ship motion; for the open symbol data (□, Δ, ∇) $Re_{trans} \approx 3500$, for the cross symbol data $Re_{trans} \approx 5400$, and for the solid symbol data (▲, ▼) $Re_{trans} \approx 7600$. Note that the PMT levels for the high laminar flow Reynolds number data (▲, ▼) are conspicuously low. 31

7b. PMT levels (same data as in figure 7a) *vs* wall shear stress. The solid line is taken from figure 6b and is representative of San Diego Bay data. The disparity in PMT levels between laminar and turbulent flow, evident in figure 7a when plotted as a function of Re, is no longer apparent. 32

7c. PMT levels *vs* wall shear stress (same data as in figure 7b) with laminar (□), turbulent (■), and transitional (⊠) flow indicated. 33

8. PMT levels *vs* wall shear stress (τ_{wall}) for the highest laminar pipe flow stimulus. Solid symbols designate laminar flow measurements taken in San Diego Bay with the 0.305-cm i.d. pipe (▼, 500–s averages, PMT is 106 cm downstream of inlet) and the 0.635-cm i.d. pipe (■, 2.2–l averages, PMT is 67 cm downstream of inlet), and off San Clemente Island with the 0.635-cm i.d. pipe (●, 100–s averages, PMT 67 cm is downstream of inlet). Open symbols designate turbulent flow measurements taken in San Diego Bay with the 0.635-cm i.d. pipe (□, 2.2–l averages, PMT is 67 cm downstream of inlet). Note that for $\tau_{wall} > 15$ dynes/cm^2, the PMT *vs* τ_{wall} dependence is similar (approximately linear) regardless of whether the flow is laminar or turbulent. 34

9. PMT levels (100–s averages) *vs* wall shear stress (τ_{wall}) for the lowest laminar pipe flow stimulus. San Diego Bay water is used in the 0.635-cm i.d. pipe-flow apparatus with the PMT positioned 67 cm from the inlet. The solid line represents a least squares power law regression to the data between 0.7 and 14.0 dynes/cm^2 and has a slope of 2.57. Threshold τ_{wall} values are seen to be around 1 dyne/cm^2. 35

10. Sample laminar (a) and turbulent (b) PMT time series data (0.1-s bins). The PMT is located 67 cm from the inlet of the 0.635-cm i.d. pipe. Each vertical spike is believed to result from an individual bioluminescent flash. Corresponding wall shear stress values are 15 dynes/cm^2 (a) and 101 dynes/cm^2 (b). It is noteworthy that although the average bioluminescent level for (b) is nearly five times larger than (a), peak values remain about the same. 36

11. Average (100 s) *vs* peak (0.1 s) PMT levels as a function of wall shear stress (τ_{wall}). The PMT is located 67 cm from the inlet of the 0.635-cm i.d. pipe. Solid symbols (◆) designate average PMT levels recorded in San Diego Bay, open symbols (◇, ○) designate peak PMT levels recorded in San Diego Bay, and cross symbols designate peak levels recorded off San Clemente Island. Note that the leveling off of peak PMT levels beginning at $\tau_{wall} \approx$ 10–20 dynes/cm^2, coincides with the reduced slope of the average PMT *vs* τ_{wall} data. 37

12. Comparison of peak (0.1 s average) PMT *vs* Reynolds number dependence for top (6 cm from inlet) and bottom (67 cm from inlet) PMT locations on the 0.635-cm i.d. pipe. 38

13. Reynolds number *vs* wall shear stress for fully developed laminar (solid line) and turbulent (dashed line) flow in a 0.635-cm i.d. pipe, with seawater at 20.6°C (U_{avg} = 0.0164 x Re). 39

14. Comparison of PMT levels expressed as counts per second (same data as in figure 8) and counts per volume as a function of wall shear stress. Laminar flow data are from San Diego Bay (14a) and off San Clemente Island (14b). Turbulent flow data are from San Diego Bay (14c). 40

14a. Laminar flow data are from San Diego Bay. 40

14b. Laminar flow data off San Clemente Island. 41

14c. Turbulent flow data are from San Diego Bay. 42

1.1a Video ISIT camera calibration curve for 50 mm lens. 1-4

1.1b Video ISIT camera calibration curve for 25 mm lens. 1-5

2.1 Experimentally observed (■, □; Laufer, 1954) distribution of the normalized turbulent shear stress, $\frac{(\rho \overline{u' v'})}{\tau_{wall}}$, across a pipe in fully developed flow. Turbulent shear stress levels have been normalized by the wall shear stress, τ_{wall}, allowing different Reynolds number experiments to be compared. The solid line shows the distribution of the theoretical values of the total normalized shear stress across the pipe. Except near the pipe wall ($r \rightarrow R$, $\rho \overline{u' v'} \rightarrow 0$; not shown) the total shear stress is essentially entirely turbulent in nature. 2-8

2.2 Photographs of dye streaks taken in the 0.635-cm i.d. pipe. 2-9

2.3a Normalized velocity profiles in fully developed pipe flow. Data from Patel and Head (1969) for Re = 2015 (laminar) and Re = 4060 (turbulent). Solid line is the theoretical laminar velocity profile. Dashed line is the empirically derived (1/7 power law; Blasius, 1913) velocity profile. 2-10

2.3b Laminar (solid line) and turbulent (dashed line) velocity profiles in fully developed pipe (0.635-cm i.d.) flow with seawater at 25°C, for Re = 4060. . . . 2-11

2.4a Representative fresh water friction factor *vs* Reynolds number data. As expected for high Reynolds number laminar flow (equation 2a), with increasing L_e/D the discrepancy between measurements and theory (solid line) decreases. Comparison with similar seawater data in figure 4 is excellent. 2-12

2.4b Wall shear stress (τ_{wall}) *vs* average velocity (U_{avg}) for fully developed pipe (0.635-cm i.d.) flow (seawater at 25°C). For U_{avg} = 89.3 cm/sec, $\tau_{wall\ laminar}$ = 10.9 dynes/cm^2 (◆) and $\tau_{wall\ turbulent}$ = 37.2 dynes/cm^2 (▼). For τ_{wall} = 10.9 dynes/cm^2, $U_{avg\ turbulent}$ = 44.3 cm/sec (■) and $U_{avg\ laminar}$ = 89.3 cm/sec (◆). 2-13

2.5. Estimated Kolmogorov length scales (L_K) as a function of Reynolds number for turbulent flow of 21°C seawater through a 0.635-cm i.d. pipe. The difference between curves result from using different dissipation values, i.e., average dissipation (solid line; equation 2.14), dissipation at the wall (long dash; equation 2.16), and dissipation throughout the central core of the pipe (short dash; Davy, 1972). A cutoff for the size of the smallest bioluminescent organisms anticipated to be present is included for comparison (dashed line). . 2-14

3.1 Relative PMT level ($I_{mean}/(I_o n)$) *vs* Reynolds number as predicted by equation (3.9). Pipe flow parameters are: D = 0.635 cm, L_1 = 65 cm, L_2 = 70 cm, ν = 0.0104 cm^2/sec (25.6°C). Decay rate of flash (γ) is assumed to be 0.1 sec. Limiting behavior for $(L_{1,2}/Uavg)/\gamma << 1$ (equation 3.11, solid line) and $(L_{1,2}/Uavg)/\gamma >> 1$ (equation 3.13, dashed line) are included. 3-4

SUMMARY

In situ luminous marine organisms are subjected to a wide range of quantifiable, hydrodynamic agitation provided by fully-developed laminar and turbulent pipe flow. The threshold for stimulation occurs in laminar flow, and in terms of the shear stress at the pipe wall, τ_{wall}, is only a few dynes/cm^2. With increasing τ_{wall}, a monotonic increase in the time averaged bioluminescence is generally observed throughout the measured range ($\tau_{wall} \leq 200$ dynes/cm^2). Peak levels associated with individual bioluminescent flashes behave differently. After an initial rapid rise from threshold to τ_{wall} values of 10–20 dynes/cm^2 (also occurring in laminar flow), peak levels remain thereafter nearly independent of shear stress.

1.0 INTRODUCTION

Awak'd before the rushing prow,
The mimic fires of ocean glow,
Those lightnings of the wave;
Wild sparkles crest the broken tides,
And flashing round, the vessel's sides
With elfish lustre lave;
While far behind, their livid light
To the dark billows of the night
a blooming splendour gave

from Lord of the Isles (1815)
by Sir Walter Scott

The photograph[1] in figure 1 attempts to display the fairy-like glow of bioluminescence. In this photograph a culture of the bioluminescent dinoflagellate, *Gonyaulax polyedra*, is poured from a beaker over a 17.5-cm model of a dolphin. The concentration of the organisms was estimated to be of the order of 10^6 c/l, representative of dinoflagellate bloom conditions (Seliger et al., 1970). Along the dolphin model, the eye and white underside is clearly illuminated by the blue-green light ($\sim$480 nm, Hastings & Sweeney (1956); Seliger et al. (1969)) emitted by the organisms ($\sim$1–2 X 10^8 photons/cell (Biggley et al. (1969); Krasnow et al. (1981)). Notice that some bioluminescent organisms are excited before striking the model. It is not known whether the shear stresses associated with the pouring motion or the accompanying acceleration is most important towards stimulating bioluminescence upstream of the model. Although there is some evidence (Christianson & Sweeney, 1972) suggesting the former, further work is necessary to differentiate between the stimulatory effects of shear and acceleration on bioluminescence.

In an overview of coastal bioluminescence, Morin (1983) discusses the photic environment wherein bioluminescence may be visually observed. At the sea surface bright daylight is about six orders of magnitude greater than maximum bioluminescent intensities (which have been determined to be greater than 10^{-1} μW cm^{-2}). However, light levels at the sea surface during a moonless night may be two orders of magnitude less than maximum bioluminescent intensities.

[1] The photograph was taken with Super HG Fujicolor 1600 film, with an f stop of 2.8, and an exposure time of 7 seconds.

Seliger et al. (1969) have made the interesting observation that while concentrations of one *Pyrodinium bahamense* per milliliter are sufficient to observe the "white" bioluminescent wake of a boat, concentrations of several hundred per milliliter provide a brilliant glow bright enough to read by.

The computer enhanced photographs of flow-induced bioluminescence, shown in figure 2, were obtained at sea from a low-light video camera. They are illustrative of the bioluminescent displays visible to the naked eye, when background lighting is suitably low, even when the stimuli is relatively weak (as compared with breaking waves or a ship's wake). In figures 2a through c the configuration of a rope, the upstream profile of a 5-gallon box, and the outline of a 24-cm diameter sphere are all discernable a few meters beneath the sea surface as a result of the bioluminescent light stimulated by passing swell. The bioluminescent irradiance of the 0.25-m diameter sphere (2c) was estimated to be about 2.9×10^{11} photons per second. Figure 2d is representative of the bioluminescent signatures of the rising bubbles (center–left of photo) and swimming motion (center–right) of divers 4 m below the sea surface.

Unfortunately, the uncontrolled flow fields associated with these pictures are not readily amenable to analysis for determination of the nature and level of the associated hydrodynamic stimulus. Moreover, most common laboratory methods for stimulating bioluminescence, e.g., bubbling (Biggley et al., 1969), stirring (Hamman & Seliger, 1972), vibration (Eckert & Sibaoka, 1968), and chemical (Hamman & Seliger, 1972) and electrical (Eckert, 1966) excitation, either do not provide hydrodynamic stimuli, or if so, can not provide a detailed description thereof. Only through observing the response of luminescent organisms in a well-characterized flow field (e.g., pipe flow) can the hydrodynamic parameters responsible for bioluminescent stimulation be best studied. It is hoped that this approach will eventually lead to reliable estimates of the bioluminescent potential of many of the flow fields encountered in the ocean. For example, once bioluminescence is determined as a function of wall shear stress from *in situ* measurements, it should be possible to estimate the bioluminescence excited by a submerged body moving through the same medium.

The objectives of the present pipe flow study are (1) to compare the response of bioluminescence in fully developed laminar and turbulent flow, (2) to determine threshold values of wall shear stress, τ_{wall}, necessary to excite bioluminescence, and (3) to examine the level of individual flashes as a function of τ_{wall}.

Section 2 describes the experimental apparatus and procedure. Wall shear stress, volume flow rates, and photomultiplier tube (PMT) measurements are presented in section 3. These sections focus respectively on: the response of luminous organisms before and after transition from laminar to turbulent flow (section 3.1a – San Diego Bay measurements, section 3.1b – San Clemente Island measurements); laminar flow stimuli (section 3.2a – high levels, section 3.2b – threshold levels); and the flash characteristics of individual organisms (section 3.3). A general discussion of the experimental results can be found in section 4 which is divided into subsections addressing: comparison with previous experiments (section 4.1), and the response of bioluminescence in laminar (section 4.2) and turbulent (section 4.3) flow. Concluding remarks follow in section 5. Appendix 1 provides a general description of the methods involved in estimating the light levels associated with the photographs in figure 2. In appendix 2 the character of fully developed laminar and turbulent pipe flow, important to this study, is briefly outlined. Finally, in

appendix 3 the mathematical framework is developed for determining the bioluminescence dependence on the convective velocity in pipe flow.

2.0 MATERIALS AND METHODS

Fully developed pipe flow is chosen to stimulate bioluminescence because it (1) is well characterized, (2) offers a wide range of laminar and turbulent stimuli, (3) provides continuous replacement of luminous organisms, and (4) levels of bioluminescence have not appeared significantly degraded by the organisms upstream transit through the pipe (Losee and Lapota, 1981). Interest in pipe flow dates back to antiquity, with the earliest pipes being composed of natural tubes such as bamboo. Clay water pipes were constructed by the Greeks at least 2500 years ago and by 312 B.C. the water supply system of Rome provided as much water per capita as is presently found in many parts of the civilized world (Rouse & Ince, 1957).

An exact solution to the governing hydrodynamic equations for fully developed laminar pipe flow, as referenced by Rouse and Ince (1957), has been known for over 150 years. Measurements which would corroborate these analytical results had been already made (Hagen, 1839; Poiseuille, 1840). In contrast, corresponding knowledge of fully developed turbulent pipe flow is predominantly empirical in nature. Nevertheless, a detailed description of the turbulent flow field has emerged (Laufer, 1954). A brief development of the relevant pipe flow equations used throughout the present study can be found in appendix 2.

The primary apparatus (figure 3) consisted of a 75-liter tank, a gently contracting inlet section, and a 0.635-cm i.d. polycarbonate pipe (Rohr et al., 1990). Dye visualization showed that the flow through the pipe inlet remained laminar throughout the range of flows used. Pressure taps were located at 28.6, 60.4, and 92.2 cm (or about 45, 95, and 145 pipe diameters) from the pipe inlet. Pressure drops were measured by variable reluctance differential transducers (Valydyne Corporation). No significant difference was found between pressure-drop measurements across the first and second taps, and the second and third taps (supporting the premise that the flow is fully developed). Wall shear stress values were calculated from pressure drop measurements employing the second and third pressure taps (see equation 2.1b).

On one occasion, for the purpose of achieving higher levels of laminar shear stress, a similar pipe-flow apparatus, but with a 0.305-cm i.d. glass pipe, was employed. The entrance section consisted of a conical section that tapered from a 5.08-cm i.d. to a 0.305-cm i.d. over a length of 7.62 cm. Pressure measurement locations were 2.41 m and 3.02 m from the pipe entrance. Here glass was extruded from the pipe, cut, and fused to a graded glass seal containing a metal pressure tap.

Volume flow rates were measured at the discharge end of each pipe using either a rising-ball flow meter or a mass flow meter (Micro Motion Corporation Model D40). To increase accuracy at low flow rates, the volume flux was also measured by weighing the volume of water collected at the pipe outlet over a measured time. The average flow velocity, U_{avg}, was obtained by dividing the volume flow rate by the pipe area. Measurements of volume flow rate, pipe diameter, and temperature (from which the kinematic viscosity can be determined) were used to determine the corresponding Reynolds number (see equation 2.3).

Figure 4 shows representative Darcy friction factor (see equation 2.5) *vs* Reynolds number data. For the 0.635-cm i.d. pipe and $Re < 2000$, there is excellent agreement between the theoretical (solid line) and measured values. Between $Re > 2000$ and transition from laminar to

turbulent flow, Re_{trans}, the friction factor data for the 0.635-cm i.d. pipe is somewhat higher than the theoretical predictions. This discrepancy results because the pressure taps for the 0.635-cm pipe were, in terms of pipe diameter, not far enough downstream (L_e/D = 95 and 145, see equation 2.2a) to ensure fully developed laminar flow for this range of Reynolds numbers. Corresponding τ_{wall} calculations will be higher, about 40% at Re = 6000, than what would be predicted for fully developed laminar flow. The pressure taps for the 0.305-cm i.d. pipe, however, were located much further downstream (L_e/D = 960). Consequently, better agreement between measurements and predicted values are found for the 0.305-cm pipe at the higher Reynolds number laminar flows. Figure 4 also shows, for $Re > Re_{trans}$, excellent agreement between the accepted turbulent values (Blasius, 1913; dashed line) and the present measurements. Simultaneous friction factor and Reynolds number values were calculated for each bioluminescent measurement throughout this investigation. This procedure allowed both the nature of the flow field (i.e., whether it was laminar or turbulent) to be determined, and shear stress levels throughout the pipe to be quantified.

Bioluminescence was measured by RCA 8575 photomultiplier tubes (PMTs) used in the photon count mode. The face of each PMT fits into an opaque housing which clamped directly onto the pipe. With this arrangement, the PMT field of view encompassed 5.0 cm of pipe length. For the 0.635-cm i.d. pipe, the center of one PMT was always positioned near the bottom of the pipe, 67 cm ($\approx$ 106 pipe diameters) from the inlet (figure 2). A second PMT was sometimes employed, positioned either near the top of the pipe with its center 6 cm ($\approx$ 9 pipe diameters) from the inlet, or near the middle of the pipe with its center 22 cm ($\approx$ 35 pipe diameters) from the inlet. For the 0.305-cm i.d. glass pipe the the PMT center was located 1.06 m ($\approx$ 350 pipe diameters) from the inlet.

Throughout these experiments, surface water from San Diego Bay and off San Clemente Island was obtained by bucket after dusk. On two occasions, luminescent organisms that passed through the pipe were identified. The majority of organisms found were *Gonyaulax polyedra* and *Noctiluca millepias*. These dinoflagellates are common to the coast of Southern California (Sweeney, 1963; Holmes et al., 1967; Kimor, 1983). Together with the genera *Ceratium* and *Protoperidinium* they are expected, to various degrees throughout the year, to be the principal sources of shallow-water bioluminescent light occurring in San Diego Bay (Sweeney, 1963; Kimor, 1983).

Most bioluminescent dinoflagellate flashes last about 100 ms (Anderson et al., 1988). For this flash duration, streaks of bioluminescent light will be less than 25 cm long at the highest flow rates achieved in the present experiments. Therefore, the light contribution to the bottom PMT from flashes initiated at the pipe inlet, 67 cm upstream, are presumed inconsequential. Even allowing for a 100 ms response time and a 200 ms flash duration, as shown in figure 5, light streaks initiated at the inlet are not measured by the bottom PMT throughout the flow range of interest. The lack of significant influence of inlet stimulus on the bottom (67 cm from inlet) PMT measurements is corroborated by recordings from a low–light video camera (Cohu Inc. ISIT) with a video analyzer (Hamamatsu model DVS–3000). Finally, lack of time correlation between the top and bottom PMTs also indicates that light is not being internally reflected down the pipe.

The average PMT measurements presented here are in the form of counts per second (Morita & Johnson, 1974; Rohr et al., 1990), as opposed to counts per volume (Widder et al., 1993; Latz et al., 1994). Threshold levels of τ_{wall} are better displayed when PMT levels are expressed as counts per second. It is also more appropriate to express individual flash PMT levels as counts per second as opposed to counts per volume. However, expressing PMT levels as counts per second may obscure the interpretation of why average PMT levels change with increasing flow rate. An inherent ambiguity results because both convective and stimulative effects determine PMT levels. In appendix 3 the dependence of the average PMT count rate on the convective velocity, for the present pipe flow configurations, is shown to be approximately linear throughout the flow regime examined. Therefore, accompanying each PMT *vs* τ_{wall} curve presented, where the PMT levels are expressed as counts per second, the corresponding relation between PMT levels expressed as counts per volume (calculated via equations 2.6b and 2.11) and τ_{wall} is also included.

The entire pipe-flow apparatus resided within a dark room and background PMT levels were typically less than 200 counts per second. Average pressure drop, PMT, and flow rate measurements were obtained for either equal flow volumes (2.2 liters for 10/1, 10/91 experiments) or equal times (100 seconds, remaining experiments), the results being essentially the same. The time series for the PMT data, containing 1000 consecutive 0.1-s increments, were also recorded. The time series were used as a diagnostic to discriminate between background noise and actual bioluminescence, and to provide information about the level of individual bioluminescent flashes.

3.0 RESULTS

3.1 BIOLUMINESCENCE BEFORE (LAMINAR) AND AFTER (TURBULENT) TRANSITION

The following experiments, which employed the 0.635-cm i.d. pipe (see figure 3), focus on the response of bioluminescence on either side of transition from fully developed laminar to fully developed turbulent pipe flow. During transition, the flow was characterized by the intermittent passage of laminar and turbulent slugs of water, which resulted in large fluctuations in the velocity and pressure measurements. Transitional flow measurements are for the most part (except some San Clemente Island measurements – see figure 7c) not included in the present study.

3.1a San Diego Bay Measurements

Bioluminescent organisms collected from San Diego Bay surface waters were allowed to dark adapt in the tank for at least 45 minutes before beginning the pipe flow experiments. Specific times marking the commencement of data collection are included throughout the text and figure legends. Laminar to turbulent transition occurred between Reynolds numbers of 5000 to 6000. The position of the single PMT for these measurements was 67 cm (106 pipe diameters) from the pipe entrance.

Representative San Diego Bay PMT measurements are presented in figure 6a as a function of Reynolds number. Each experiment involved a single tank ($\sim$65 liters full) of bay water and was divided into two runs. The open symbols in figure 6a represent measurements from the initial run, designated run 1, which employed about half of the reservoir. The sequence of flow rates was monotonically decreasing during run 1. The solid symbols in figure 6a are measurements collected from the final run, designated run 2, which comprised the remaining half of the reservoir. Here the sequence of flow rates was continually increasing. Each data point in figure 4a represents an average over 2.2 liters of seawater.

An increasing difference between PMT values associated with the first and second runs, for nearly the same Reynolds number, is observed in figure 6a for both experiments. This divergence between runs 1 and 2 may reflect, due to the different tank residency times between runs, the different prestimulus recovery times of the luminous organisms. Biggley et al. (1969) have found *Gonyaulax polyedra*, during their dark cycle, to recover exponentially after being stimulated to exhaustion with half times of about 20 minutes. While the stimulus accompanying the collection, transportation, and tank filling is presumably much less than that associated with total depletion, a similar "hysteresis" effect, as shown in figure 6a, is normally evident throughout the data where this flow-rate sequence is followed. Another possible explanation for this apparent tank residency time dependence is that stratification of the luminous organisms had either occurred prior or during the experiment. Also apparent in figure 6a is an increase in the slope of the PMT *vs* Re data around transition ($5000 \leq Re_{trans} \leq 6000$). This behavior was normally observed and often more dramatic for larger values of Re_{trans}.

Figure 6b plots the same PMT measurements of figure 6a, but as a function of the corresponding wall shear stress, τ_{wall}. Included in figure 6b are additional measurements taken from

San Diego Bay throughout the same flow regime and with similar Re_{trans} values. (The cross symbols are comparison data from Rohr et al. (1990) which are addressed in section 4.) The abrupt increase in bioluminescence appearing at transition in figure 6a is no longer evident in figure 6b.

The solid line in figure 6b represents the slope (1.03, $R^2 = 0.49$) of the least–squares power law regression for all the San Diego Bay data for $\tau_{wall} > 25$ dynes/cm^2 (turbulent flow). Dividing the PMT measurements in figure 6a by the corresponding volume flux (via eq. 2.11) results in a slope of 0.46, i.e., PMT levels expressed as counts per volume $\propto \tau_{wall}^{0.46}$. As shown in appendix 3, this latter representation eliminates the flow's convective contribution towards increasing PMT levels.

3.1b At–Sea Measurements Off San Clemente Island

To complement the San Diego Bay studies, the same pipe-flow apparatus was used in a series of at-sea experiments conducted from the research vessel USNS *De Steiguer*. The experiments were performed a few miles off the southeast coast of San Clemente Island (32° 47.6′–56.1′ N, 118° 25.1′–25.5′ W) from 3/7/92 to 3/11/92. In an attempt to mitigate the bias introduced by different reservoir residency times of the organisms, dark adaption times were reduced to 20 minutes and the at-sea flow-rate sequence alternated between high and low flow rates.

Two PMTs were employed throughout these at-sea experiments. The PMTs were located 22 cm (middle position) and 67 cm (bottom position) from the pipe inlet (see figure 3). Measurements from the two PMTs usually exhibited good agreement and consequently were averaged. Transitional Reynolds numbers were found to vary significantly throughout this series of experiments ($Re_{trans} \approx$ 3500, 5400, and 7600 in figure 7a). Presumably, this was due to the changing background motion accompanying the evolving sea state. The most conspicuous differences between the PMT *vs* Re data sets shown in figure 7a occurred between Reynolds numbers of 3000 and 9000. For example, throughout this range the PMT levels associated with low Re_{trans} were significantly higher than those corresponding to high Re_{trans}. This disparity reflects the two different states of the flow, i.e., turbulent (higher PMT values) and laminar, existing for the same Re number because of the different Re_{trans} values. Similar arguments can be made for the behavior of the middle-of-the-range Re_{trans} data (i.e. $Re_{trans} \approx 5400$). As before, when comparing laminar and turbulent flows at similar Reynolds numbers in figure 7a, the PMT values associated with turbulent flow are usually greater.

Plotting the same average PMT values in figure 7a as a function of wall shear stress in figure 7b, both laminar and turbulent flow data appear to lie along a single curve. Note that the highest laminar τ_{wall} value (3/9/92, ▲; Re $\approx$ 7600, $\tau_{wall} \approx$ 35 dynes/cm^2) overlaps the lowest turbulent τ_{wall} value (3/9/91–3/10/92, □; Re $\approx$ 4500, $\tau_{wall} \approx$ 30 dynes/cm^2). Also noteworthy is that within the laminar flow region of each data set in figure 7b, a change of slope around $\tau_{wall} \approx$ 15–20 dynes/cm^2 is apparent. This feature, also evident in figure 6b, will be addressed in the discussion section. For $\tau_{wall} > 25$ dynes/cm^2, the San Clemente Island PMT laminar and turbulent data in figure 7b increase approximately as the first power (slope = 0.82, $R^2 = 0.72$) of wall shear stress. (Expressing these PMT levels as counts per volume results in a slope of 0.25.) The solid line appearing in figure 7b, included for comparison purposes, has a slope of 1.03 as determined from the San Diego Bay data (figure 6b).

In figure 7c the previous data from figure 7b are replotted to show the overlap between experiments of the different flow regimes. For all data sets laminar flow is indicated by the open square symbol, turbulent flow data by the solid square symbol, and transitional flow by an open box with x inside. In general the response of bioluminescence to wall shear stress in pipe flow, as shown in figure 7c, does not appear to be significantly dependent on the nature of the flow. However, two caveats should be mentioned. First, unlike the transitional data appearing in figure 7c, there have been similarly acquired measurements collected in San Diego Bay, which show a significant increase in bioluminescence during transition. Secondly, although equation 2.1b was invoked, neither the transitional nor the higher laminar flow (Re > 2000) measurements were obtained in fully developed flow.

3.2 BIOLUMINESCENCE IN LAMINAR FLOW

A rise in PMT levels with increasing laminar flow is evident to various degrees throughout figures 6 and 7. The present section focuses on the effect on bioluminescence of both high and low τ_{wall} levels of laminar flow stimuli. High τ_{wall} levels obtained in laminar flows may overlap low τ_{wall} values obtained in turbulent flows, thereby providing an opportunity to compare the stimulative effect of laminar and turbulent flows for the same average shear field. Low levels of τ_{wall} in laminar flow are important toward determining threshold values of the hydrodynamic stimulation of bioluminescence.

3.2a High Levels of Laminar Flow Stimulus, $\tau_{wall} > 15$ dynes/cm^2

The highest laminar flow Reynolds number ($Re_{trans} \approx 10{,}000$) measurements were obtained during the USNS *De Steiguer* experiments conducted off San Clemente Island (32° 55.1′ N, 118° 27.7′ W) on 12/18/91 and 12/19/91. The 0.635-cm i.d. pipe-flow apparatus was again utilized with the PMT positioned 67 cm from the pipe inlet. No significant differences were observed between the six consecutive runs executed. Consequently, all PMT *vs* τ_{wall} data were plotted collectively in figure 8.

The highest laminar flow shear stress data were obtained in the 0.305-cm i.d. pipe-flow apparatus with seawater collected from San Diego Bay on 12/12/91. The PMT was 106 cm from the pipe inlet. The smaller diameter pipe, while providing a greater range of fully developed laminar flow than the 0.635-cm pipe, significantly reduced the volume flux for equal τ_{wall} values. This resulted in lower signal levels and greater variability. To reduce variability, each data point from the 0.305-cm i.d. pipe in figure 8 is composed of an average of five consecutive 100-s records. For comparison with the 0.635-cm i.d. data in figure 8, the PMT levels obtained from the 0.305-cm i.d. glass pipe are adjusted by the ratio of their areas. No discernable time dependence was found on the sequence in which the five consecutive, constant flow-rate measurements were taken. However, this was not the case for data sets obtained when tank residency times were much different. For example, the last data set taken, which had the highest tank residency time, was conspicuously high (τ_{wall} = 45 dynes/cm^2, PMT = 44,000 counts per second) and consequently is not included in figure 8.

Representative laminar and turbulent flow data from figure 6b (10/1/91) are also shown in figure 8. There is a conspicuous gap between $\tau_{wall} \approx 12$ and 40 dynes/cm^2 for the 10/1/91 data, where transition occurs, which is spanned by the high shear laminar flow data. The lines in

figure 8 represent the slopes of a least-squares power law regression to each data set where τ_{wall} > 15 dynes/cm^2. These slopes are 1.00 (laminar flow; R^2 = 0.71; 12/18/91–12/19/91) for the large dashed line, 1.26 (laminar flow; R^2 = 0.89; 12/12/91) for the solid line, and 1.10 (turbulent flow; R^2 = 0.96; 10/01/91) for the small dashed line. Expressing the PMT levels as counts per volume results in respective slopes of 0.00, 0.26, and 0.53.

3.2b Low Levels of Laminar Flow Stimulus, τ < 15 dynes/cm^2

Figure 9 displays PMT levels as a function of wall shear stress from the most extensive low Reynolds number experiments. These experiments used San Diego Bay water in the 0.635-cm pipe with the PMT 67 cm downstream from the pipe inlet. Threshold values of wall shear stress in figure 7 occur around 1 dyne/cm^2. Corresponding Reynolds numbers are less than 1000. At these low Reynolds numbers the flow is unquestionably laminar. Similar experiments (not shown) throughout the year corroborate that threshold values always occur in laminar flow and at levels usually between 0.5 and 3 dynes/cm^2.

The increase of bioluminescence with τ_{wall} shown in figure 9 is much faster than what is found (figures 6b, 7b, and 8) for τ_{wall} > 15 dynes/cm^2, where the relationship is approximately linear. The solid line in figure 9 represents a least squares power law regression to the PMT data between 0.7 and 14.0 dynes/cm^2 and has a slope of 2.57, R^2 = 0.59. (Accounting for the convective velocity component, see appendix 2, the bioluminescent levels expressed per unit volume are proportional to $\tau_{wall}^{1.57}$.) The corresponding Reynolds numbers for these data are always less than 5000, and since Re_{trans} for these experiments occurs around 6000, all the data in figure 9 were obtained in laminar flow.

The associated f *vs* Re measurements for much of the data found in figures 8 and 9 can be found in figure 4. The corresponding PMT *vs* Re data are not presented because, in fully developed laminar flow, τ_{wall} is proportional to Re.

3.3 INDIVIDUAL FLASH LEVELS

Representative PMT time series data are shown in figure 10a for τ_{wall} = 15 dynes/cm^2 (Re = 5000, laminar flow) and figure 10b for τ_{wall} = 112 dynes/cm^2 (Re = 9950, turbulent flow). The PMT is located 67 cm from the inlet of the 0.635-cm i.d. pipe. Measurements are composed of PMT counts in consecutive 0.1-s bins. Each vertical spike in figures 10a and b is believed to be indicative of a single flashing organism. Considering that the corresponding 100-s average PMT level for figure 10a is about five-fold larger than for figure 10b, it is remarkable that the peak 0.1-s PMT level for either figure remains nearly the same (within 10%).

Representative peak levels from the bottom PMT (located 67 cm from the inlet of the 0.635-cm i.d. pipe) are plotted in figure 11 as a function of τ_{wall} for both San Clemente Island and San Diego Bay experiments. Peak PMT levels are obtained by taking the highest count in any 0.1-s bin within each 100-s record (constant τ_{wall}). To compare with average PMT values which are in counts per second, peak values in figures 11 and 12 are divided by 0.10.

Transition from laminar to turbulent flow for all the experiments in figure 11 was between Reynolds numbers of 5000 and 6000. This range of Re_{trans} resulted in the gap in the shear stress

data between 20 to 35 dynes/cm^2. Between threshold and τ_{wall} values of about 10 dynes/cm^2, where the flow is always laminar, peak PMT levels grow rapidly with increasing shear suggesting a graded bioluminescent response. For $\tau_{wall} > 10$ dynes/cm^2, which includes both the highest levels of laminar shear stress and the entire range of turbulent shear stress, peak PMT levels remain nearly constant[2]. Included in figure 11 are representative 100-s average bottom PMT levels. An abrupt change in functional dependence of both peak (0.1 s) and average (100 s) PMT levels around $\tau_{wall} \approx 10$–20 dynes/cm^2 is evident.

Peak top (6 cm from pipe inlet) and bottom (67 cm from pipe inlet) PMT data sets taken from the 0.635-cm i.d. pipe are compared in figure 12 as a function of Reynolds number. With increasing Reynolds number both top and bottom peak levels initially grow, followed by a flow regime where they assume a nearly constant value. The onset of bioluminescence for the top PMT is seen to occur at a lower Reynolds number, which is in agreement with the 100-s average PMT measurements and visual observations.

The 0.1-s peak PMT data in figure 12 are not plotted as a function of τ_{wall}, because τ_{wall} is not known at the location of the top PMT where the flow is not fully developed. Nevertheless, for the same Reynolds number gross comparisons between the flow fields opposite the top and bottom PMTs can be made. For example, via dye visualizations the flow past the top PMT was found to remain laminar throughout the entire range of Reynolds numbers investigated, whereas $Re_{trans} \approx$ 5000–6000 for the bottom PMT. Comparing top and bottom peak PMT data for Re > 6000, it appears that the nature of the flow field (laminar *vs* turbulent) is not particularly important towards determining flash levels of individual bioluminescent organisms.

[2] This constant value is about half the level where the PMT signal becomes clipped. Similar behavior, i.e., peak PMT level independence at τ_{wall} values from about 10 – 200 dynes/cm^2, is found when the experiment is repeated with a 10^{-1} filter.

4.0 DISCUSSION

4.1 COMPARISON WITH PREVIOUS EXPERIMENTS

There have been several previous bioluminescent experiments that are relevant to the present study. While these experiments did not usually include direct measurements of shear stress, for comparison sake, estimates of τ_{wall} are made when possible.

4.1a Christianson and Sweeney (1972)

Christianson and Sweeney (1972) have studied bioluminescent stimulation of *Gonyaulax polyedra* cultures in a 0.86-mm i.d. coiled capillary tube through a range of laminar flows. A PMT monitored the emitted light from the entire coil, including its centrally located inlet. They noted that luminescence was observed to take place principally within the coil as the cells passed through the capillary. Assuming that the shear stress in the coiled tube is approximately equal to that in a straight tube with an equivalent diameter[3], τ_{wall} values can be estimated (equation 2.6b) and are included parenthetically. Christianson and Sweeney (1972) observed night phase luminescence ($\propto$ counts per second) to initially increase faster than the flow rate, but then from about 7 ml/min (20 dynes/cm^2) to 12 ml/min (35 dynes/cm^2), the increase was nearly proportional to the flow rate. A triggering flow rate of 0.8 ml/min (2.3 dynes/cm^2) was inferred by extrapolating to the lower flow rate data.

The above results of bioluminescent excitation are in good agreement with those reported here. Moreover, Christiansen and Sweeney (1972) hypothesized that the change in the rate at which the average bioluminescence grows with shear stress may be related to an initial gradation of peak flash levels. This hypothesis is supported by the present data.

4.1b Anderson, Nosenchuck, Reynolds and Walton (1988)

Anderson et al. (1988) repeated the experiments of Christianson and Sweeney (1972), using the same coiled capillary tube and cultures of *Gonyaulax polyedra*. An image intensifier was employed to image the entire capillary coil. Anderson et al. (1988) found, contrary to Christianson and Sweeney's (1972) visual observations, that bioluminescence was not stimulated in the uniform section of the capillary tube, but only at the abrupt transition at its entrance. This result, together with additional measurements obtained in a converging-diverging capillary tube, led Anderson et al. (1988) to conclude that bioluminescence is stimulated principally by changes in shear, acceleration, and pressure.

The present experiments also indicate greater (2–3 times downstream values) bioluminescent stimulus occurring near the pipe inlet. However, stimulation is now found to continue throughout

[3] Strictly speaking the friction factor in a curved pipe is often greater than that of an equivalent straight pipe at identical Reynolds number. In a coiled tube the presence of centrifugal forces result in a secondary (i.e., radial) flow pattern which is a function of the Dean number, De, defined as follows:

$$De = Re^*(D/d)^{1/2}.$$

Here d is the diameter of the pipe coil, and as before, Re is the pipe Reynolds number, and D is the pipe diameter. For Dean numbers less than 10, the secondary flow is small and the friction factor is nearly equivalent to the corresponding straight pipe values. For larger Dean numbers the friction factor of the coil exceeds that of an equivalent straight pipe. The Dean numbers in the Christian and Sweeney (1972) experiments ranged from 0 to about 35 (U_{avg} = 0–12 ml/sec).

the pipe when threshold shear stress levels are exceeded. Note in particular, contrary to Anderson et al.'s (1988) findings, bioluminescent stimulation is also observed in laminar flow even though the shear stress is constant along the organism's trajectory. The reason for this discrepancy is not known.

4.1c Morita and Johnson (1974)

Morita and Johnson (1974) have performed pipe flow studies in a 0.71-cm i.d. glass pipe, also with cultures of *Gonyaulax polyedra*. Transition was assumed to occur between a Reynolds number of 2000 and 4000. Estimates of τ_{wall} were made assuming laminar flow for Re < 2000 (equation 2.6b) and turbulent flow for Re > 4000 (equation 2.9b). Morita and Johnson (1974) found that for τ_{wall} > 25 dynes/cm^2, which was assumed to be fully developed turbulent flow, the stimulated emission ($\propto$ counts per second) appeared to be linearly related to shear. This observation is in good agreement with the present measurements (figures 4b and 5b). However, at lower shear stress levels, their results are contradictory to those reported here. Morita and Johnson (1974) reported more light at τ_{wall} = 2–3 dynes/cm^2 than at τ_{wall} = 10–15 dynes/cm^2. It was hypothesized that this anomalous behavior may have resulted because the flash signature (i.e., the rise time and/or decay rate of the stimulable light emission) is dependent on stimulation intensity.

4.1d Latz, Case and Gran (1994)

Most recently Latz et al. (1994) reported a study of the excitation of cultures of bioluminescent dinoflagellates (including *Gonyaulax polyedra*) by laminar and turbulent Couette flow. The general PMT *vs* τ behavior they observed, for shear stresses between 0.3 and 16 dynes/cm^2, is in excellent agreement with the present pipe flow measurements. In particular, they have found laminar flow excitation of bioluminescence, threshold shear values of about 1 dyne/cm^2, a graded response of individual flashes at low shear stress levels, and a lack of sensitivity to the nature (laminar or turbulent) of the hydrodynamic stimuli.

4.1e Rohr, Losee and Hoyt (1990)

The at-sea (Sea of Cortez) bioluminescent experiments of Rohr et al. (1990) employed essentially the same 0.635-cm i.d. pipe apparatus (with the exception of pressure taps) and procedure as used here. Rohr et al. (1990) reported:

1. an often abrupt increase in bioluminescence as a function of Re number around transition,

2. essentially no bioluminescent stimulation in laminar flow,

3. constant peak PMT values in turbulent flow.

Each of these observations need to be reevaluated in the context of the present work.

1. Throughout the current measurements, an abrupt increase in bioluminescence at Re_{trans} is also often observed (e.g., figures 6a and 7a), particularly when occurring at high Reynolds numbers. Concerning the reason for this increase in bioluminescent stimulation at transition, Rohr et al. (1990) had written:

"Whether this principally results from the corresponding increase in shear stress or the sudden appearance of fluctuating stresses associated with the turbulent eddy field remains to be resolved."

Where comparisons can be made (see figures 7b and 8), the present PMT measurements (expressed as counts per sec) suggest that shear stress, regardless of whether it is laminar or turbulent, reasonably characterizes bioluminescent stimuli in fully developed pipe flow. Therefore, when plotted as a function of Re number, the increase in bioluminescence observed at transition appears to be at least partly accounted for by the accompanying jump in τ_{wall} (presumably the increased mixing and reduced average velocity associated with turbulence has some effect also). For fully developed pipe flow, τ_{wall} increases by a factor of $0.005(Re)^{3/4}$ at transition. The increase in shear stress for Re_{trans} values of 6000 and 10000 are, respectively, by factors of 3.4 and 5.0 throughout the pipe.

Another example of increased bioluminescence occurring at transition may be the following. Dolphins swimming through phosphorescent seas have been reported to produce interesting displays of light (Stevens, 1950; Hill, 1950; Thompson, 1971; Ridgeway and Carter, 1993). Pronounced bioluminescence beginning below the dorsal fin of a swimming Pacific white-sided dolphin has been reported (Wood, 1973). On a dolphin's spindle-shaped body, Re_{trans} might be expected to occur in this area (Ridgeway and Carter, 1993), and would result in both higher shear stresses and a thicker boundary layer. A representative Re_{trans} value for a dolphin is 6.5×10^6 (Newman and Wu, 1975). For comparison, the increase in shear stress along a flat plate at $Re_{trans} = 6.5 \times 10^6$ is a factor of 6.0. Note even when $\tau > 20$ dynes/cm^2, where peak levels of individual organisms are independent of τ, transition may still be associated with increased bioluminescence. Increased bioluminescence could result from a larger volume of flow experiencing shear stresses greater than threshold, as well as a greater fraction of the organisms present being stimulated.

2. The lack of significant bioluminescence reported in laminar flow by Rohr et al. (1990) deserves comment. If a value of Re_{trans} is assumed for Rohr et al.'s (1990) PMT *vs* Re data shown in their figure 4, then τ_{wall} values for fully developed laminar (equation 2.6b) and turbulent (equation 2.9b) flow can be estimated. Based on Rohr et al.'s (1990) accompanying dye visualization experiments, $Re_{trans} \approx 6000$. Included with the present San Diego Bay data in figure 6b, are the 2.2 l average PMT levels from Rohr et al. (1990) as a function of the estimated τ_{wall} values. When plotted with logarithmic coordinates in figure 6b, a rise of luminescence with increasing laminar τ_{wall} levels is clearly evident for the Rohr et al. (1990) data. Although the light intensity of the Rohr et al. (1990) measurements shown in figure 6b are about an order of magnitude less than the present data, the similarity in general dependence of bioluminescence *vs* τ_{wall} is noteworthy. The dashed line in figure 6b represents the slope (1.30, $R^2 = 0.96$) of the least-squares power law regression to the turbulent Rohr et al. (1990) data. Expressed as counts per volume, this slope would be 0.73.

3. Rohr et al. (1990) have also reported that the growing bioluminescent intensity, which they normally observed with increasing turbulent pipe flow, did not appear to be accompanied by a heightening of individual flash levels. The time series measurements presented here offer finer resolution (0.1-s time averages) than those (1.0-s time averages) of Rohr et al. (1990). Where wall shear stress measurements overlap, $\tau_{wall} > 40$ dynes/cm^2 (turbulent flow), the present results

show a similar behavior. Throughout this range it can again be concluded that the increase in bioluminescence with τ_{wall} results from more organisms being stimulated, rather than an increase in individual peak intensity. However, for $\tau_{wall} < 10$ dynes/cm^2 (laminar flow), outside the measurement range of Rohr et al. (1990), a graded response by individual luminescent organisms is now found. The data in figure 11 suggest that the graded bioluminescent response of individual flashes may have an important influence on the form of the 100-s average PMT data, which also exhibit a dramatic change in form around $\tau_{wall} = 10$ dynes/cm^2. The details of this influence cannot be inferred from figure 11, however, since additional information regarding the fraction of organisms excited as a function of τ_{wall} is not known.

4.2 RESPONSE OF BIOLUMINESCENT ORGANISMS IN LAMINAR FLOW

Previously, hydrodynamic stimulation of bioluminescence has been almost exclusively associated with turbulent flow (Anderson et al., 1989; Rohr et al., 1990). Bathyphotometers developed for *in situ* bioluminescent measurements have always provided highly turbulent flow as the hydrodynamic stimulus (Seliger et al., 1969; Losee et al., 1985; Widder et al., 1993). The present study shows, however, that laminar flow stimulates bioluminescence. The question arises as to why, within a biological context, should luminescent dinoflagelates be excited in laminar flow?

Natural dinoflagellate bioluminescence is often observed in the presence of predatory copepods (Buskey et al., 1983). Studies have shown (Esaias & Curl, 1972; H. White, 1979) that marine copepods ingest highly bioluminescent dinoflagellates at a lesser rate than their nonbioluminescent counterparts. Furthermore, copepods have also been found to exhibit a 'startle' or photophobic response to natural and stimulated dinoflagellate bioluminescence (Buskey et al., 1983; Buskey & Swift, 1985). Since most luminous flashes are several orders of magnitude greater than the visual threshold of their predators (Nicol, 1978; Lythgoe, 1979), temporary blinding ("flash bulb effect") by the flash seems likely (Morin, 1983). The possibility (Burkenroad, 1943) also exists that luminescent dinoglagellates might expose the copepod feeding on them to the copepod's predator ("burglar alarm effect").

Taken together, these observations strongly suggest that the luminescent response of dinoflagellates serves as a defense strategy and as such, should be stimulated by the predatory motions of copepods. These motions are unambiguously laminar. A representative Reynolds number for copepod motion, even at a pulse speed of 20 cm/s, is only around 300 (Vogel, 1981), which is low enough to ensure laminar flow about the body. Food capture by copepods is also thought (Koehl & Stricker, 1981) to be viscously dominated and laminar in nature. In retrospect, considering both the natural flow fields that excite luminescent dinoflagellates and the possible advantage that their bioluminescence may serve, a sensitivity of these organisms towards shear stresses induced by laminar flow is to be expected.

The threshold for bioluminescent stimulation found in the present study is of the order of a few dynes/cm^2 (figure 9; $\tau_{wall} \approx 1$–2 dynes/cm^2, $\tau_{avg} \approx 0.5$–1 dynes/cm^2), and deserves some discussion as to the possible advantage this level of threshold excitation might serve. Clearly for bioluminescence to be an effective defense mechanism for an organism, the level of threshold stimulus must be lower than the excitation field caused by the approach of its predators. Threshold levels must also be much higher than oceanic background levels to avoid bioluminescent exhaustion. The possibility of continual random stimulation by ambient motion would severely

limit whatever useful purpose bioluminescent might otherwise have. In this regard Harvey (1929) has written:

> "who can suggest the use of light . . . to a protozoan, living at the surface of the sea, blown hither and thither by the wind."

Estimates regarding the magnitude of ocean surface shear stress that marine dinoflagellates are exposed to have been previously made (Thomas & Gibson, 1990, 1992). The expected range of shear stress at the sea surface for light winds is about two orders of magnitude less than the bioluminescent threshold levels reported here. A wind of 3.5 m/s (measured 10 m above the sea surface) would only produce maximum shear stresses at the ocean surface equal to one-tenth that required for bioluminescent stimulation. Typical shear stress levels measured throughout the deep surface mixed layer are around 0.001 dynes/cm^2 (Evans, 1982), about three orders of magnitude less than that necessary for bioluminescent excitation.

On the other hand, order of magnitude estimates of the average shear stress experienced by a dinoflagellate about to be devoured are not significantly greater than these same threshold values. The entrainment of the common bioluminescent dinoflagellate *Gonyaulax polyedra* (modeled as an equivalent 35–μm diameter sphere; Kamykowski, 1992), by water swept (U_o = 3.2 cm/s; Koehl & Strickler, 1981) towards a devouring copepod results in a Reynolds number around 1.1. At these low Reynolds numbers, Stokes flow is a reasonable approximation for our purposes (Bird et al., 1960). The shear stress on a sphere in Stokes flow is of the form (White, 1974):

$$\tau_{r\theta} = -1.5\,[\mu U_o/R]\,\sin(\theta)\,.$$

The above equation yields, for our *Gonyaulax polyedra* model, average and maximum surface shear stresses of about 20 and 30 dynes/cm^2 respectively. A similar calculation shows that the organism's own propulsion ($\approx$ 0.03 cm/s, Kamykowski et al., 1992) subjects it to shear stresses that are about an order of magnitude less than threshold values. While these estimates are encouraging, it must be realized that on a cellular level the exact mechanism by which mechanical stimulation triggers light emission remains unclear. Also, the present experiments do not address the effects of acceleration (conceivably an important precursor to consumption), and large fluctuating shear stresses for stimulating bioluminescence.

Latz et al. (1994) provide a much more comprehensive comparison between bioluminescent threshold levels and various oceanic flow fields. Based on essentially identical threshold values of shear stress (determined in Couette flow), they predict that surface breaking waves, adult scombrid fish, and copepod burst swimming should all excite bioluminescence. All of these predictions have been confirmed by observation.

4.3 RESPONSE OF BIOLUMINESCENT ORGANISMS IN TURBULENT FLOW

The general behavior of the laminar and turbulent flow data exhibited in figure 8 suggests the following results if two pipe flow experiments are performed under identical conditions, except with greatly different Re_{trans} values. Under these conditions, the laminar flow data of the high Re_{trans} experiment should both bridge the transition gap of the low Re_{trans} experiment and overlap its turbulent data. In other words, for the same value of τ_{wall}, bioluminescent levels expressed

as counts per second do not appear (at least for range of overlap studied, 20 dynes/cm^2 < τ_{wall} < 70 dynes/cm^2) particularly sensitive to whether the fully developed pipe flow is laminar or turbulent.

In a fluid dynamics context, it is somewhat surprising that for equal τ_{wall} values in laminar and turbulent pipe flow, average levels of bioluminescence are nearly the same. The length scale of the turbulent eddies, which are of the order of the size of the luminescent organisms (see figure 2.5, appendix 2), has been previously believed to be a significant factor in effective stimulation (Morita & Johnson, 1974; New Scientist, 1990; Rohr et al., 1990; Widder et al., 1993). The lack of increased sensitivity to small scale turbulence, however, is consistent with the luminous response of individual organisms as inferred from 0.1-s peak PMT counts. For τ_{wall} > 10–20 dynes/cm^2 peak flash values were found in figure 11 to have remained essentially unchanged with increasing flow stimulus throughout both laminar and turbulent flow. This behavior suggests that whatever additional stimulus accompanies turbulent flow, it is largely superfluous towards eliciting higher peak luminescent levels from individual organisms.

There remains the question: For the same shear stress profile across the pipe, why doesn't the increased mixing associated with turbulent flow result in more bioluminescence? It is possible that for the same τ_{wall}, the increase in bioluminescence due to turbulent mixing is approximately compensated by the associated decrease in convective velocity. For example (see figure 13), consider turbulent pipe flow at a Reynolds number of 6,000. The necessary laminar mean flow to provide the same shear stress profile is nearly 3.5 times as great (Re_{lam} = 20,400). As shown in appendix 3, throughout the present flow regime where bioluminescence is excited, the contribution to PMT levels (measured as counts per second) due to the convection of luminous organisms past the PMT sensor varies nearly linearly with U_{avg}.

Conversely, our interpretation of the response of bioluminescence (expressed as counts per second) to increasing pipe flow will depend on whether the flow is laminar or turbulent. Consider, for example, figure 8, and τ_{wall} values greater than 15 dynes/cm^2. Here bioluminescent levels for both laminar and turbulent flow increase approximately linearly with τ_{wall}. Since in fully developed, laminar pipe flow $\tau_{wall} \propto U_{avg}$ (equation 2.6b), the near linear increase of bioluminescence with τ_{wall} can be attributed primarily due to convection alone. For fully developed turbulent pipe flow, however, $\tau_{wall} \propto U_{avg}^{1.75}$ (equation 2.11). Consequently U_{avg} (or Re) in turbulent flow increases much more slowly than in laminar flow over the same range of τ_{wall} (see figure 13). Therefore, in turbulent flow, a linear increase of bioluminescence with τ_{wall} represents a greater increase (consistent with the enhanced mixing) than what the associated change in convective velocity can alone provide.

In figure 14, each data set of figure 8, with its PMT levels expressed as counts per second (14a1, b1, and c1), is replotted with its PMT levels expressed as counts per volume (14a2, b2, and c2). After removing the influence of convection, a greater increase in bioluminescence with τ_{wall} is now apparent for turbulent flow (compare figures 14a and 14b with figure 14c). Note, the difference in slope between what is shown in figure 14b2 (0.3; which was calculated from mean velocity measurements) and what was stated previously in the text (0.0; which was calculated from equation (2.6b)). This discrepancy reflects the poorer approximation to fully developed pipe flow for the laminar, high Reynolds number data.

5.0 CONCLUSIONS

"Although in most ways the exact manner in which water moves is difficult to perceive and still more difficult to define, as are the forces attending such motion, certain general features both of the forces and motions stand prominently forth, as if to invite or defy theoretical treatment."

Osborn Reynolds (1883)

While the present effort provides neither an adequate identification of the luminescent organisms involved nor a detailed description of their interaction with the flow field, nevertheless, certain unmistakable trends in the data appear "as if to invite or defy" explanation. These trends include the repeated observation that bioluminescence is stimulated in laminar flow, with threshold values of the order of a few (0.5–3) dynes/cm^2. With respect to the estimates made herein of the natural hydrodynamic stimulus these organisms would normally be subjected to, this level of threshold stimulus should have antipredation value. Another general feature of these measurements is that with increasing wall shear stress a conspicuous break in the rate of increase of average bioluminescence is normally observed between τ_{wall} = 10–20 dynes/cm^2, with the greater increase occurring initially. This break, which occurred in laminar flow, is believed to be at least partly related to the behavior of the peak PMT levels associated with individual bioluminescent flashes. Peak PMT levels initially exhibited a graded response, increasing with τ_{wall} from threshold to τ_{wall} values of about 10 dynes/cm^2, and then remaining nearly constant thereafter. Finally, throughout the figures for τ_{wall} > 20 dynes/cm^2, an approximate linear dependence between average PMT levels (expressed as counts per sec) and wall shear stress is usually observed, regardless of whether the flow is laminar or turbulent. The interpretation of the stimulatory nature of this relationship, as previously discussed, depends on the relationship between τ_{wall} and U_{avg} which is different in laminar and turbulent flows.

The few bioassays complementing the present data set, as well as the historic record, suggest that the luminous organisms responsible for the stimulated light belong only to a few species of dinoflagellates. In coastal environments, the proportion of bioluminescent species is only 1 to 2% (Morin, 1983) of that found in oceanic waters. However, higher productivity in coastal waters may result in a greater amount of bioluminescence potential per unit volume of near surface water (Buskey et al., 1987). In reference to figures 6b, 7b, 8, and 11 it is compelling to suggest that there may be certain regimes of flow agitation where coastal dinoflagellates share similar bioluminescent fingerprints (i.e., similar peak and average PMT dependance on τ_{wall}). It is hoped that this work will lead to better predictive capabilities towards assessing bioluminescent stimulation in a variety of oceanic flow fields. Further work, particularly with offshore organisms and cultures of luminous dinoflagellates (where species, concentration, and prestimulus history can be better controlled) is necessary to corroborate this initial study.

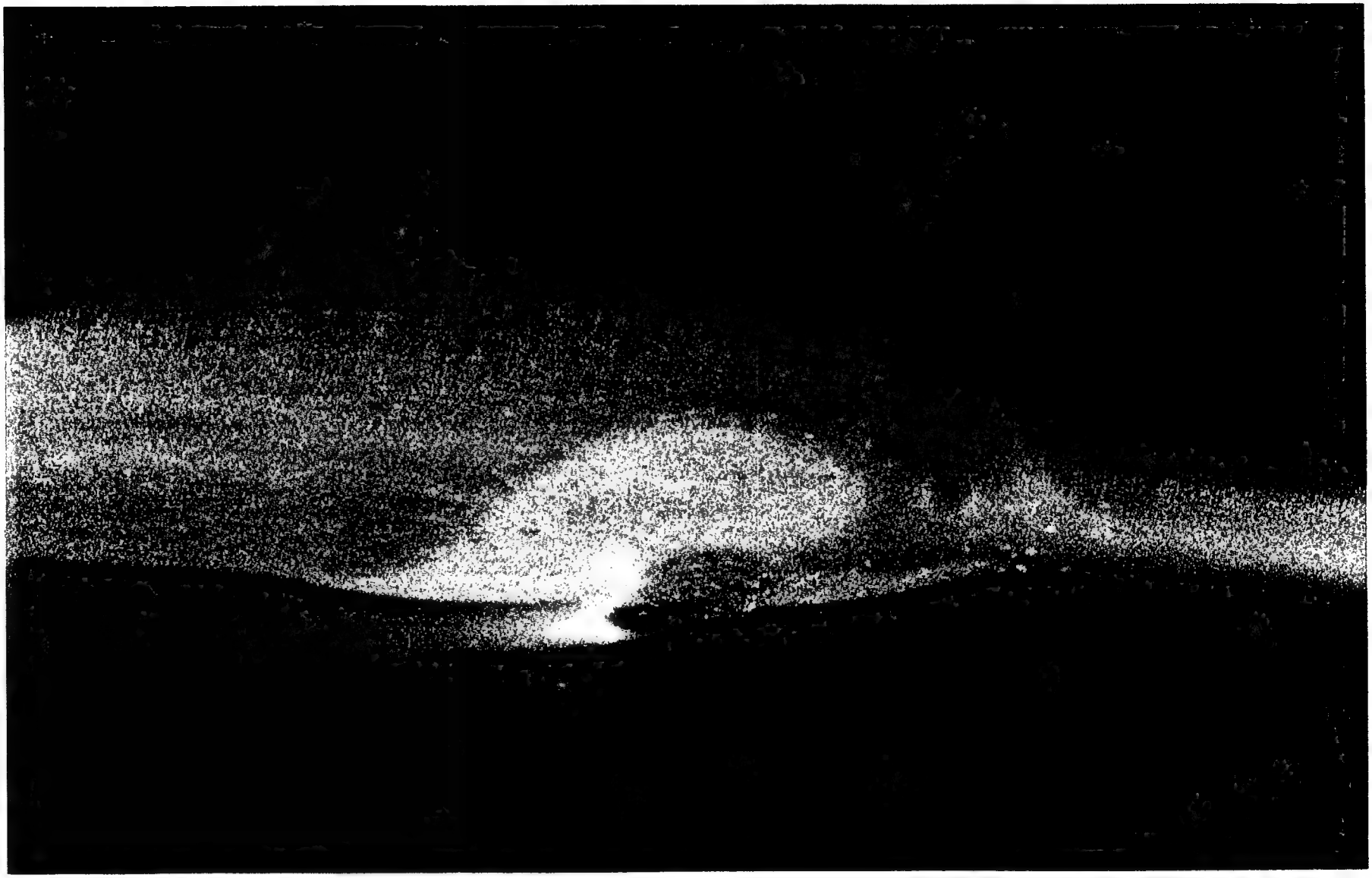

Figure 1. Photograph of bioluminescence. The marine bioluminescent dinoflagellate, *Gonyaulax polyedra* (culture of ~10^6 cells per liter), are stimulated as they are poured over a 17.5 cm model of a dolphin.

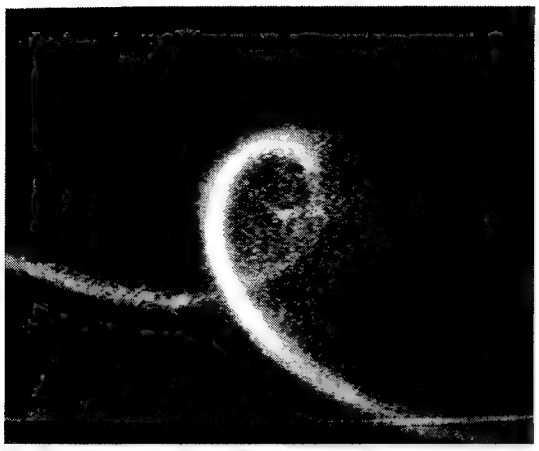

a. The outline of a rope.

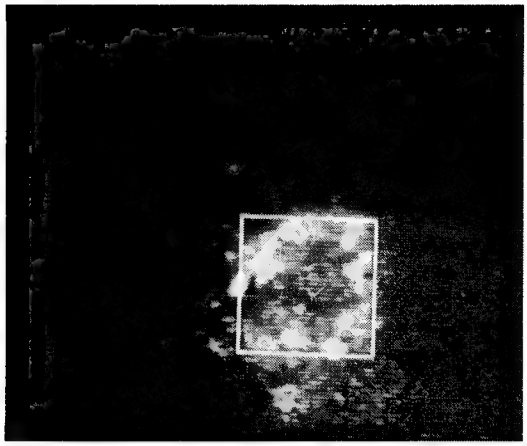

b. A 0.25-m diameter sphere.

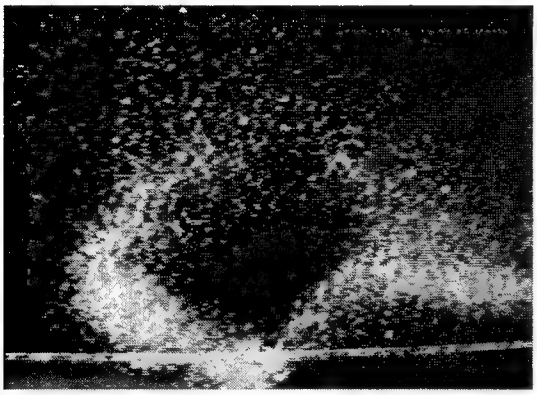

c. A 5-gallon box.

d. The presence of divers.

Figure 2. Computer enhanced photographs of *in situ*, flow induced bioluminescence obtained via a low-light video camera. Objects can be identified 3-5 meters beneath the sea surface as a result of stimulated bioluminescence. At these depths it is likely that one or more species of dinoflagellates are responsible for the emitted light.

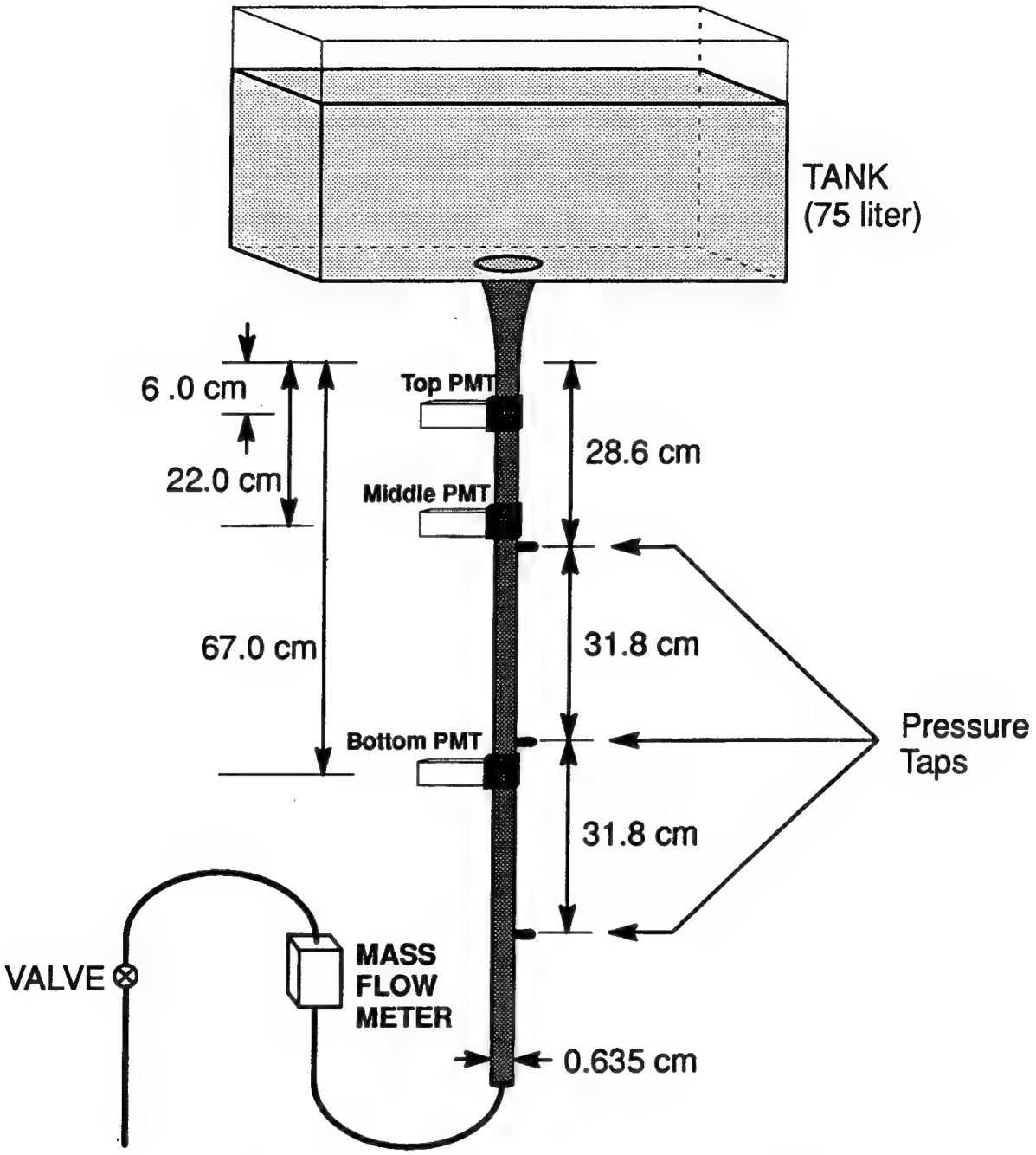

Figure 3. Diagrammatic illustration of the primary pipe flow apparatus.

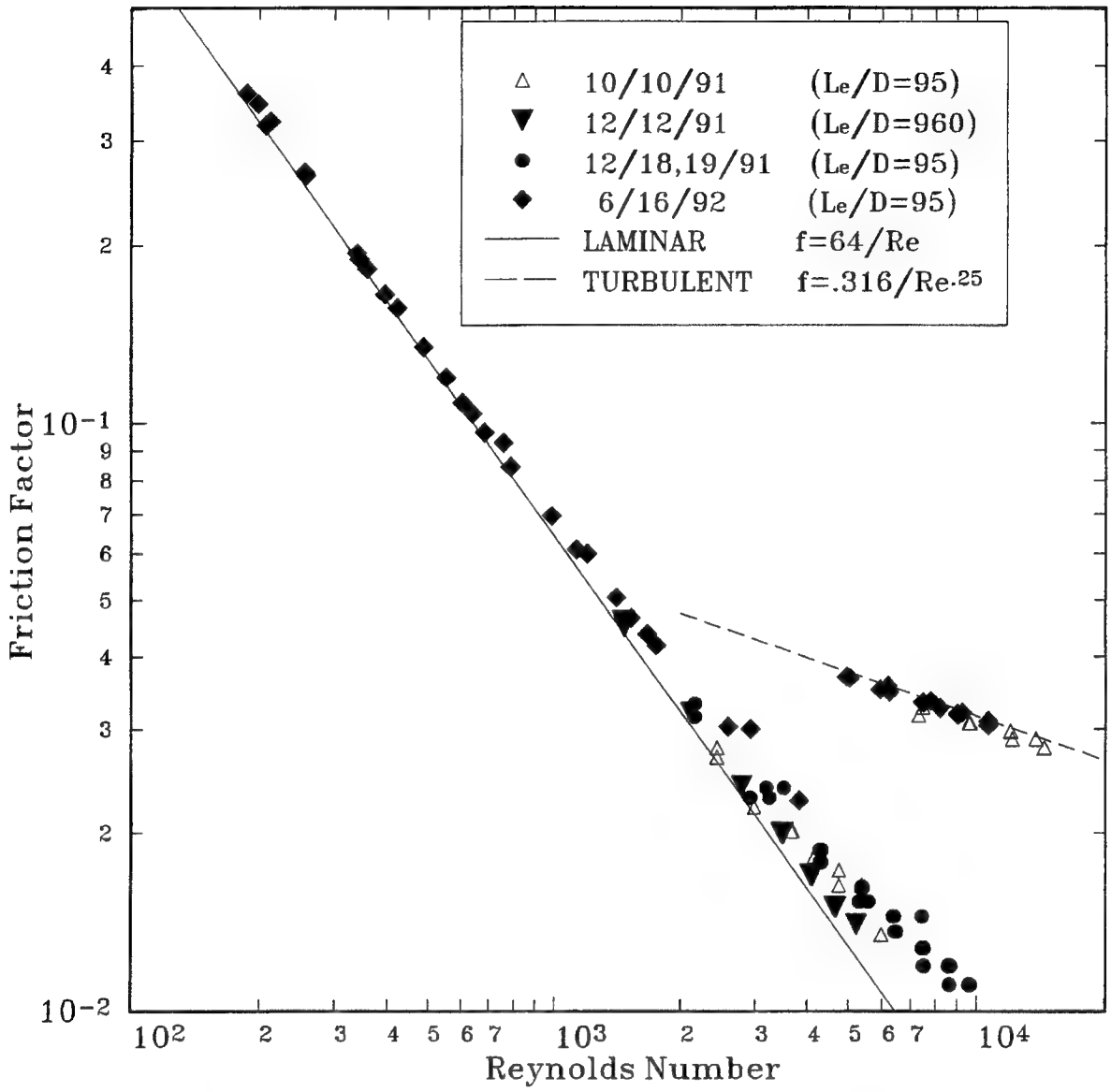

Figure 4. Representative seawater friction factor *vs* Reynolds number data. Most of the measurements show good agreement with theoretical (laminar flow - solid line) and empirically derived (turbulent flow - dashed line) values. Laminar flow measurements taken in the 0.635-cm i.d. pipe (● , ◆ , △) for Re > 2000, however, begin to diverge from theoretical values because the pipe's dimensionless entrance length (L_e/D) is not long enough to support fully developed flow. Measurements obtained in the 0.305-cm i.d. pipe (▼), with its much longer entrance length, exhibit better agreement.

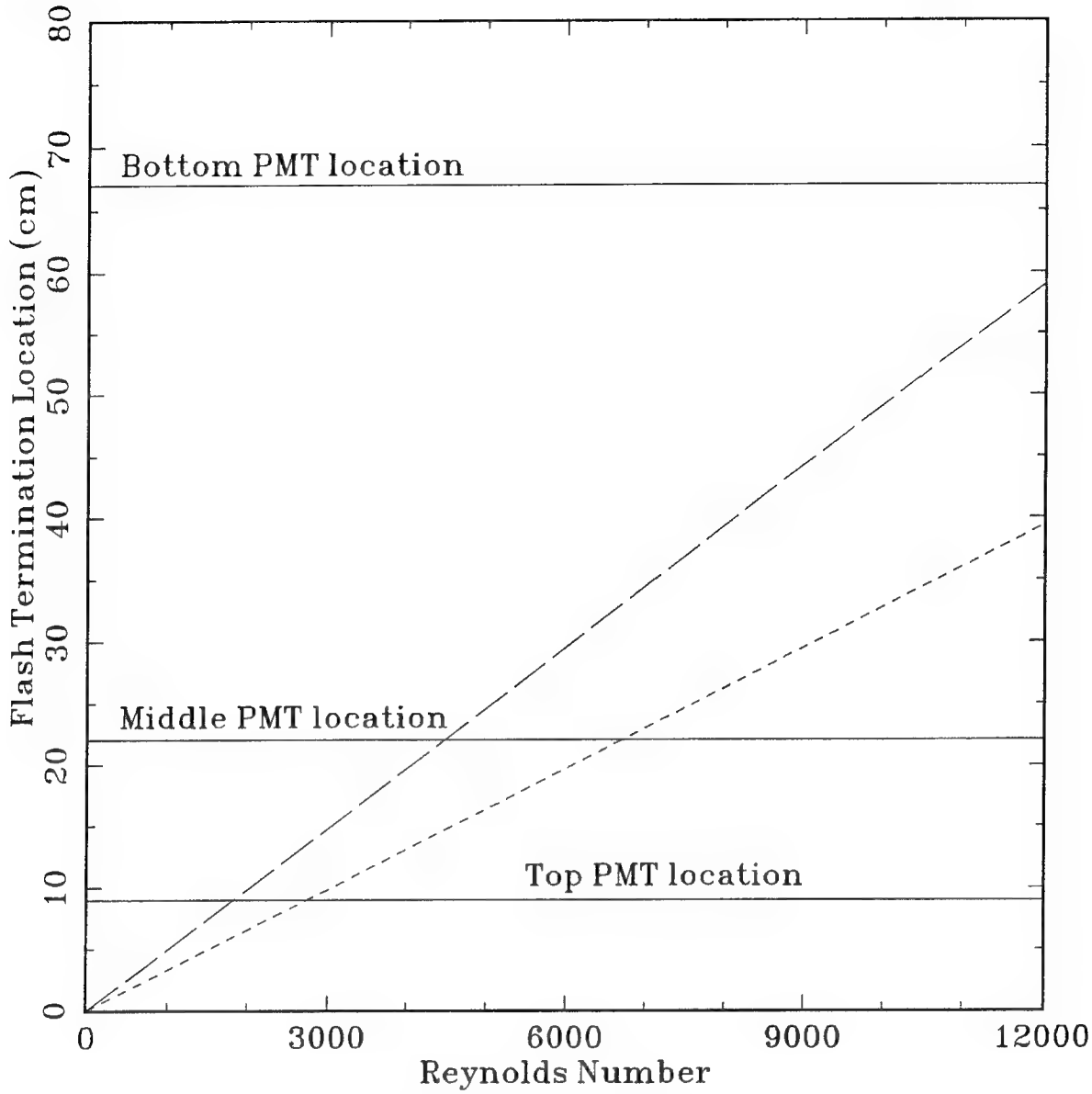

Figure 5. Downstream flash termination location of bioluminescent organisms stimulated at the pipe inlet as a function of Reynolds number. A response time of 100 ms is assumed, followed by flash durations of 100 ms (short dash) and 200 ms (long dash). PMT positions are indicated by solid lines. Pipe i.d. = 0.635 cm; 69°F ($\nu = 0.0104$ cm^2/sec)

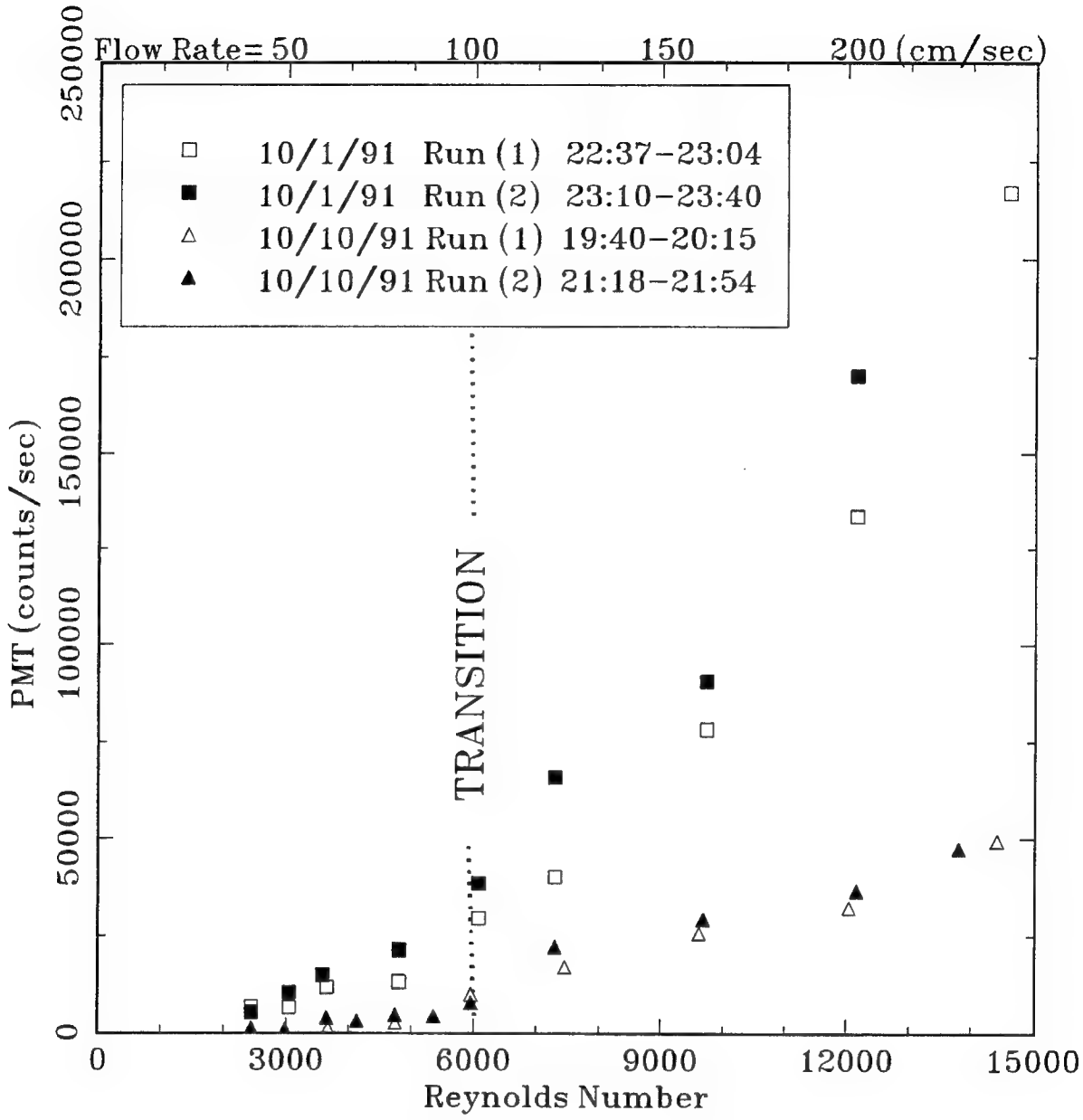

Figure 6a. Representative San Diego Bay PMT levels *vs* Reynolds number. The PMT is located 67 cm from the inlet of the 0.635-cm i.d. pipe. Each data point represents an average of 2.2-1 of seawater. Open symbols (Run 1; □ , △) refer to measurements taken from the bottom half of the 75-1 tank, where the flow sequence is monotonically decreasing. Solid symbols (Run 2; ■ , ▲) refer to measurements taken from the remaining half of the tank, where the flow sequence is monotonically increasing. Transition (dotted line) from laminar to turbulent flow occurs at $Re_{trans} \approx 6000$, where a change in the PMT *vs* Re dependence is evident.

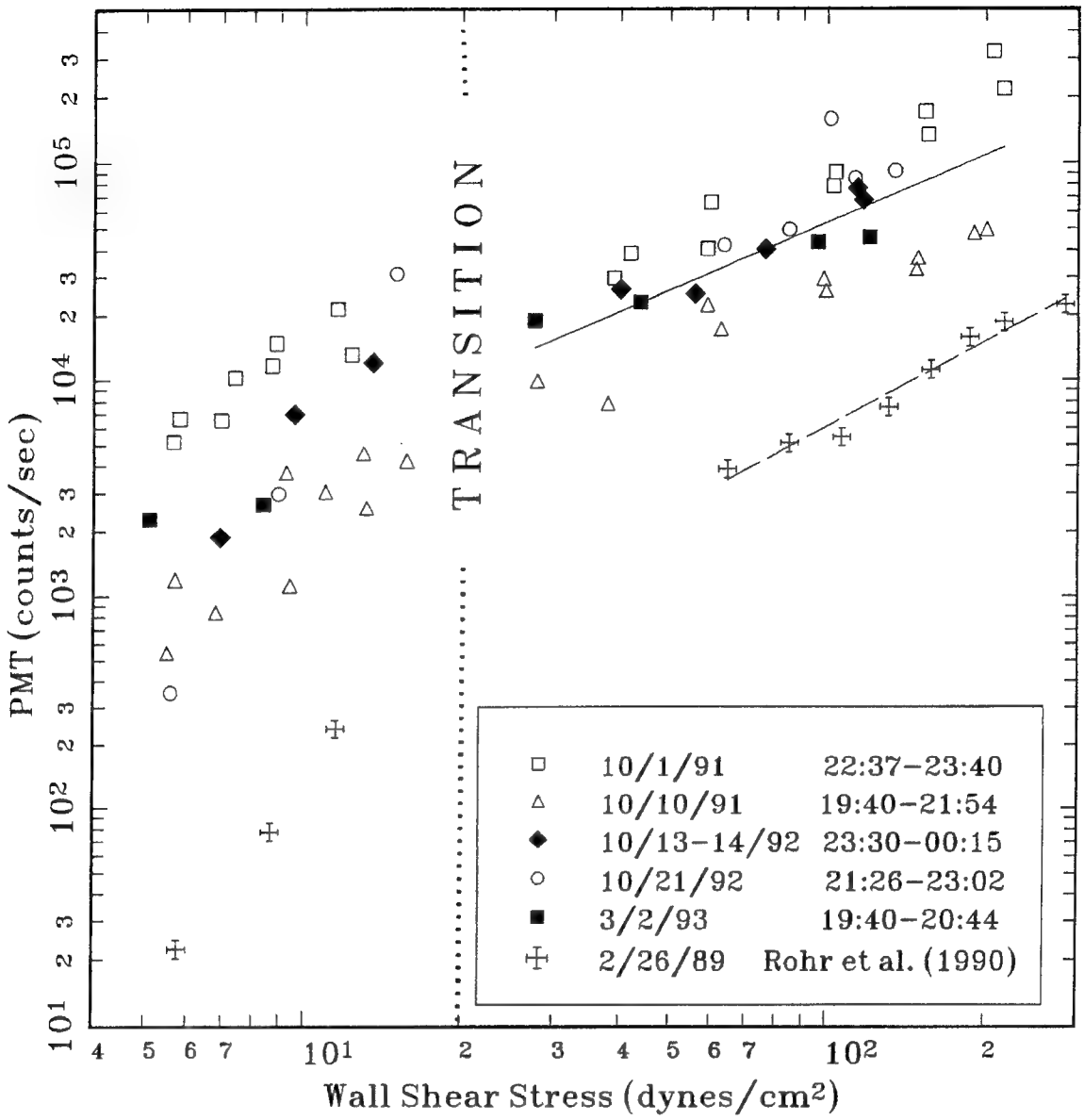

Figure 6b. PMT levels *vs* wall shear stress. San Diego Bay data, collected 67 cm from the 0.635-cm i.d. pipe inlet, are represented by symbols and composed both of 2.2-1 (□ , △ ; same PMT data as in figure 6a) and 100-s (◆ , ○ , ■) averages. Sea of Cortez data, collected 65 cm from the 0.635-cm i.d. pipe inlet, are represented by crosses and composed of 2.2-1 averages. Transition (dotted line) from laminar to turbulent flow, for all the experiments, occurs around a Reynolds number of 6000.

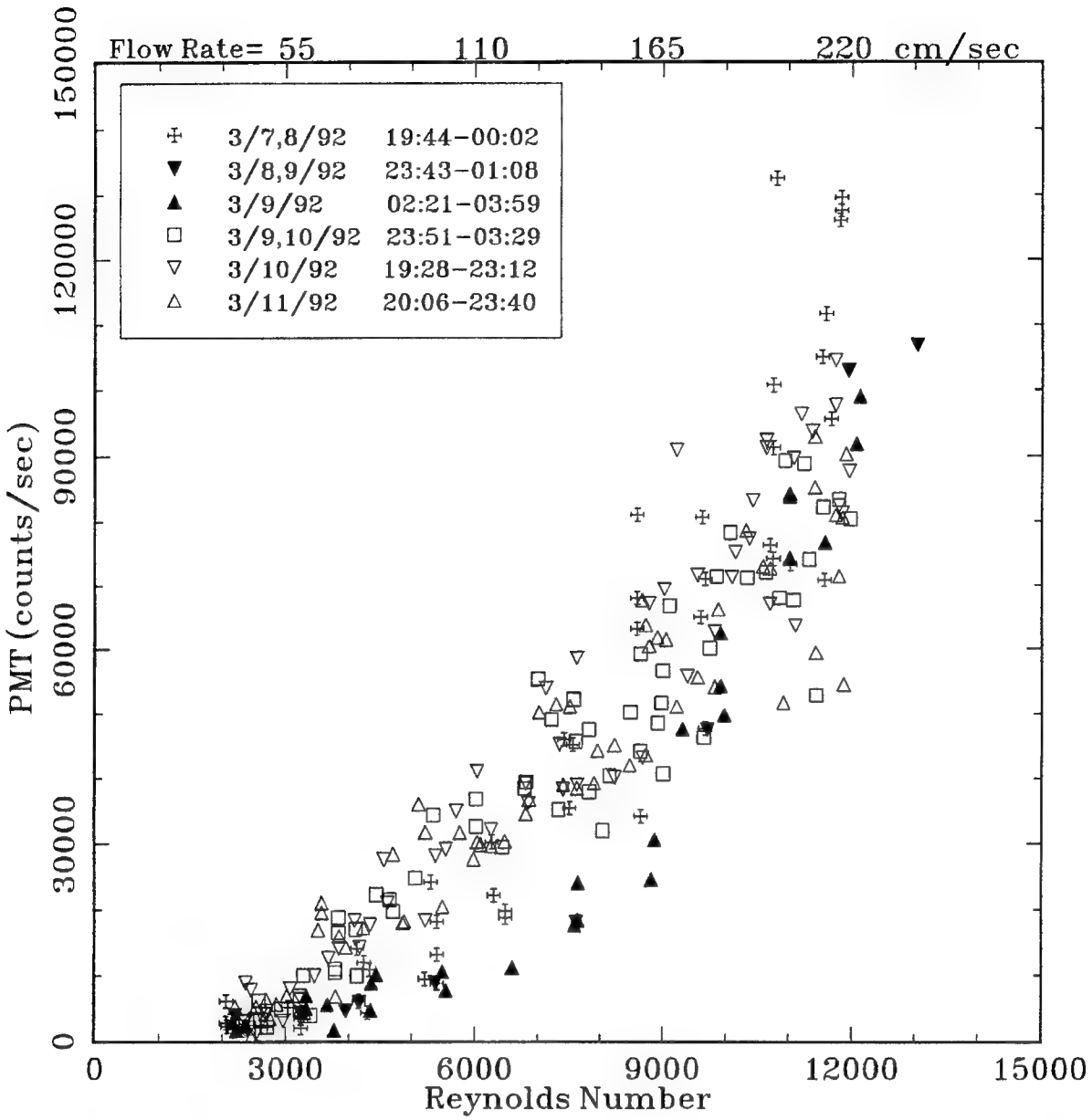

Figure 7a. Representative San Clemente Island PMT levels *vs* Reynolds number. Each data point represents a 100-s average of two PMTs, located 22 and 67 cm from the inlet of the 0.635-cm i.d. pipe. Transition from laminar to turbulent flow varies due to ship motion; for the open symbol data (□, △, ▽) $Re_{trans} \approx 3500$, for the cross symbol data $Re_{trans} \approx 5400$, and for the solid symbol data (▲, ▼) $Re_{trans} \approx 7600$. Note that the PMT levels for the high laminar flow Reynolds number data (▲, ▼) are conspicuously low.

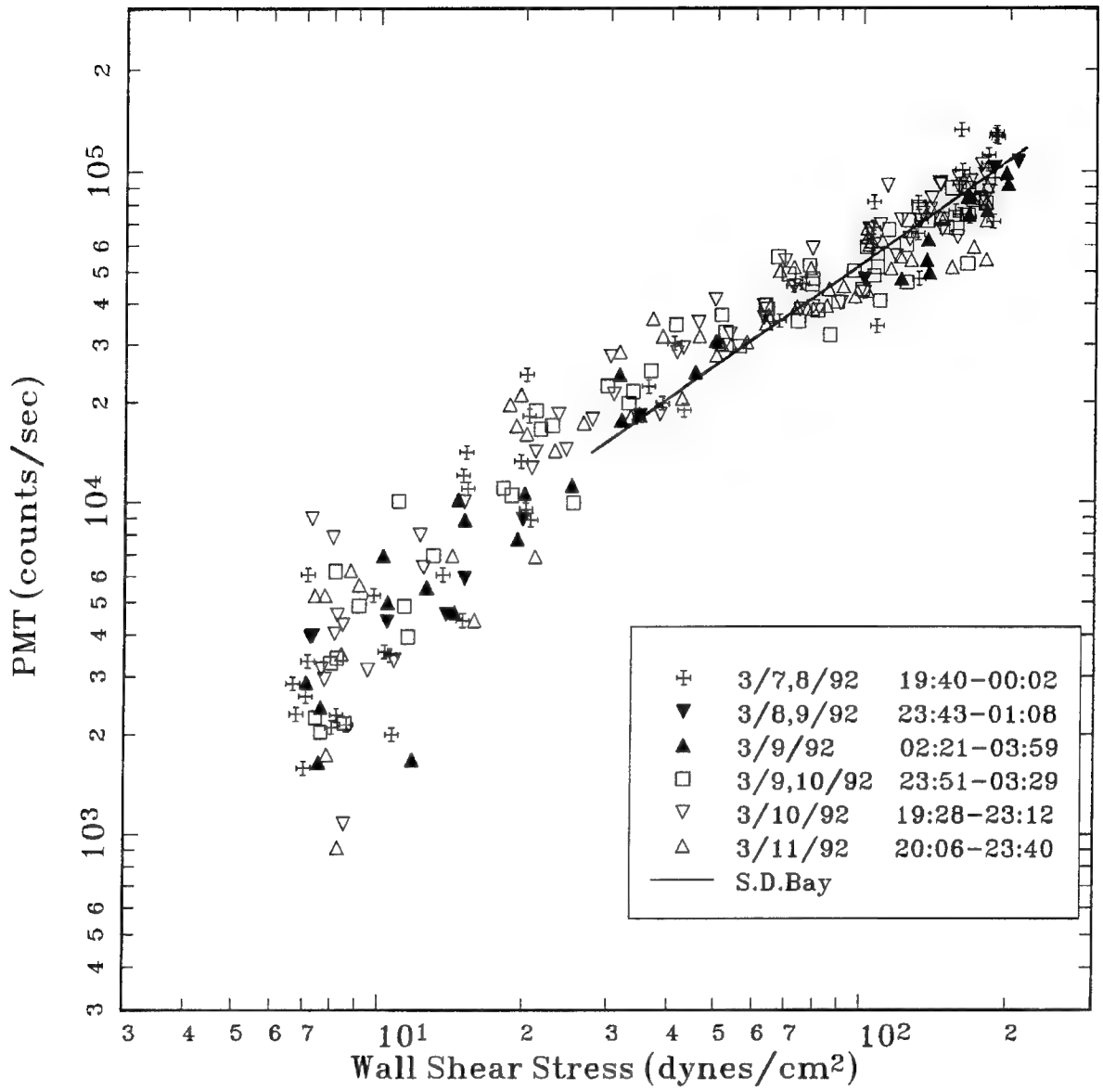

Figure 7b. PMT levels (same data as in figure 7a) *vs* wall shear stress. The solid line is taken from figure 6b and is representative of San Diego Bay data. The disparity in PMT levels between laminar and turbulent flow, evident in figure 7a when plotted as a function of Re, is no longer apparent.

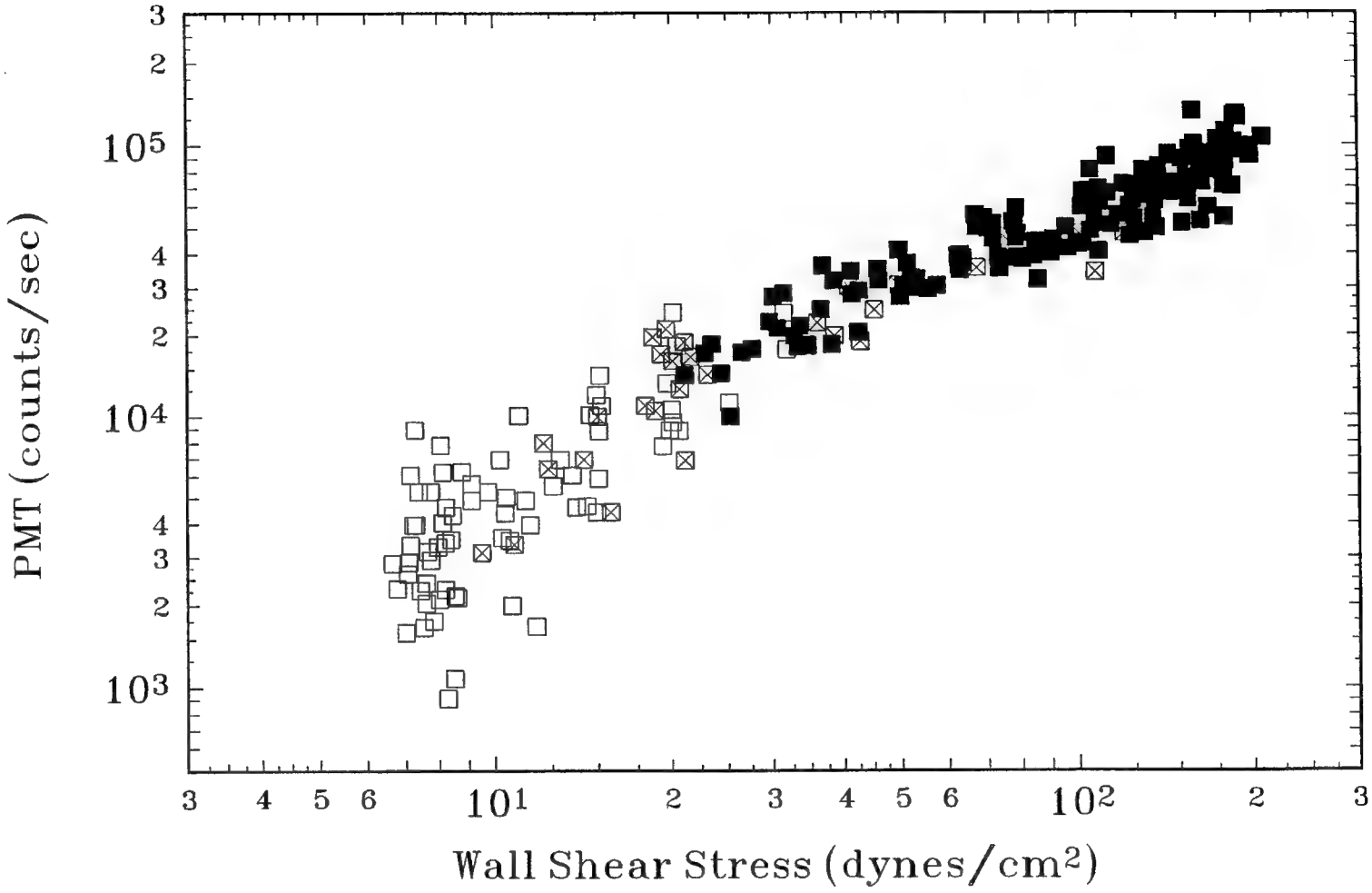

Figure 7c. PMT levels *vs* wall shear stress (same data as in figure 7b) with laminar (□), turbulent (■), and transitional (⊠) flow indicated.

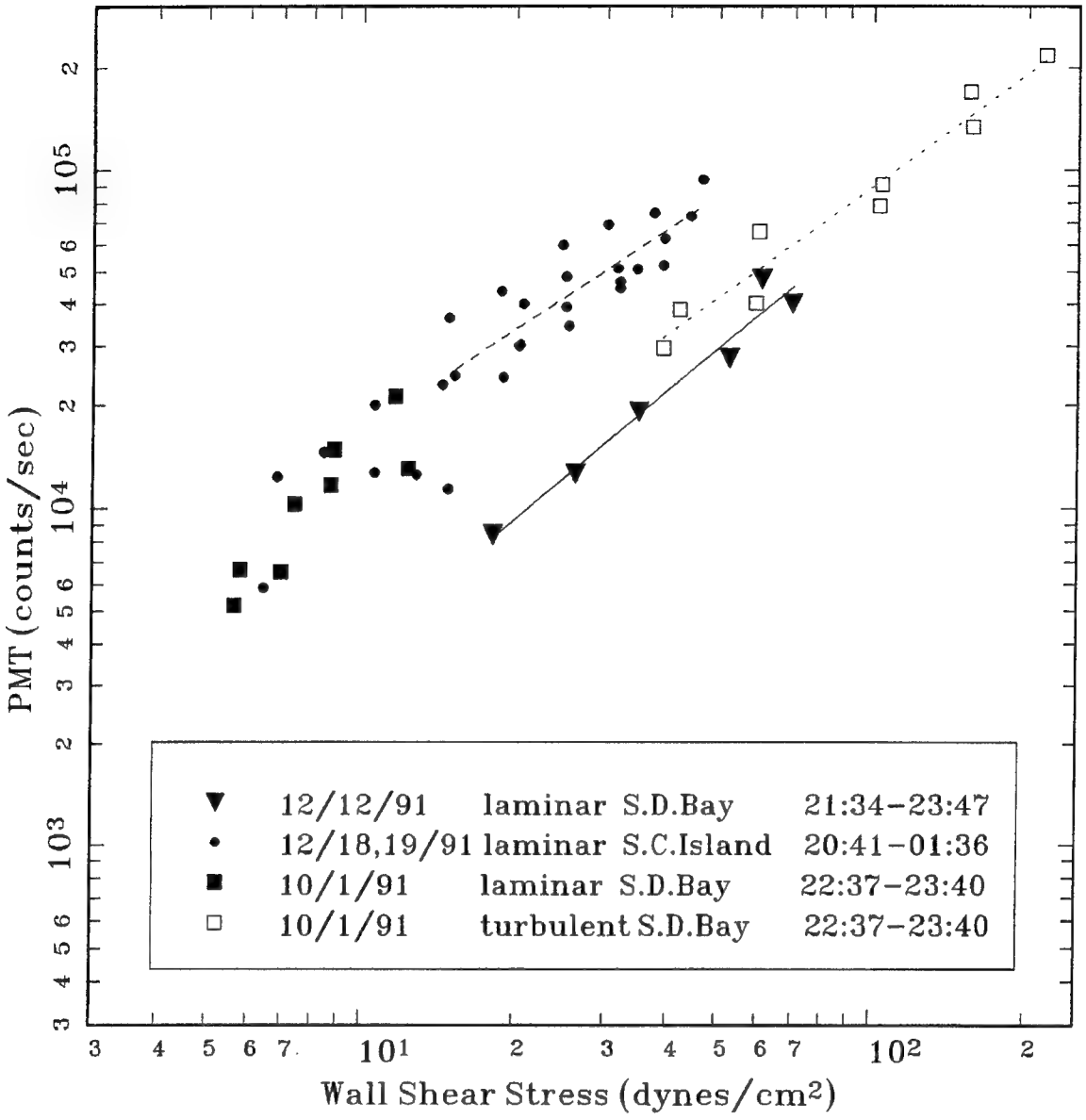

Figure 8. PMT levels vs wall shear stress (τ_{wall}) for the highest laminar pipe flow stimulus. Solid symbols designate laminar flow measurements taken in San Diego Bay with the 0.305-cm i.d. pipe (▼, 500-s averages, PMT is 106 cm downstream of inlet) and the 0.635-cm i.d. pipe (■, 2.2-1 averages, PMT is 67 cm downstream of inlet), and off San Clemente Island with the 0.635-cm i.d. pipe (●, 100-s averages, PMT 67 cm is downstream of inlet). Open symbols designate turbulent flow measurements taken in San Diego Bay with the 0.635-cm i.d. pipe (□, 2.2-1 averages, PMT is 67 cm downstream of inlet). Note that for $\tau_{wall} > 15$ dynes/cm^2, the PMT *vs* τ_{wall} dependence is similar (approximately linear) regardless of whether the flow is laminar or turbulent.

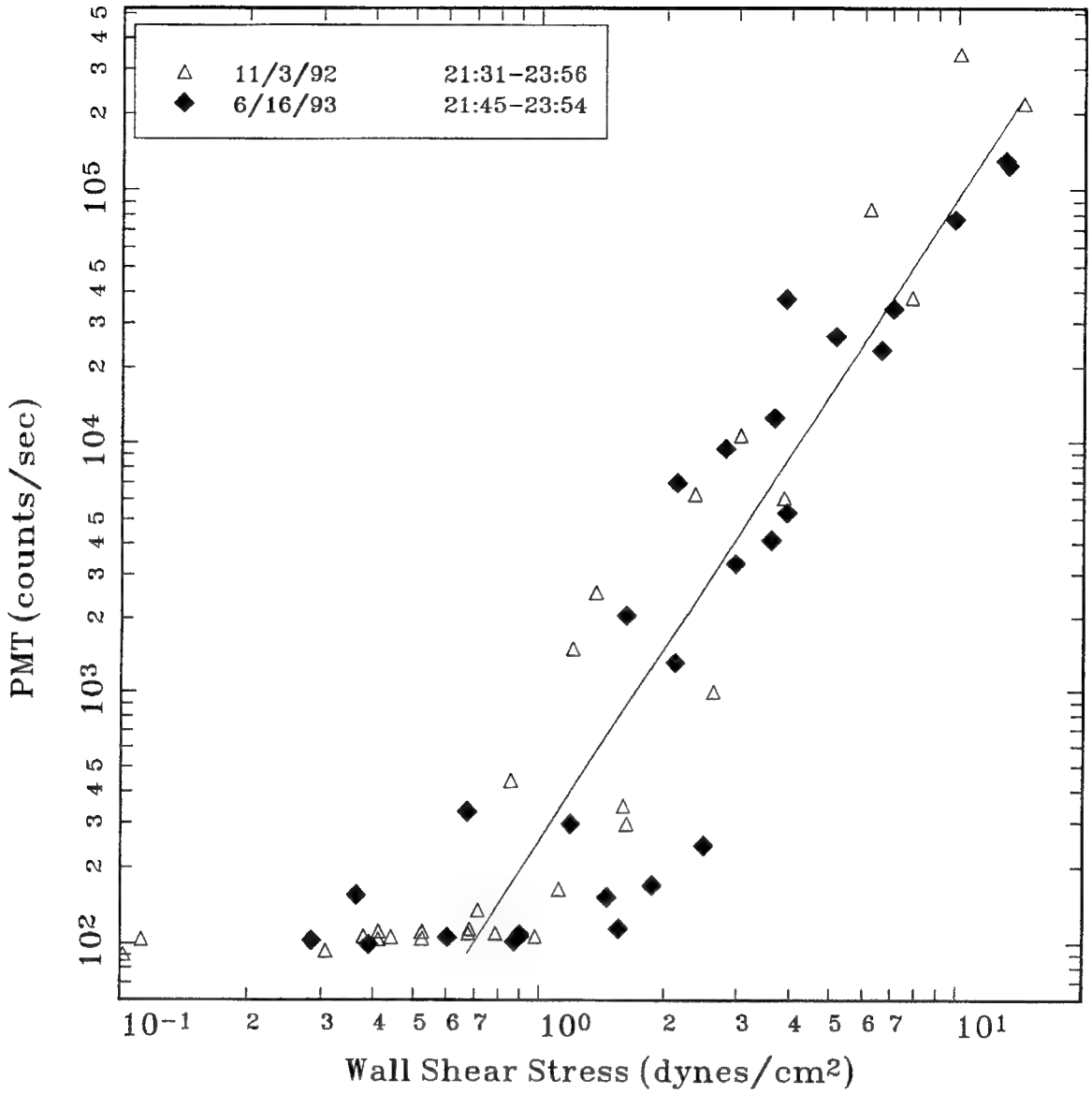

Figure 9. PMT levels (100-s averages) *vs* wall shear stress (τ_{wall}) for the lowest laminar pipe flow stimulus. San Diego Bay water is used in the 0.635-cm i.d. pipe-flow apparatus with the PMT positioned 67 cm from the inlet. The solid line represents a least squares power law regression to the data between 0.7 and 14.0 dynes/cm^2 and has a slope of 2.57. Threshold τ_{wall} values are seen to be around 1 dyne/cm^2.

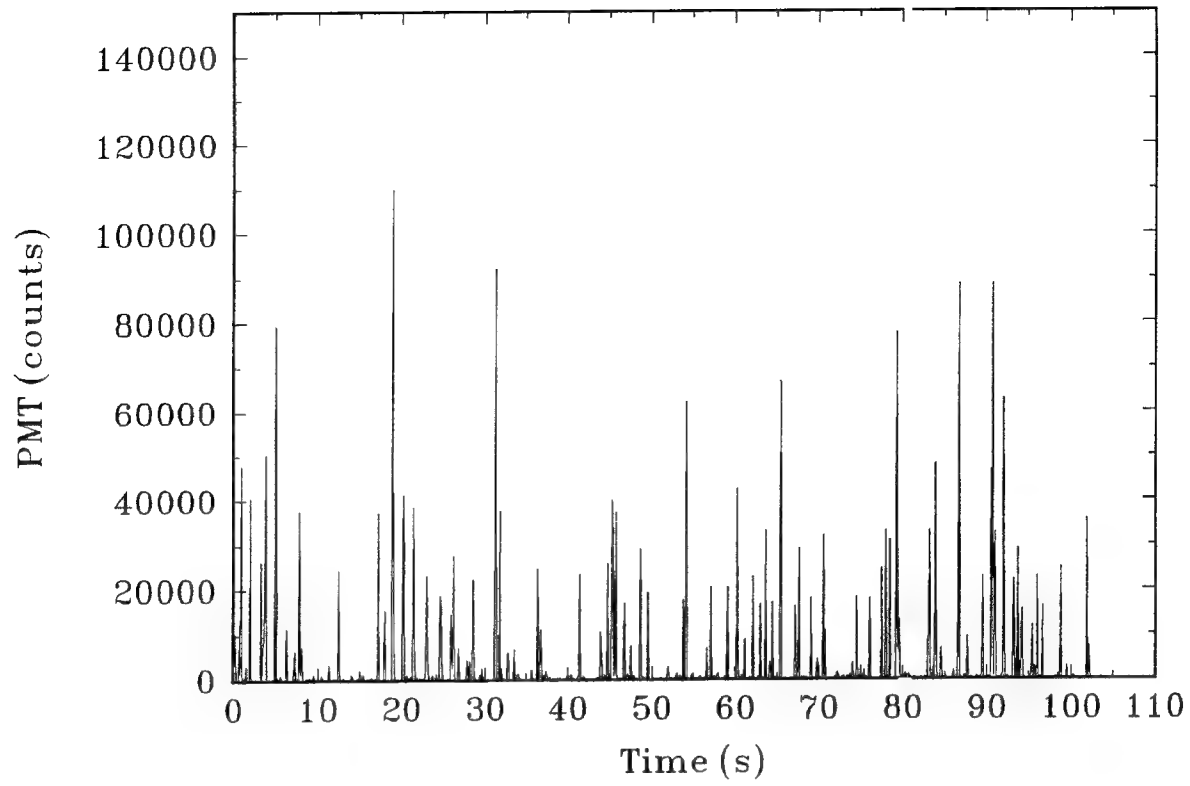

Figure 10a.

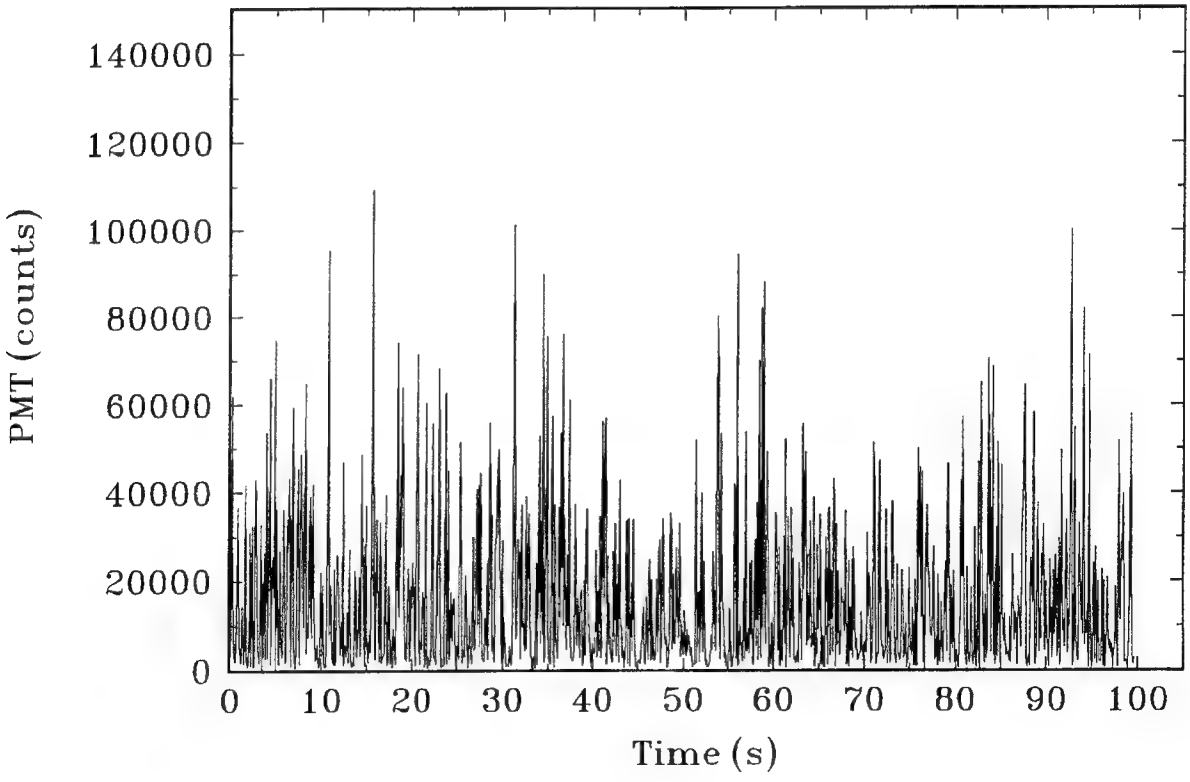

Figure 10b.

Figure 10. Sample laminar (a) and turbulent (b) PMT time series data (0.1-s bins). The PMT is located 67 cm from the inlet of the 0.635-cm i.d. pipe. Each vertical spike is believed to result from an individual bioluminescent flash. Corresponding wall shear stress values are 15 dynes/cm^2 (a) and 101 dynes/cm^2 (b). It is noteworthy that although the average bioluminescent level for (b) is nearly five times larger than (a), peak values remain about the same.

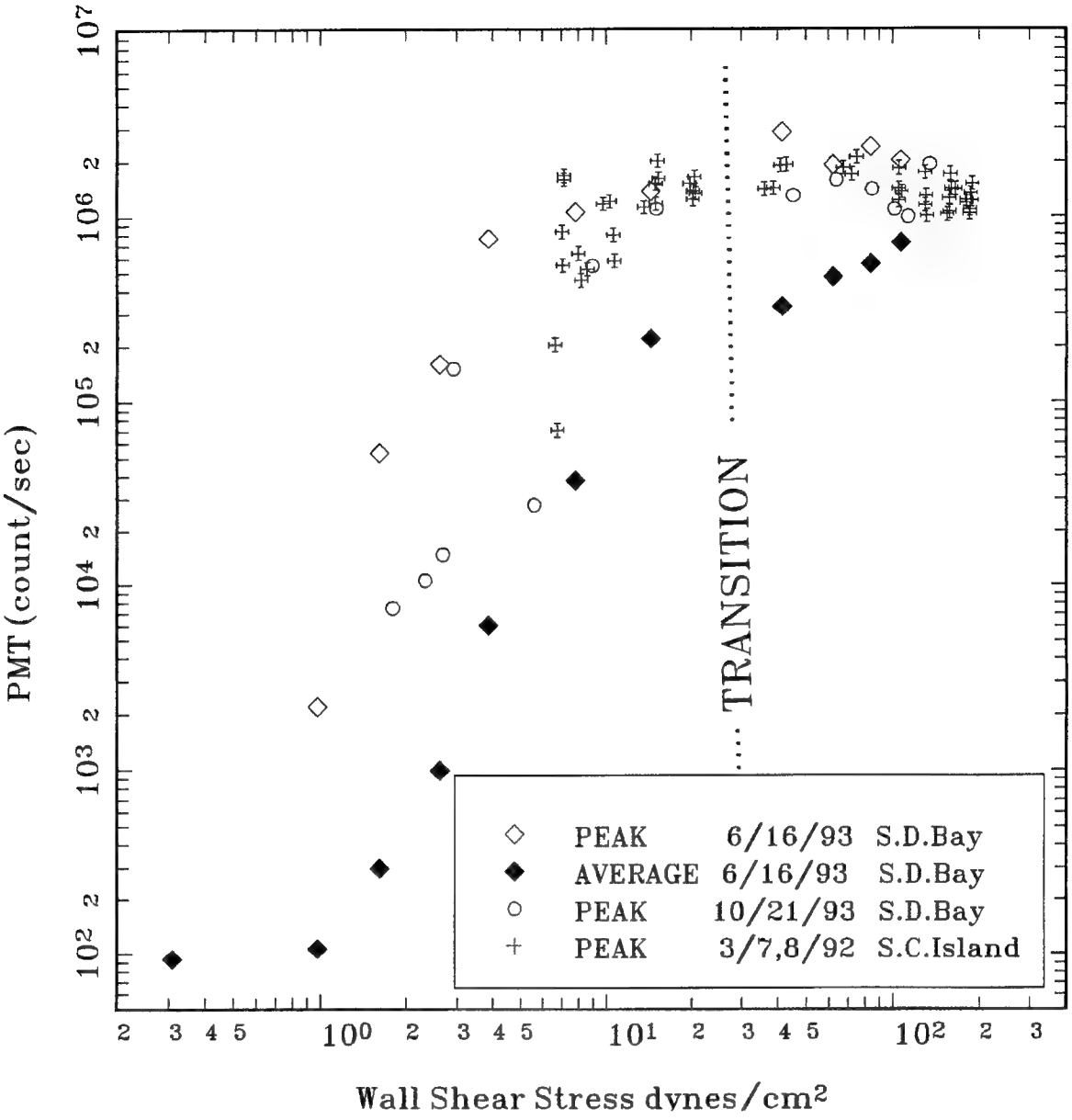

Figure 11. Average (100 s) *vs* peak (0.1 s) PMT levels as a function of wall shear stress (τ_{wall}). The PMT is located 67 cm from the inlet of the 0.635-cm i.d. pipe. Solid symbols (◆) designate average PMT levels recorded in San Diego Bay, open symbols (◇ , ○) designate peak PMT levels recorded in San Diego Bay, and cross symbols designate peak levels recorded off San Clemente Island. Note that the leveling off of peak PMT levels beginning at $\tau_{wall} \approx$ 10-20 dynes/cm^2, coincides with the reduced slope of the average PMT *vs* τ_{wall} data.

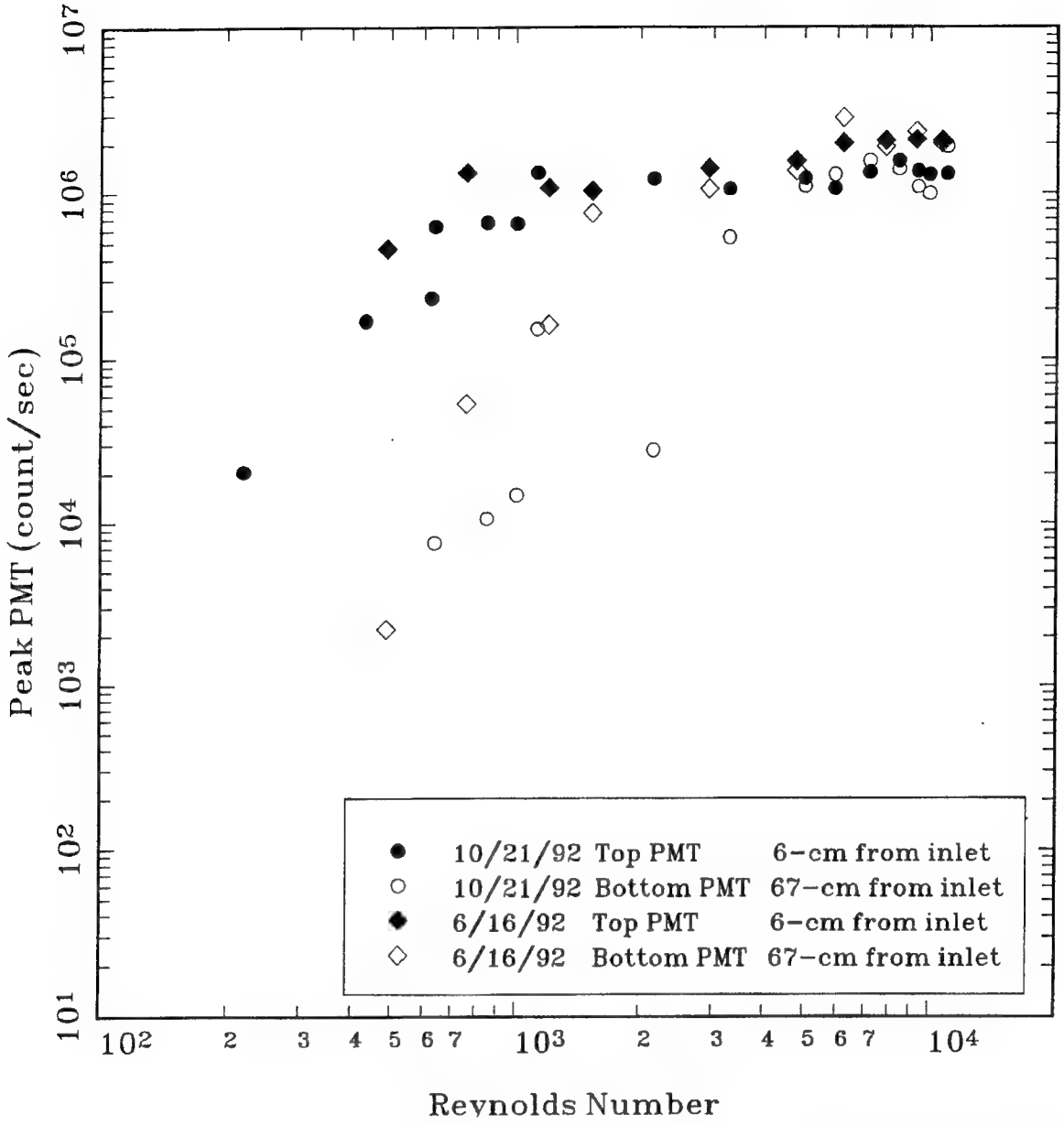

Figure 12. Comparison of peak (0.1 s average) PMT *vs* Reynolds number dependence for top (6 cm from inlet) and bottom (67 cm from inlet) PMT locations on the 0.635-cm i.d. pipe.

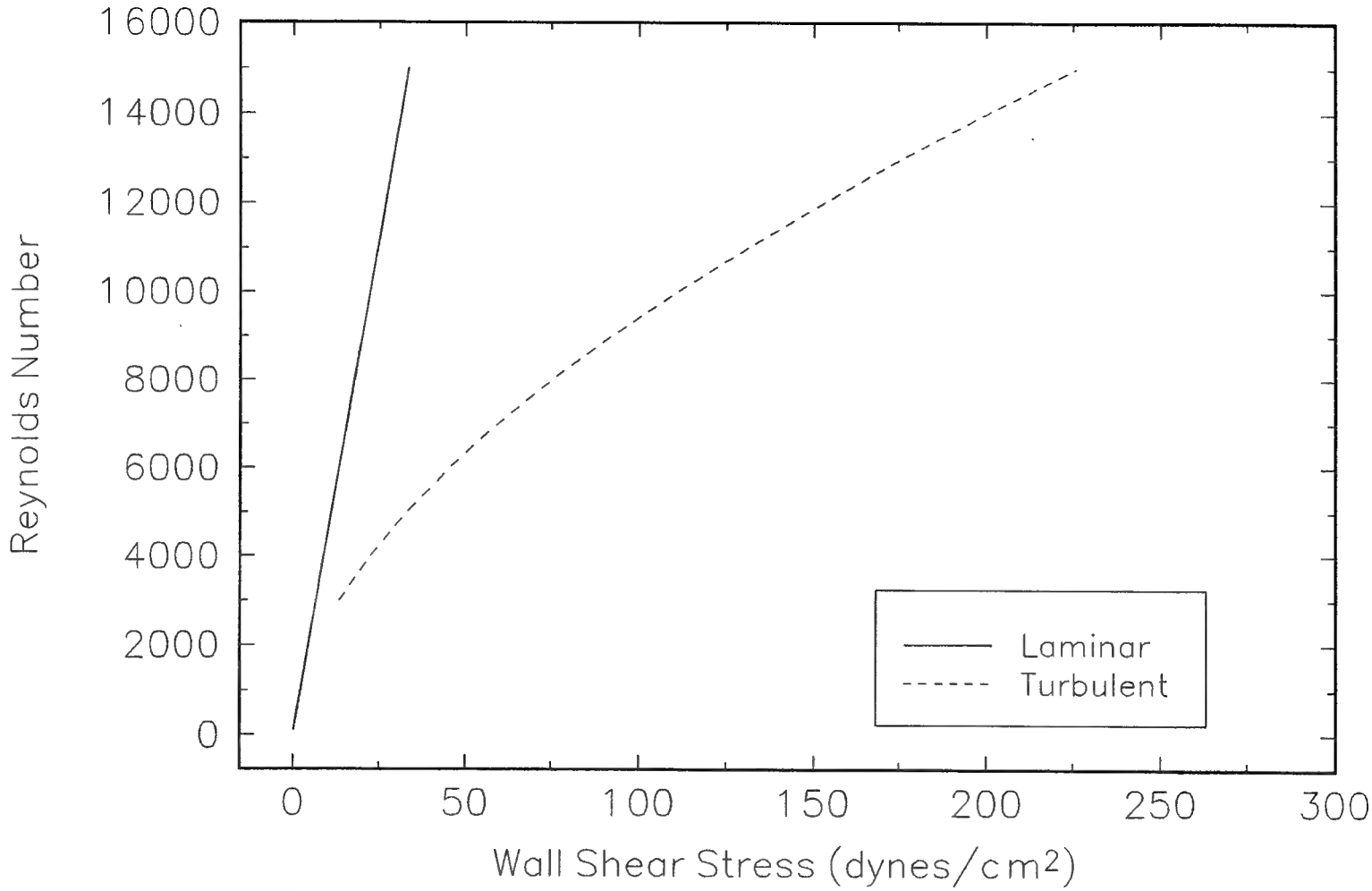

Figure 13. Reynolds number *vs* wall shear stress for fully developed laminar (solid line) and turbulent (dashed line) flow in a 0.635-cm i.d. pipe, with seawater at 20.6°C (U_{avg} = 0.0164 x Re).

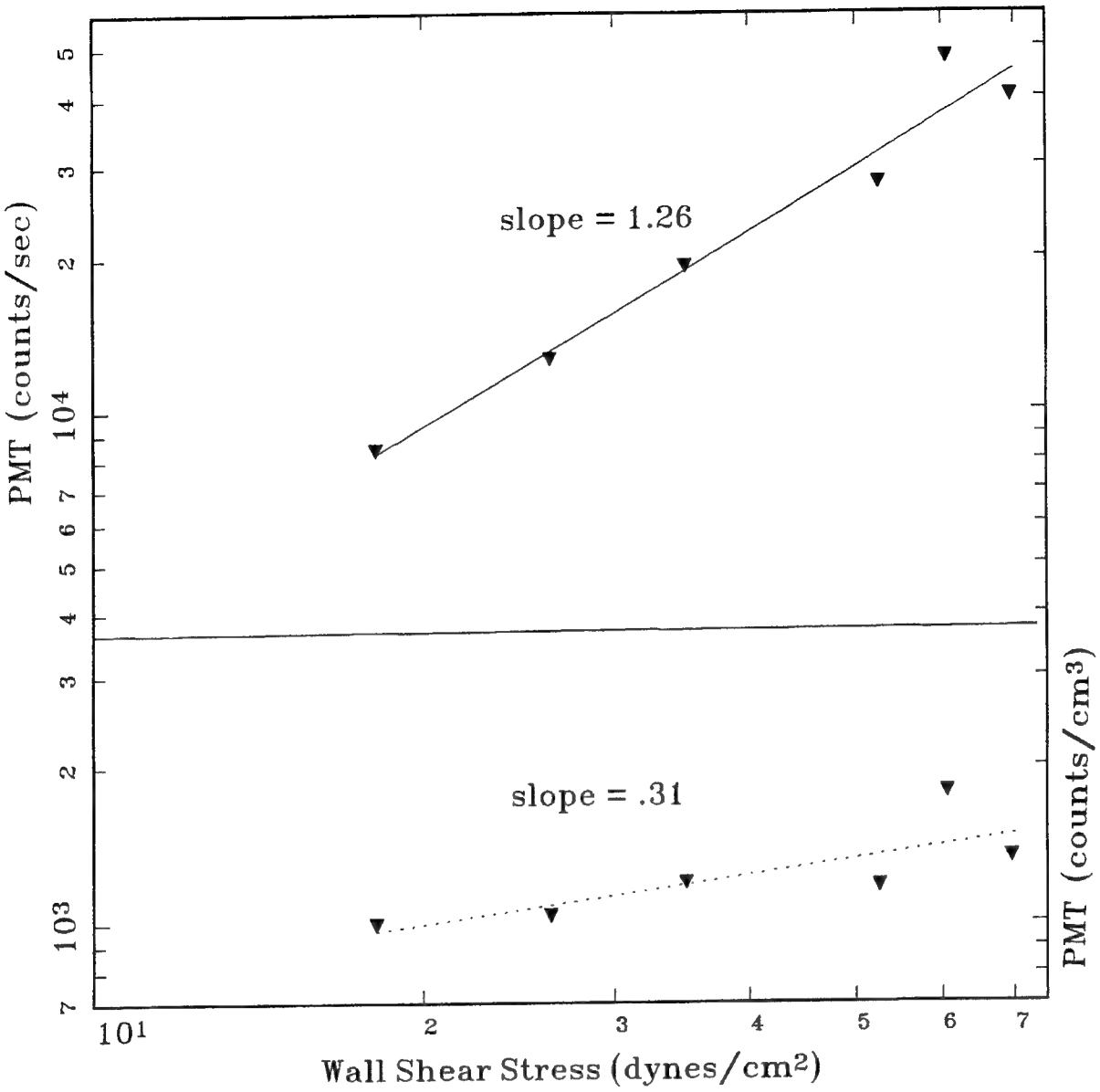

Figure 14a. Laminar flow data are from San Diego Bay.

Figure 14. Comparison of PMT levels expressed as counts per second (same data as in figure 8) and counts per volume as a function of wall shear stress. Laminar flow data are from San Diego Bay (14a) and off San Clemente Island (14b). Turbulent flow data are from San Diego Bay (14c).

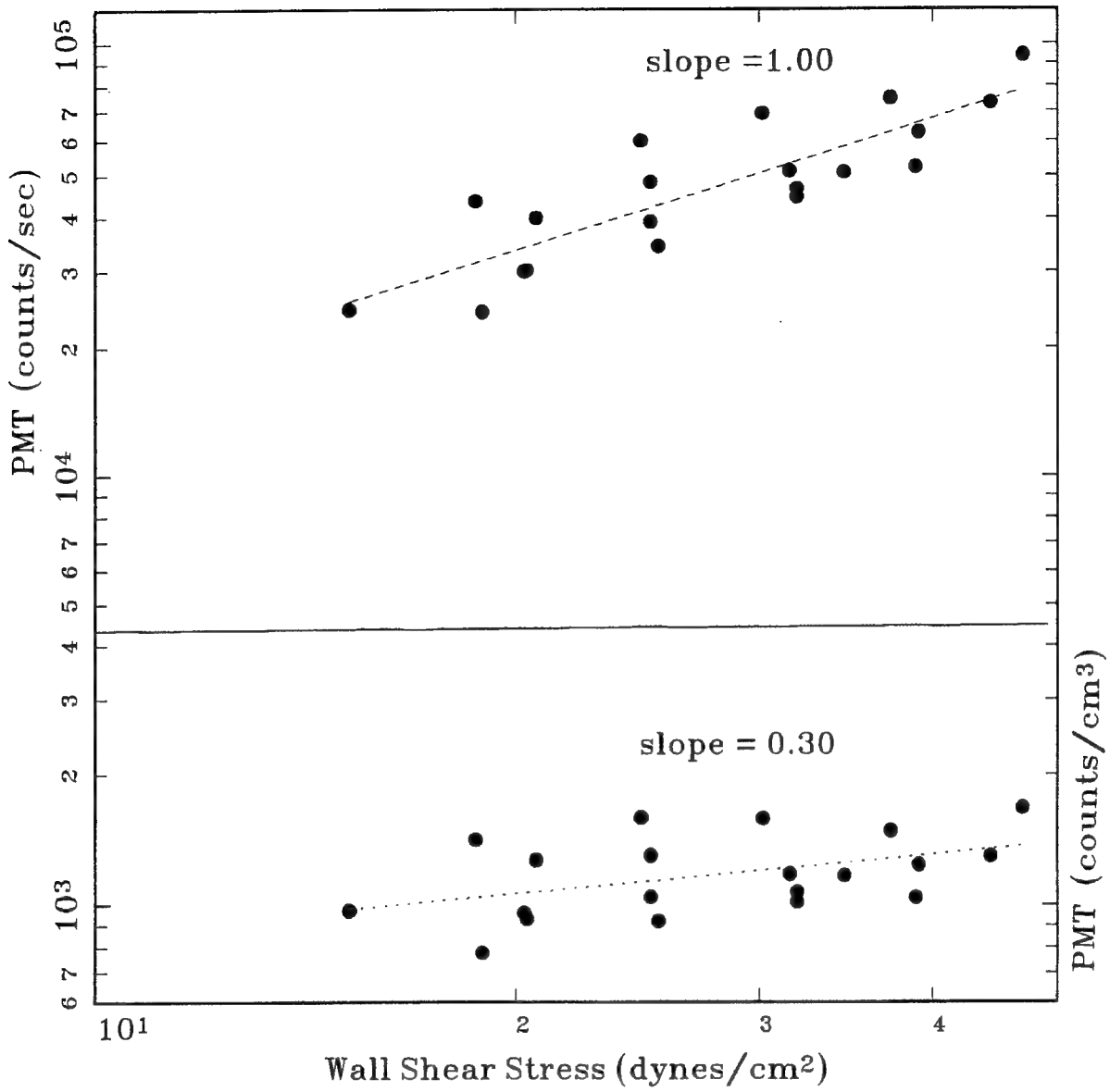

Figure 14b. Laminar flow data off San Clemente Island.

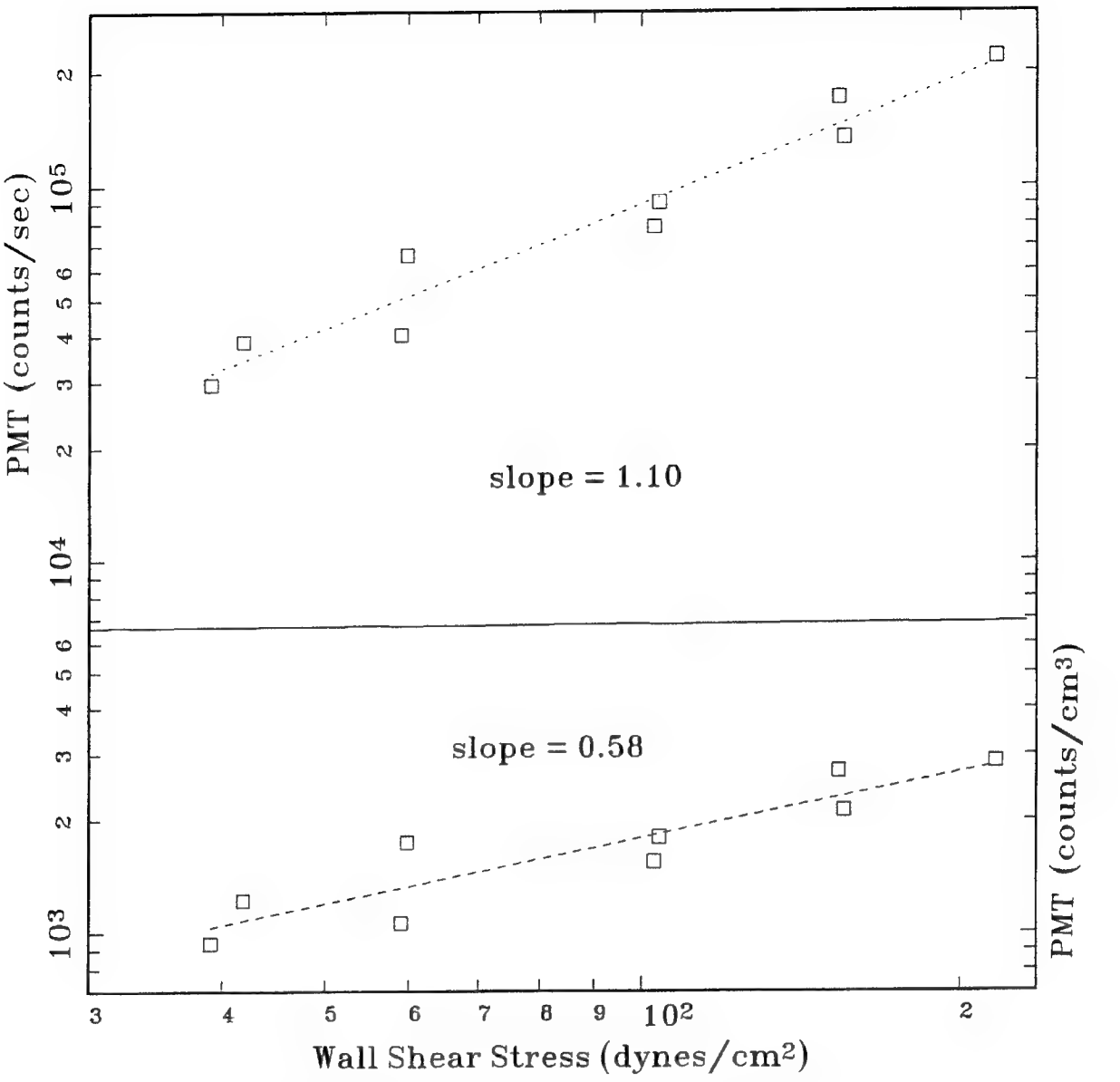

Figure 14c. Turbulent flow data are from San Diego Bay.

REFERENCES

Anderson, D.M., D.M. Nosenchuck, G.T. Reynolds, and A.J. Walton. 1988. "Mechanical stimulation of bioluminescence in dinoflagellate *Gonyaulaux polyedra stein*," *J. Exp. Mar. Biol. Ecol.*, 122:277–288.

Bakhmeteff, B., 1936. *The mechanics of turbulent flow.* p. 4, Princeton University Press, Princeton, New Jersey.

Biggley, W.H., E. Swift, R.J. Buchanan, and H.H. Seliger. 1969. "Stimulable and spontaneous bioluminescence in marine dinoflagellates, *Pyrodinium bahamenese, Gonyaulax polyedra, and Pyrocystis lunula*," *J. Gen. Physiol.*, 54:96–123.

Bird, R.B., W.E. Stewart, and E.N. Lightfoot. 1960. *Transport Phenomenon*, p. 59 John Wiley and Sons, New York.

Blasius, H., 1913. Das Ahnlichkeitsgesetz bei Reibungsvorgangen in Flussigkeiten. Forschg. Arb.Ing.–Wes. No. 134, Berlin.

Burkenroad, M.D. 1943. "A possible function of bioluminescence," *J. Mar. Res.*, 5:161–164.

Buskey, E.J., L. Mills, and E. Swift. 1983. "The effects of dinoflagellate luminescence on the swimming behavior of a marine copepod," *Limnol. Oceanogr.*, 28:575–579.

Buskey, E.J., and E. Swift. 1985. "Behavioral responses of oceanic zooplankton to simulated bioluminescence," *Biol. Bull.*, 168:263–275.

Buskey, E.J., C.G. Mann, and E. Swift. 1987. "Photophobic responses of calanoid copepods: possible adaptive value," *J. Plankton Res.*, 9: (5), 657–870.

Cajori, F. 1946. *Sir Isaac Newton's Mathematical Principles*. Berkeley.

Childress, S. 1981. *Mechanics of swimming and flying*. p. 5, Cambridge University Press, Cambridge, England.

Christianson, R., and B.M. Sweeney. 1972. "Sensitivity to stimulation, a component of the circadian rhythm in luminescence in *Gonyaulaux*," *Plant Physiol.*, 49:994–997.

Davies, J.T. 1972. *Turbulence Phenomenon*. p. 54, Academic Press, London, England.

Eckert, R., 1966. "Excitation and luminescence in *Noctiluca miliaris*." In *Bioluminescence in Progress.* pp. 269–300, F. Johnson and Y. Haneda, Eds.

Eckert, R., and T. Sibaoka. 1968. "The flash-triggering action potential of the luminescent dinoflagellate *Noctiluca*," *J. Gen. Physiol.*, 52:258–282.

Esias, W.E., and H.C. Curl, Jr. 1972. "Effect of dinoflagellate bioluminescence on copepod ingestion rates," *Limnol. Oceanogr.*, 17:901–906.

Evans, D.L. 1982. "Observations of small-scale shear and density structure in the ocean," *Deep-Sea Res.*, 29:581–595.

Hagen, G.H.L. 1839. "On the motion of water in narrow cylindrical tubes," (German) Pogg. Ann., 46:423–440.

Hamman, J.P., and H.H. Seliger. 1972. "The mechanical triggering of bioluminescence in marine dinoflagellates: chemical basis," *J. Cell. Physiol.*, 80:397–408.

Harvey, E.N. 1929. "Phosphorescence," *Encycl. Brittanica*, p. 780, 14th ed. 17.

Hastings, J.W., and B.M. Sweeney. 1956. "The luminescent reaction in extracts of the marine dinoflagellate, *Gonyaulax polyedra*," *J. Cellular Comp. Physiol.* 49:209–226.

Hill, A.V. 1950. "The dimensions of animals and their muscular dynamics," *Science Progress*, 38: 209–230.

Holmes, R.W., P.M. Williams, and R.W. Eppley. 1967. "Red Water in La Jolla Bay," 1964–1966. *Limnol. Oceanogr.*, 12:503–512.

Jayesh and Z. Warhaft. 1992. "Probability distribution, conditional dissipation, and transport of passive temperature fluctuations in grid-generated turbulence," *Phys. Fluids A*, 4:(10).

Kamykowski, D., R.E. Reed, and G.J. Kirkpatrick. 1992. "Comparison of sinking velocity, swimming velocity, rotation and path characteristics among six marine dinoflagellate species," *Mar. Biol.*, 113:319–328.

Kessler, J.O. 1985. "Co–operative and concentrative phenomena of swimming microorganisms," *Contemp. Phys.*, 26:2, 147–166.

Kimor, B. 1983. "Seasonal and bathymetric distribution of thecate and nonthecate dinoflagellates off La Jolla, California," CalCOFI Rep., Vol. XXII.

Koehl, M.A.R., and J.R. Strickler. 1981. "Copepod feeding current: Food capture at low Reynolds numbers," *Limnol. Oceanogr.*, 26:(6), 1062–1073.

Krasnow, R., J. Dunlap, W. Taylor, J.W. Hastings, W. Vetterling, and E. Hass. 1981. "Measurements of *Gonyaulax* bioluminescence, including that of individual cells." In *Bioluminescence: Current Perspectives,* pp. 52–63, K. Nealson, Ed.

Latz, M.I., J.F. Case, and R.L. Gran. 1994. "Excitation of bioluminescence by laminar shear associated with simple Couette flow," *Limnol. Oceanogr.,* 39(6), 1994, 1424–1439.

Laufer, J. 1954. "The structure of turbulence in fully developed pipe flow," Natl. Advisory Comm. Aeronaut. Tech. Repts. No. 1174.

Losee, J., and D. Lapota, 1981. "Bioluminescence measurements in the Atlantic and Pacific." In *Bioluminescence: Current Perspectives,* pp. 143–152, K. Nealson, Ed.

Losee, J., D. Lapota, and S.H. Lieberman. 1985. "Bioluminescence: a new tool for oceanography." In *Mapping strategies in chemical oceanography, Amer. Che. Soc.,* pp. 211–234, A. Zirino, Ed.

Lythgoe, J.N. 1979. *The ecology of vision.* p. 344, Clarendon Press, Oxford.

Morin, J.G. 1983. "Coastal bioluminescence: patterns and functions," *Bulletin of Marine Science*, 33:(4), 787–817.

Morita, M., and R. Johnson. 1974. "Field induced luminescence," TRW Report AT–SVD–TR–74–5.

New Scientist (1990). "Miniscule eddies make plankton grow in the dark," p. 35, 10 March 1990.

Newman, J.N., and T.Y. Wu. 1975. "Hydromechanical aspects of fish swimming." In *Swimming and flying in nature,* pp. 615–634, vol. 2, Wu et al., Ed.

Nicol, J.A.C. 1978. "Bioluminescence and vision." In *Bioluminescence in action,* pp. 367–398, P.J. Herring, Ed.

Patel, V.C., and M.R. Head. 1969. "Some observations on skin friction and velocity profiles in fully developed profiles in fully developed pipe and channel flows," *J. Fluid Mech.* 38:(part 1), 181–201.

Pfenninger, W. 1961. In *Boundary layer and flow control.* 2 vols. G. V. Lachmann, Ed. Pergamon, Oxford.

Poiseuille, J.L. 1840. Recherches experimentales sur le movement des liquides dans les tuyaux de tres petits diametres. Comptes Rendus 11:961–967 and 1041–1048.

Prandtl, L., and O.G. Tietjens, 1934. *Applied hydro- and aeromechanics.* Dover Publications Inc., p. 33, New York, NY.

Reynolds, O. 1883. "An experimental investigation of the circumstances which determine whether the motion of water will be direct or sinuous, and the law of resistance in parallel channels," *Philosophic Transactions of the Royal Society of London*, 174:935–982.

Ridgeway, S.H., and D.H. Carder. 1993. "Features of dolphin skin with potential hydrodynamic importance," *IEEE Engineering in Medicine and Biology*, Sept., pp. 83–88.

Rizk, M.A. and S. E. Elghobashi. 1984. "The motion of a spherical particle suspended in a turbulent flow near a plane wall," *Phys. Fluids* 28:(3) 806–817.

Rohr, J., J. Losee, and J. Hoyt. 1990. "Stimulation of bioluminescence by turbulent pipe flow," *Deep Sea Research,* 37:(10) 1639–1646.

Rouse, H., and S. Ince. 1957. *History of hydraulics.* Iowa Institute of Hydraulic Research, State University of Iowa, p. 161.

Rouse, H. 1938. "Fluid mechanics for hydraulic engineers," pp. 171–172. Dover Publications, Inc. New York.

Schlichting, H. 1979. *Boundary-layer theory,* p. 599, 7th ed., McGraw–Hill Inc., NY.

Schonberg, J. A., and E. J. Hinch. 1989. "Inertial migration of a sphere in Poiseuille flow," *J. Fluid Mech.* 203:517–524.

Segre, G., and A. Silberberg. 1962. "Behavior of macroscopic rigid spheres in Poiseuille flow: Part 1. Determination of local concentration by statistical analysis of particle passage through crossed light beams," *J. Fluid Mech.* 13:115–135.

Seliger, H.H., W.H. Biggley, and E. Swift. 1969. "Absolute values of photon emission from the marine dinoflagellates *Pyrodinium Bahamanese, Gonyaulax Polyedra and Pyrocistus Lunula*," *Photochemistry and Photobiology*, 10:227–232.

Seliger, H.H., W.G. Fastie, and W.D. McElroy. 1969. "Towable photometer for rapid area mapping of concentrations of bioluminescent marine dinoflagellates," *Limnol. Oceanogr.*, 14:(5) 806–813.

Seliger, H.H., J.H. Carpenter, M. Loftus, and W.D. McElroy. 1970. "Mechanisms for the accumulation of high concentrations of dinoflagellates," *Limnol. Oceanogr.*, 15:234–245.

Stevens, G.A. 1950. "Swimming of dolphins," *Science Progress*, 38:524–525.

Sweeney, B.M. 1963. "Bioluminescent Dinoflagellates," *Biol. Bull.*, 125:177–181.

Tennekes, H., and J.L. Lumley. 1972. *A first course in turbulence,* p. 19, MIT Press, Cambridge, MA.

Thomas, W.H., and C.H. Gibson. 1990. "Quantified small-scale turbulence inhibits a red tide dinoflagellate, *Gonyaulax polyedra* Stein," *Deep-Sea Research*, 37:1583–1593.

Thomas, W.H., and C.H. Gibson. 1992. "Effects of quantified small-scale turbulence on the dinoflagellate, *Gymnodinium sanguineum (splendens)*: contrasts with *Gonyaulax (Lingulodinium) polyedra*, and fishery implication," *Deep-Sea Research*, 39:(7/8)1429–1437.

Thompson, D. 1971. *On growth and form*, p. 32, Cambridge University Press, Cambridge.

Van Atta, C.W., and W.Y. Chen. 1968. "Correlation measurements in grid turbulence using digital harmonic analysis," *J. Fluid Mech.*, 34:(3)497–515.

Van Dyke, M. 1982. *An album of fluid motion,* p. 61. The Parabolic Press, Stanford, California.

Vogel, S. 1981. *Life in moving fluids*, p. 67. Willard Grant Press, Boston Massachusetts.

Wells, M.R., and D.E. Stock. 1983. "The effects of crossing trajectories on the dispersion of particles in a turbulent flow," *J. Fluid Mech.* 136:31–62.

White, F.M. 1974. *Viscous fluid flow,* p. 206. McGraw–Hill, Inc. New York, NY.

White, F.M. 1979. *Fluid mechanics*, p. 312. McGraw–Hill, Inc. New York, NY.

White, H.H. 1979. "Effects of dinoflagellate bioluminescence on the ingestion rates of herbivorous zooplankton," *J. Exp. Mar. Biol. Ecol.*, 36:217–224.

Widder, E.A., J.F. Case, S.A. Bernstein, S. MacIntyre, M.R. Lowenstine, M.R. Bowlby, and D.P. Cook. 1993. "A new large volume bioluminescence bathyphotometer with defined turbulence excitation," *Deep-Sea Research*, 40:607–627.

Wood, F.G. 1973. *Marine mammals and man*, p. 89, R.B. Luce Inc., New York.

Young, J. B., and T. J. Hanratty. 1991. "Optical studies on the turbulent motion of solid particles in a pipe flow," *J. Fluid Mech.*, 231:665–688.

APPENDIX 1: VIDEO CALIBRATION AND LIGHT ESTIMATES FOR PROJECT BONS (Bioluminescence for Ocean Night Surveillance)

1.1 INTRODUCTION

NRaD, Code 524, and the Naval Oceanographic Office (NAVOCEANO), Code N3212, have been involved in bioluminescence measurements in many areas of the Northern Hemisphere (references 3–17). This work shows that night bioluminescence is omnipresent in the marine environment, and most intense in near shore regions and in the upper mixed layer of the ocean (upper 20–50 meters) (references 3, 4, 6, 7, 9, 12–17). Luminous plankton are known to be easily stimulated (references 1, 6, 8, 10) and stimulated bioluminescence from swell and/or current-induced flow has been observed around submerged objects (references 6, 18–21).[1] An ISIT video camera was used successfully to image bioluminescence generated from submerged objects at night during tests at sea (reference 2).[2] Four at-sea operations have been completed and video pictures of stimulated bioluminescence around objects were obtained. This appendix presents the procedure leading to the calibration curves which allow *in situ* bioluminescence levels to be estimated. As an example, a bioluminescence image of a sphere taken from the cruise of February/March 1989 in the Gulf of California is analyzed.

Methods

A Cohu Inc., ISIT camera, model #5162–2000/0000 and serial #144104, and a Hamamatsu video analyzer, model #DVS–3000 and serial #88020041, were obtained as part of NRaD Code 524 capital equipment. The camera has both automatic and manual controls for both the video gain and intensifier high voltage. The video gain and high voltage settings were digitally read so camera settings can be reproduced to allow for calibration. The video and intensifier gains were manual and set at: video +0.02 V and HV +0.04 V. The DVS–3000 video analyzer brightness was set at 0.5 (center of range) and the contrast/gain was set at 1.0 (center of range). Two Fujinon lenses were used on the camera: 50 mm f/0.7 and 25 mm f/0.85, aperture areas 40 and 6.8 cm^2 respectively.

The DVS–3000 was used to put date/time information on each frame during data acquisition. During video playback, the analyzer captures (digitizes) individual frames and allows pixel data from areas within a video frame to be integrated. The integration allows a quantified video signal to be obtained which can be calibrated to an absolute light level.

Quantifiable light sources were prepared from solutions of luminescent marine bacteria. One ml samples of the solution were measured in a Quantalum luminescence photometer calibration unit (model #2000 and serial #882). The Quantalum unit itself was calibrated by using secondary light standards (Ni^{63} in conjunction with phosphors). The one ml bacteria solutions measured in the Quantalum calibration unit provide a known source strength (photons/sec). The one ml bacteria solutions were placed at a distance of 5.5 m from the ISIT camera lens and the image was recorded using a VCR.

[1] For induced laminar flows of as little as 1/2 kt (26 cm/s), wall shear stress on a 20-cm-long flat plate will everywhere exceed bioluminescence threshold levels ($\sim$1 dyne/cm^2, as determined in the work herein).

[2] NOSC Technical Notes (TNs) are working documents and do not represent an official policy statement of NCCOSC RDT&E Div. (formerly NOSC). For further information, contact the author.

To quantify the video signals and the corresponding variance, 800 frames of the imaged bacteria solution were averaged 100 frames at a time. The image spot (20 x 20 pixels) of each 100 frame average was integrated. A similar 20 x 20 pixel area was integrated without a source to determine the background video signal. The source video signals, minus background of these eight integrations, were then averaged to obtain the final video signal for each bacteria light source. The bacteria source was measured immediately before and after the image was recorded, and these Quantalum readings were averaged to obtain the source strength.

The one ml bacteria solution source strength was divided by $4\pi r^2$ and multiplied by the lens area to obtain the solid angle, and thus the light entering the lens (photons/sec). The number of pixels illuminated in the image is four times greater for the 50 mm lens relative to that of the 25 mm lens. This difference in pixels is due to the x2 magnification of the 50 mm lens relative to the 25 mm lens. The number of pixels for the images was estimated to be 100 (10 x 10) for the 25 mm lens and 400 (20 x 20) for the 50 mm lens. To express the calibration in fundamental units, the light entering the lens and the video signal were divided by the estimated image pixels to give: photons/sec/pixel vs video signal per pixel. A range of light intensities was obtained by using various dilutions of the bacteria solutions and the resulting calibration curves (Video ISIT calibration 50 mm lens, figure 1.1a and Video ISIT calibration 25 mm lens, figure 1.1b) were obtained. A second order polynomial curve was fit to each calibration curve as shown in figures 1.1a and 1.1b.

The camera video calibration provided an estimate of the bioluminescence signal generated by a 24-cm diameter black float. Video pictures were obtained on the nights of 2/26/89 and 2/27/89 in the southern Gulf of California about 40 miles off La Paz, Mexico. There was background light from the upper levels of the ship (USNS *De Steiguer*), the sky was clear with no moon, and there was little or no wind. The surface water was smooth with a slight swell and the depth was on the order of 1000 m. The bioluminescence measured (about 1E8 photons/sec/ml) with the NRaD Code 524 photometer system was typical for the area. The float was a Benthos glass sphere wrapped in black shade cloth and suspended from a black electrical cable (1.4 cm in diameter) with a weight suspended below it. The float was lowered from the ship's side winch. The video camera was mounted on a tripod which was on the second deck at a height of 5.3 m above the sea surface and pointed down at about 30 degrees from the vertical. The float was suspended at a depth of 6.1 m and at a horizontal distance of about 3.6 m from the camera.

A video frame containing the float image was captured (figure 2c) and a 50 x 50 pixel square centered around the image was integrated. A similar 50 x 50 pixel square in the background was integrated to obtain an equivalent background signal. The background signal was subtracted from that of the float image to give a net video signal of about 9E4. The average video signal per pixel is then 36, which is equivalent to 175 photons/sec/pixel from the 50 mm lens calibration curve. The light flux at the lens is then 175 ph/s/pixel * 2500 pixels/40 cm^2 aperture which equals: 1.09E4 photons/sec/cm^2.

The next step is to determine what fraction of the bioluminescence from the submerged object gets to the camera lens. This was done by writing a Quick Basic program (the program VIDEOATT.BAS listing is included). The program calculates the primary ray light path from the submerged object to the camera lens and then calculates the light attenuation along that path. Having the light path, the attenuation fraction is determined by the following calculations:

1. The fraction of light transmitted through the water/air interface. For this case: 0.95

2. The inverse square distance from the underwater virtual image to the lens. For this case: 7.38E–8/cm^2

3. The attenuation due to the water path (the attenuation length is assumed to be 10 m which is typical for the area). For this case: 0.53

The bioluminescence estimate is then simply the light flux at the camera lens divided by the attenuation fraction, which in this case is [(1.09E4 photons/sec)/cm^2]/[3.74e–8/cm^2], which gives 2.9e11 photons/sec. The bioluminescence can be estimated from other video images in the same way.

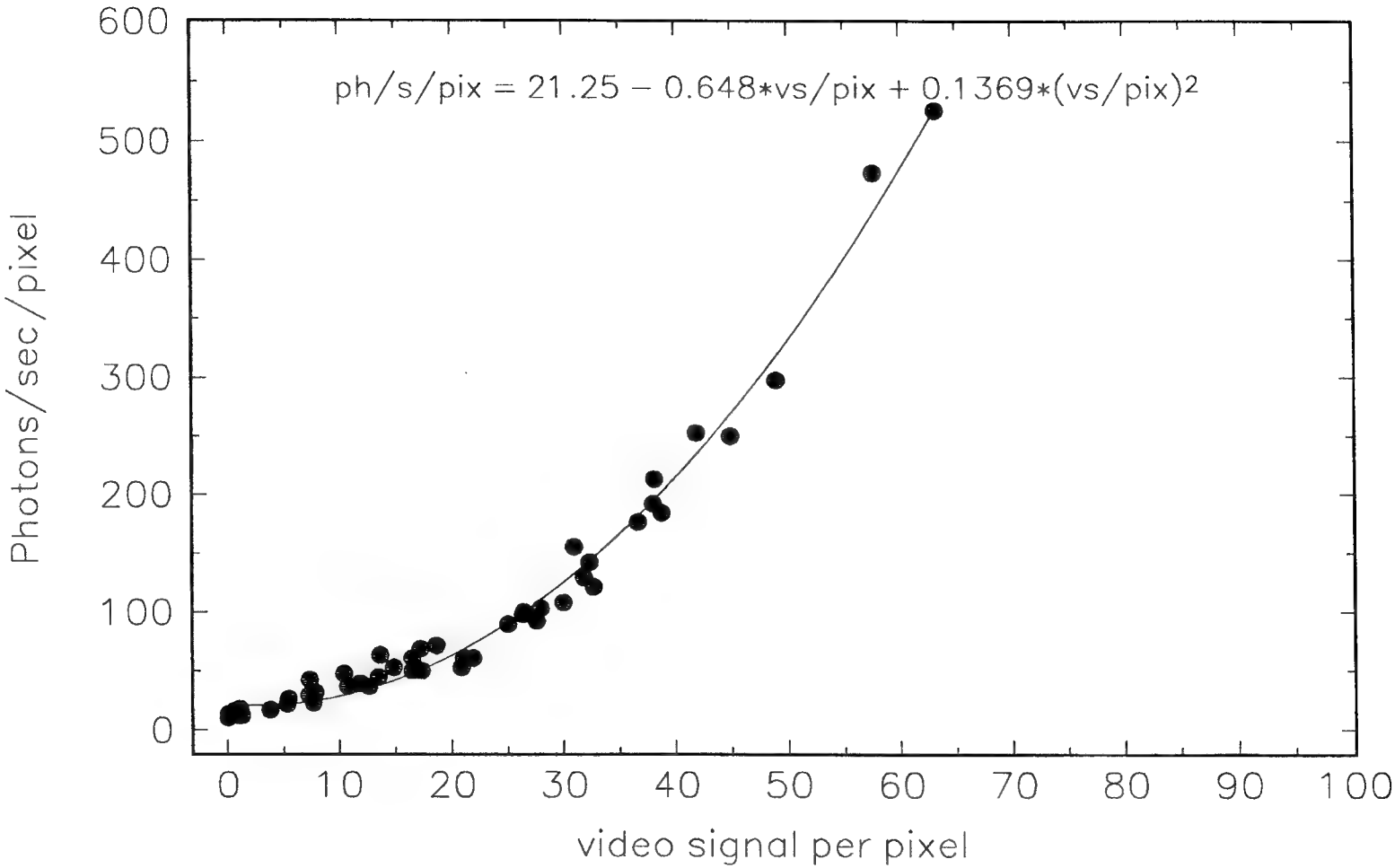

Figure 1.1a. Video ISIT camera calibration curve for 50 mm lens.

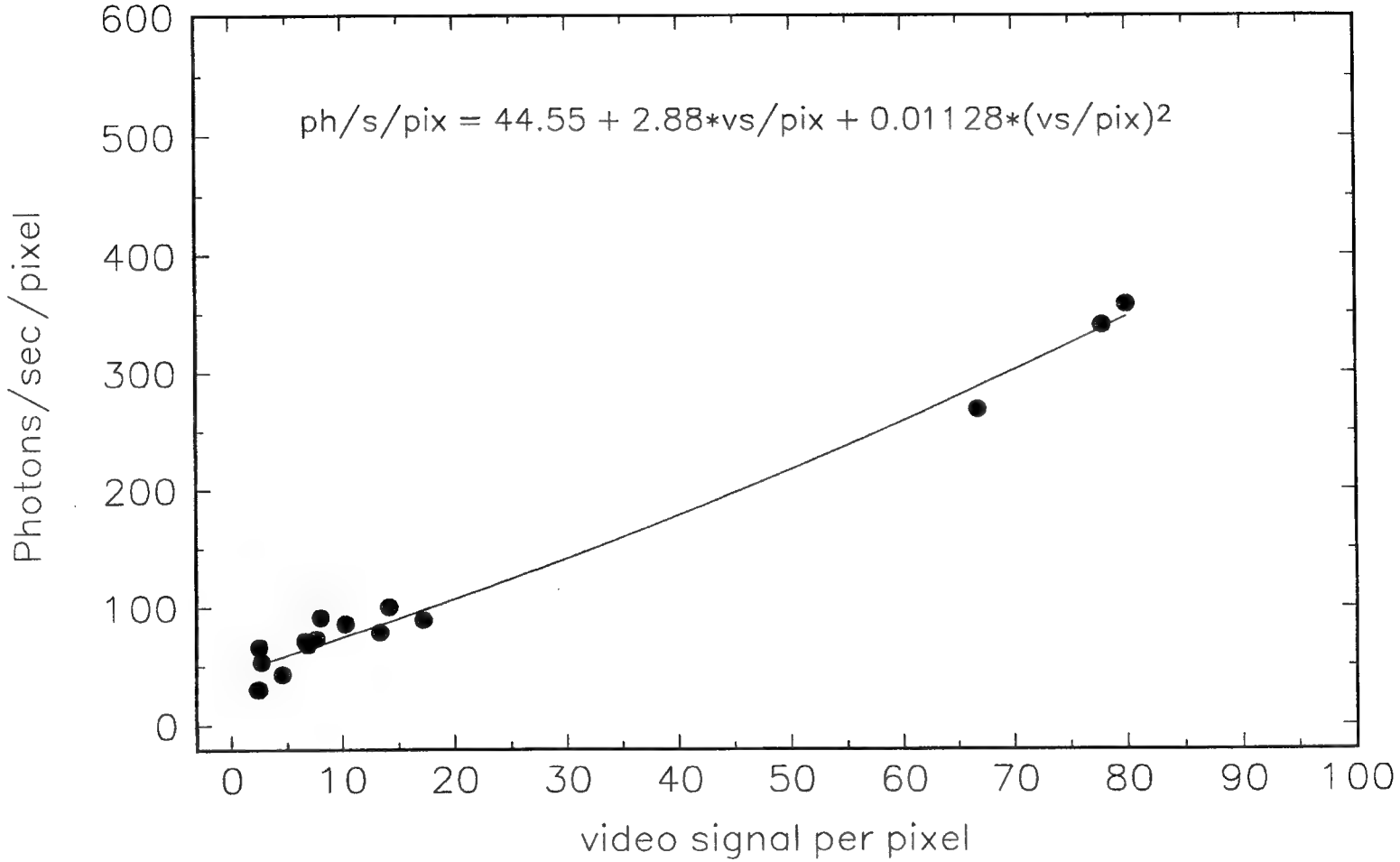

Figure 1.1b. Video ISIT camera calibration curve for 25 mm lens.

```
    'Program:   VIDEOATT.BAS
    CLEAR : CLS
    prog$  =  "Program  to  calculate source strengths underwater
10/12/94"
    PRINT prog$
restart:
    H = 17.34 'height above sea surface in feet: 89 Baja
    X0 = 12   'horizontal distance lens to object in feet: 89
Baja
    INPUT "Attenuation  length  in  feet  for  light  (480 nm) in
seawater <33ft (10m)>"; attlen
    IF attlen = 0 THEN attlen = 33
'default attenuation length
    INPUT "What is the depth of the object in feet"; D2

    'determines the actual horizontal distance (X) the primary
ray leaves water surface
    'this distance (X) determines the angle of the primary ray
due to refraction above the water surface
    HS = H ^ 2                    'height squared
    DS = D2 ^ 2                   'depth squared
    wis = (4 / 3) ^ 2             'water index squared
    FOR i% = 1 TO 500             'iteration loop
    X = .01 * i% + X0 - 8         'start iteration 8 ft less than
actual horizontal distance
    X0S = (X0 - X) ^ 2           'horizontal distance primary ray
at surface from object squared
    XS = X ^ 2                    'horizontal distance primary ray
at surface squared
    E = DS * XS + XS * X0S - wis * X0S * (HS + XS)      'error
in: index^2 - (sin(refracted)/sin(incident))^2 = 0
    E = ABS(E)
'absolute value of error
    IF i% = 1 THEN EM = E                    'start at initial
error
    IF E < EM THEN im% = i%: EM = E          'find minimum error
    NEXT i%                                  'end of iteration loop

    PRINT "i% at minimum = "; im%; "  error= ";  EM   'print
loop count and minimum error
    X = .01 * im% + X0 - 8                    'calculate X from
loop count at minimum error
    PRINT "X= "; X; "ft", X / 3.28; "m"          'print X in ft
and metres
    phi = ATN(X / H)                             'refracted angle
in radians from X and H
    PRINT "phi= "; 57.296 * phi                'print refracted
angle in degrees

    GOSUB intensity                  'gosub to calculate
fractional intensity
    INPUT q$                         'input dummy before
restarting
```

```
    GOTO restart                    'go back to start to
calculate another
intensity:

    'fraction transmitted through water surface:
    waterindex = 4 / 3                          'index for water
= 4/3
    SINincident = SIN(phi) / waterindex                    'index
= sin(refracted)/sin(incident)
    COSinc = SQR(1 - SINincident ^ 2)          'cos =
sqr(1-sin^2)
    COSref = SQR(1 - SIN(phi) ^ 2)             'cos =
sqr(1-sin^2)
    RN = COSref / COSinc                       'ratio of
cos(refracted)/cos(incident)
    TS = (4 / SQR(3)) / (RN + waterindex) * (RN)
'transmitted wave amplitude polarization perpendicular to plane
of rays
    TP = (4 / SQR(3)) / (RN * waterindex + 1) * (RN)
'transmitted wave amplitude polarization in plane of rays
    fractrans = (TS ^ 2 + TP ^ 2) / 2
'intensity transmitted
    PRINT "fraction intensity transmitted through water surface=
"; fractrans

    'inverse square plus water attenuation:
    PRINT
    pathuw = SQR((X0 - X) ^ 2 + D2 ^ 2)        'actual path
length underwater
    auw = EXP(-pathuw / attlen)             'attenuation
underwater
    PRINT "underwater attenuation factor= "; auw
    invSqrpath = 1 / (((X0 - X) / SIN(phi)) + (SQR(X ^ 2 + HS)))
^ 2   'inverse square ratio from virtual source to camera
    FractionAtLensFt =   auw * invSqrpath * fractrans *  1  /  (4
* 3.14)   'per sq ft
    PRINT
    FractionAtLens = FractionAtLensFt / (144 * 2.54 ^ 2)
 'per sq cm
    PRINT "Fractional Light Flux from object at lens=
"; FractionAtLens; " /cm^2"
    PRINT
    INPUT "Input  photons/sec/cm^2  into  camera  lens  from
video signal calibration of image"; VSphotons
    PRINT  "Source   strength   from   object   =  ";  VSphotons
/ FractionAtLens; " ph/s"
    RETURN

    END
```

REFERENCES FOR APPENDIX 1

1. Rohr, J. J., J. R. Losee and J. W. Hoyt. 1990. "Stimulation of bioluminescence by turbulent pipe flow," *Deep Sea Research,* 37:(10) 1639–1646.

2. Losee, J. R. 1989. "Bioluminescence for ocean night surveillance (BONS)," NOSC TN 1561 (Jan).

3. Losee, J., K. Richter, S. Lieberman, and D. Lapota. 1989. "Bioluminescence: spatial statistics in the North Atlantic," *Deep Sea Research*, vol. 36, no. 5, pp. 783–801.

4. Lieberman, S., D. Lapota, J. Losee, and A. Zirino. 1987. "Planktonic bioluminescence in the surface waters of the Gulf of California," *Biological Oceanography*, vol. 4, no. 1.

5. Two papers given at AGU/ASLO meeting in Jan 1986, New Orleans: Losee, J.R. and D. Lapota, "Bioluminescence in diverse oceanic regions"; and Lapota, D., J. Losee, H.D. Huddell, C. Galt, K. H. Nealson and J. K. Orzech, "Measurements and observations of bioluminescence in the western Indian Ocean and Arabian Sea."

6. Losee, J. R., D. Lapota, and S.H. Lieberman. 1985. "Bioluminescence: A new tool for oceanography," chapter 11 in *Mapping Strategies in Chemical Oceanography*, No. 209 Advances in Chemistry Series, American Chemical Society.

7. Invited paper: Losee, J.R., D. Lapota, M. Geiger, and S. Lieberman. 1984. "Bioluminescence in the marine environment," *Ocean Optics VII SPIE Conference*, Naval Postgraduate School, Monterey, California, 25–28 June.

8. Lapota, D. and J.R. Losee. 1984. "Observations of bioluminescence in marine plankton from the Sea of Cortez," *Journal of Experimental Marine Biology and Ecology,* 77: 209–240.

9. Greenblatt, P.R., D.F. Feng, A. Zirino, and J.R. Losee. 1984. "Observations of bioluminescence in the euphotic zone of the California current," *Marine Biology,* 84:75–82.

10. Lapota, D. and J.R. Losee. 1984. "Records of bioluminescence in marine plankton from the Norwegian Sea and waters off North Cape," Abstract. *EOS 64* (52):1102.

11. Losee, J., and D. Lapota. 1982. "Ultraviolet bioluminescence in the marine environment," *EOS 63*, 944.

12. Griswold, C.A., J.R. Losee, and D. Lapota. 1984. "Correlation of zooplankton community structure and measured bioluminescence throughout the water column using a manned submersible," Abstract. *EOS 64* (52):1102.

13. Griswold, C.A. and J.R. Losee. 1984. "Observations of gelatinous zooplankton and measurements of vertical bioluminescence in the Gulf of Maine and on Georges Bank," Undersea Research Symposium: Scientific Applications and Future Needs. May 22–24, 1984.

14. Losee, J. and D. Lapota. 1981. Section Six, Chapter 3 of *Bioluminescence Current Perspectives, Bioluminescence Measurements in the Atlantic and Pacific.*

15. Naval Oceanographic Office, Biological data from North Pacific transits, BDR 7110–2–87, June 1987.

16. Naval Oceanographic Office, Biological and chemical data from the Arabian Sea, BDR 7110–1–87, June 1987.

17. Naval Oceanographic Office, Biological and chemical data from the Northeast Pacific, BDR 01–89, May 1989.

18. Biggley, W.H., E. Swift, R.J. Buchanan, and H.H. Seliger. 1969. "Stimulable and spontaneous bioluminescence in marine dinoflagellates, *Pyrodinium bahamenese, Gonyaulax polyedra, and Pyrocystis lunula," J. Gen. Physiol.*, 54:96–123.

19. Christianson, R., and B. M. Sweeney. 1972. "Sensitivity to stimulation, a component of the circadian rhythm in luminescence in *Gonyaulaux*," *Plant Physiol.,* 49, pp. 994–997.

20. Morita, M., and R. Johnson. 1974. "Field induced luminescence," TRW Report AT–SVD–TR–74–5.

21. Anderson, D. M., D. M. Nosenchuck, G. T. Reynolds, and A. J. Walton. 1988. "Mechanical stimulation of bioluminescence in dinoflagellate *Gonyaulaux polyedra stein*," *J. Exp. Mar. Biol. Ecol.,* 122:277–288.

APPENDIX 2: PROPERTIES OF FULLY DEVELOPED PIPE FLOW

2.1 FULLY DEVELOPED FLOW

Pipe flow is considered fully developed when its velocity profile is no longer evolving downstream. With no mean acceleration, the pressure drop, dP/dx, across the face of any concentric, cylindrical control volume of radius r must be balanced by the shear stress τ acting on its perimeter. This relationship can be expressed as

$$\tau(r) = (dP/dx) * (r/2), \tag{2.1a}$$

which at the pipe wall, R, becomes

$$\tau_{wall} = (dP/dx) * (R/2). \tag{2.1b}$$

Eliminating dP/dx, equations (2.1a) and (2.1b) reduce to

$$\tau(r) = \tau_{wall} (r/R). \tag{2.1c}$$

This linear stress distribution expresses a general law, regardless of whether the flow is laminar or turbulent.

Fully developed pipe flows are approached asymptotically in the downstream direction, and experiments have determined appropriate entrance lengths (L_e). The accepted relations for laminar and turbulent pipe flows are the following (F. White, 1979):

$$(L_e/D)_{laminar} \approx 0.06\ Re, \tag{2.2a}$$

and

$$(L_e/D)_{turbulent} \approx 4.4\ (Re)^{1/6}, \tag{2.2b}$$

where D is the pipe diameter and Re is the Reynolds number. The Reynolds number is indicative of the ratio of the force acting on a small parcel of fluid, to the force developed on the parcel by the viscous stresses, and has become the basic dynamic characteristic, qualifying the state of fluid motion (Childress, 1981). Here Re is defined as

$$Re = \rho U_{avg} D/\mu, \tag{2.3}$$

where ρ is the fluid density, U_{avg} is the average flow speed, and μ is the kinematic viscosity.

2.2 LAMINAR FLOW

The sole source of shear stress in laminar flow is due to viscosity. The viscous stresses developed in laminar flows of most common fluids (such as air, water, and sea water) are found to be equal to the product of the kinematic viscosity and the local velocity gradient. This relationship was first proposed by Isaac Newton in 1687 (Cajori, 1946):

> "The resistance arising from want of lubricity in the parts of the fluid, is, other things being equal, proportional to the velocity with which the parts of the fluid are separated from one another."

Fluids adhering to this linear relationship between shear stress and velocity gradient[1] are referred to as Newtonian. In fully developed laminar pipe flow of a Newtonian fluid the following relationship holds:

$$\tau_{laminar} = \tau_{wall}(r/R) = \mu(du/dr), \qquad (2.4)$$

where u(r) is the velocity along the pipe axis, measured at radius r from the pipe centerline. (As a matter of notation, u(r), U(r), and u′(r) refer, respectively, to the instantaneous, average, and fluctuating velocity at r. The average velocity through the pipe is designated U_{avg}.) For fully developed laminar flow, equation (2.4) predicts (Schlichting, 1979) both the correct parabolic velocity profile and dimensionless relationship between pressure drop (Darcy friction factor, λ) and average flow rate (Reynolds number, Re). The Darcy friction factor is defined[2] as

$$\lambda = (dp/dx)D/(1/2\rho U_{avg}^2). \qquad (2.5)$$

The theoretical relation between λ and Re for fully developed laminar pipe flow is

$$\lambda = 64/Re \qquad (2.6a)$$

which can also be expressed, via equations (2.1b), (2.5), and (2.6a), as

$$\tau_{wall\ lam} = 8\rho U_{avg}^2/Re \propto U_{avg}. \qquad (2.6b)$$

2.3 TURBULENT FLOW

In turbulent flow, another mechanism for momentum exchange arises. Turbulent shear stress[3] results from the correlation of two components of velocity fluctuation at the same point. For fully developed turbulent pipe flow the total shear stress becomes

$$\tau_{total} = \tau_{wall}(r/R) = \mu(du/dr) + \rho\,\overline{u'v'} \qquad (2.7)$$

where $\overline{u'v'}$ represents the time-averaged product of the fluctuating velocities in the longitudinal and radial directions. While individual velocity fluctuations are only a few percent of the average mean velocity[4], turbulent shear stresses, except within the viscous sublayer at the wall, essentially constitute the total shear stress throughout the pipe (Laufer, 1954). This is illustrated in figure 2.1 where the theoretical, total shear stress (solid line), identical for both laminar and turbulent flow, is compared with the turbulent shear stress measurements of Laufer (1954). Both the total and turbulent shear stress shown in figure 2.1 are normalized by τ_{wall}. The Reynolds numbers for Laufer's (1954) pipe flow experiments were 50,000 and 500,000. Note that on the pipe wall the velocity is zero (no slip condition). Therefore, as the wall is approached, equation (2.7) will reduce to equation (2.4).

---

[1] In the limit of infinitesimal changes the shear strain rate is equal to the velocity gradient (White, 1979).

[2] Unfortunately, a dimensionless shear stress is sometimes used instead of λ. This dimensionless shear stress, f, is referred to as the Fanning friction factor and is equivalent, via equation 1b, to 1/4 λ.

[3] The correlation term $\overline{u'v'}$ is commonly called a turbulent stress because it has the same dimensions as the laminar stress and has the same mathematical effect. Actually $\overline{u'v'}$ is a convective acceleration term which is why the density appears (White, 1979).

[4] The peak longitudinal, radial, and azimuthal turbulent velocity fluctuations occur near the pipe wall ($r/D \approx 0.001$), are respectively about 8%, 4%, and 6% of the centerline velocity, and decrease monotonically to zero at the wall and to about 3% at the pipe centerline (Laufer, 1954).

The nature of turbulent shear stress greatly increases mixing. Whereas in laminar flow, filaments of dye remain intact as they pass down the pipe, at the onset of turbulence they appear to "explode", mixing rapidly across it. Figures 2.2a through c are photographs of dye taken 30 pipe diameters (D = 0.635-cm) from the pipe inlet where the dye was introduced for respective Reynolds numbers of 13,500 (beginning of turbulent flow), 10,500 (beginning of transitional flow), and 3200 (laminar flow). At higher Reynolds numbers, and at the same position along the tube, the dye streak could no longer be distinguished. At the pipe entrance the filament was always intact[5], regardless of the Reynolds number. Toward the end of the pipe the dye streak was always distinguishable for laminar flows, intermittently intact for transitional flows, and completely mixed for turbulent flows.

The photographs in figures 2.2a through c were taken 18 hours after the water had been transferred to the aquarium. Normally experiments began 45–60 minutes after the aquarium was filled and transition was usually observed to occur at the significantly lower Reynolds number of 6000. Lower Reynolds number transition resulting from the residual motion associated with the filling of the reservoir is a common occurrence (Reynolds, 1883). Reynolds (1883) had achieved, after painstaking effort, transitional Reynolds around 12,000 (Prandtl, 1934; Rouse, 1938). It is interesting to note that when Reynolds' experiment was repeated using the original apparatus a century later, such relatively high transition values could not be duplicated due to the increased background vibrations introduced by modern traffic (Van Dyke, 1982)[6].

Another fundamental difference between turbulent and laminar shear stress is that the former is not determined by the local mean velocity gradient, but now is primarily dependent on the previous history of the flow which carries the turbulent eddies. Therefore mean and turbulent velocity profiles, and the functional relationship between wall shear stress and turbulent flow rate, must be empirically determined. It has been found (Schlicting, 1979) for the range of Reynolds numbers important to this study, Re < 20,000, that a suitable representation for the mean velocity profile (except very near the wall) for fully developed turbulent pipe flow is the following:

$$U(r)/U_{max} = (r/R)^{1/7} \qquad (2.9)$$

where U_{max} is the centerline velocity.

Figure 2.3a compares the theoretical laminar and experimentally derived turbulent pipe velocity profiles, normalized by the centerline velocity, with the measurements of Patel and Head (1969) at Reynolds numbers of 2015 and 4060. Figure 2.3b illustrates the laminar and turbulent velocity profiles one would expect to find in a 0.635-cm diameter pipe, with sea water at 25° C[7], flowing at 60.26 cm/sec (Re = 4060). Note, as a result of increased turbulent mixing, the mean velocity levels in turbulent flow change much less (profile is flatter) than laminar flow

[5] Discussion and photographs of the stabilizing effect of a contracting inlet can be found in Rouse (1938).

[6] It has been empirically observed that pipe flow remains laminar for Reynolds numbers less than about 2000 (White, 1974) no matter how rough and noisy the entrance conditions are made. Laminar pipe flow, after taking great care in minimizing the inlet and background disturbance levels, has been maintained until Reynolds numbers of around 100,000 (Pfenninger, 1961).

[7] Temperature throughout the experiments reported herein ranged between 15°C to 25°C. This difference in temperature results in a 20% change (decrease with increasing temperature) in kinematic viscosity, ν. Consequently, whatever the temperature chosen for a particular figure, the resulting pipe flow curves are fairly representative of the entire experimental flow range tested herein.

across the central core of the pipe. The wall shear stress supporting this turbulent velocity profile is about two and one half times the laminar velocity profile for the same Reynolds number.

As in the laminar case, a relation between the nondimensional pressure drop and mean flow (i.e., λ vs Re) can be found. This empirical relation, established by Blasius (1913) is

$$\lambda = 0.316/Re^{1/4} \tag{2.10}$$

or equivalently, via equations (2.1b), (2.5), and (2.10),

$$\tau_{wall\ turb} = 0.04\rho U_{avg}^2/Re^{1/4} \propto U_{avg}^{1.75}. \tag{2.11}$$

It can be shown (Schlicting, 1979) that equation (2.11) is related to the velocity profile specified in equation (2.9). In figure 2.4a the theoretical laminar and empirically derived turbulent relations for λ *vs* Re are compared to tap water data obtained in various pipes of different lengths and diameters. As the ratio of entrance length (L_e) to pipe diameter (D) increases, either by increasing L_e or decreasing D, the high laminar Re flow becomes more fully developed. Note also the excellent agreement between tap (figure 2.4a) and ocean (figure 4) water data.

Although the dimensionless variable λ decreases with increasing Reynolds number, it is important to realize that both dp/dx and τ_{wall} increase with flow speed. This is illustrated in figure 2.4b where values of wall shear stress and average flow speed for fully developed flow in a 0.635-cm-diameter pipe, with seawater at 25°C flowing through it, are presented. Wall shear stress values increase monotonically with flow speed in both laminar and turbulent flow, exhibiting a discontinuous increase at transition. As seen in figure 2.4b, when transition occurs at an average pipe velocity of 89.3 cm/sec (Re $\approx$ 6000) an accompanying increase in the total shear stress of almost 3-1/2 fold is found throughout the pipe. With transition occurring at higher Reynolds numbers, the accompanying increase in shear stress becomes larger.

2.4 LENGTH SCALES OF TURBULENT EDDIES

In fully developed turbulent pipe flow the range of eddy length scales can be inferred. The largest turbulent eddy length scale is of the order of the pipe radius. The smallest turbulent eddy length scale, where inertial and viscous forces are nearly equal, is of the order on the Kolmorgorov length scale, L_K. The Kolmorgorov length scale is obtained from dimensional analysis after making the reasonable assumption that the dissipation rate per unit mass, ε, and the kinematic viscosity, ν ($\nu = \mu/\rho$), govern the small scale motion (Tennekes & Lumley, 1972). The Kolmogorov length scale, L_K, is defined as

$$L_K = (\nu^3/\varepsilon)^{1/4}. \tag{2.12}$$

Experiments measuring the energy spectra of grid turbulence (Van Atta & Chen, 1969; Jayesh & Warhaft, 1992) have shown a cut-off close to the wavenumber corresponding to L_K.

In fully developed pipe flow, the average dissipation is equal to the work performed by the wall shear stress acting on the fluid surface over a displacement corresponding to the average velocity of the flow (Bakhmeteff, 1936). Consequently for turbulent flow between Re = 2300–20000, where equation (2.10) is valid, the average dissipation, ε_{avg}, can be estimated (Davies, 1972) as

$$\varepsilon_{avg} = 0.16(Re)^{-0.25}(U_{avg})^3/D. \quad (2.13)$$

After substituting equation (2.13) into equation (2.12), one arrives at an expression (Rohr et al., 1990) for L_K,

$$L_K = 1.58D(Re)^{-0.69}. \quad (2.14)$$

Near the pipe wall a better approximation for ε can be made. Because the velocity is zero everywhere on the pipe boundary (no slip condition), at the pipe wall only derivatives with respect to the pipe radius are not equal to zero. Consequently

$$\varepsilon_{(r\to R)} \approx \nu[(du/dr]^2 \quad (2.15a)$$

and via equation (2.7) with $\overline{u'v'} \to 0$

$$\varepsilon_{(r\to R)} \approx \tau_{wall}^2/(\mu\rho). \quad (2.15b)$$

Therefore

$$L_{K(r\to R)} \approx \nu/(\tau_{wall}/\rho)^{1/2}. \quad (2.16)$$

Figure 2.5 contains various estimates of the Kolmorgorov length scale over the flow range of interest (pipe i.d. = 0.635 cm and temperature = 20.6°C). The solid and long dashed lines are calculated from equations (2.14) and (2.16) which respectively employ average and wall dissipation values. The short dashed line is from a derivation by Davies (1972), who uses a dissipation representative of eddies near the pipe axis. As can be seen in figure 2.5, regardless of the estimate used for ε, L_K is almost always less than the size of bioluminescent dinoflagellates, the smallest of which are typically about 30 μm in diameter (Morin, 1983). When the turbulent eddies are less than the size of the organisms, they should be much more effective in distorting, as opposed to convecting, the organisms.

Two issues concerning the above development and interpretation of L_K should be discussed. First, the dissipation, ε, is not uniform across the pipe, but decreases rapidly from the wall (Hinze, 1975; Laufer, 1954). But because ε enters into the equation for L_K as $\varepsilon^{1/4}$, an approximate value, such as ε_{avg}, $\varepsilon_{(r\to 0)}$, or $\varepsilon_{(r\to R)}$ may be sufficient. Second, significant shear energy may only exist in turbulent scales 10 times and greater than L_K (Lazier & Mann, 1989). Accordingly, L_K would have to be about 3 μm to ensure adequate stimulation for the smallest bioluminescent dinoflagellates present. As seen in figure 2.5, higher Reynolds number flows are necessary to achieve this.

2.5 CAVEATS

It has been tacitly assumed throughout this analysis that the presence of the organisms do not significantly effect the pipe flow field described, and remain roughly homogeneously distributed throughout it. While we believe these assumptions are reasonably justifiable, there are several flow-organism interactions worth noting:

1. Gyrotactic focussing. Kessler (1985) has reported that for small laminar flow rates ($Re \approx 10$, $U_{avg} \approx 0.1$ cm/sec for D = 0.635-cm) the swimming direction of algal cells can be

directed by compensating gravitational and viscous torques. In downward pipe flow an initially uniformly distributed cell population becomes focused along the pipe centerline.

2. Inertial migration. Suspensions of neutrally buoyant spheres under laminar flow conditions (Re = 3–30) have been found to migrate, due to the inertia of the fluid, to an equilibrium position between the pipe wall and centerline (Segre & Silberg, 1962a, b). This equilibrium position has been predicted (Schonberg & Hinch, 1989) to move toward the wall with increasing Reynolds number.

3. Turbophoresis. Particle drift velocities arise in turbulent flow when the statistical properties of the velocity fluctuations vary in space, resulting in a migration of particles from regions of high fluid turbulence to regions of low fluid turbulence (Young & Hanratty, 1991).

4. Drag and lift forces. Particles close to the wall experience an augmented response to fluid turbulence (Rizk & Elghobashi, 1984).

5. Effect of crossing trajectories. The trajectories of particles heavier than the suspending medium will tend to cross the trajectories of fluid elements, resulting in a reduced dispersion (Wells & Stock, 1983).

Assuming the bioluminescent organisms follow the fluid flow, thereby ignoring the aforementioned complexities, is believed to be a reasonable first approximation for the following reasons:

1. For the most part, the pipe flows pertinent to this investigation are several orders of magnitude greater than the swimming speed[8] of the organisms.

2. The ratio of organism to fluid density is significantly smaller than the particle experiments which exhibited anomalous dispersion[9].

3. Concentrations of the organisms are believed to be much less than necessary to effect flow. Direct numerical simulations of particle dispersion in decaying isotropic grid turbulence have shown (personal communication, Said Elgobashi) that 10^{-4} volume fractions must be exceeded for the particles to significantly effect the flow field. This is much greater than the concentrations found in the samples which were inspected.

4. Finally, throughout the present experiments the friction factor *vs* Reynolds number data for tap and seawater are (except for transition) essentially identical, suggesting that the flow fields are similar.

Even if one knew everything about the flow field in which bioluminescence occurs, there is still the inherent ignorance of the organisms' prestimulus history. This is unavoidable regardless

[8] In general, single celled organisms, typically between 2 and 1000 μm long, can sustain swimming speeds up to 100 body lengths per second (Yates, 1986). For the organisms of interest (*Gonyaulax polyedra* is about 45 μm long and 41 μm wide [Morita & Johnson, 1974]), this relationship would predict swimming speeds less than 1 mm/sec, in agreement with measurements by Kamykowski et al. (1992).

[9] When Young and Hanratty (1991) measured the turbulent motion of 100–μm diameter glass spheres (density = 2.42 g/cm^3) suspended in water flowing through a pipe, they found excellent agreement with Laufer's (1954) classic pipe-flow measurements made without particles. The density of six marine dinoflagellates studied by Kamykowski et al. (1992) were between 1.06 and 1.09 g/cm^3. (Note, some dinoflagellates can achieve positive buoyancy in seawater. Noctiluca have a large vacuole in which they concentrate ammonia and exclude potasium and divalent anions to reduce density (Vogel,1981).)

of the flow field chosen (see for example Latz's (1994) comments on the prestimulus associated with start up in Couette flow). To test the effect on bioluminescence intensity and color spectra due to transit in a hose, Losee and Lapota (1981) pumped San Diego Bay water at 0.38 l/s through different lengths of 2.54-cm inside diameter (i.d.) hose[10]. A viewing chamber fitted with quartz windows was positioned at the end of the hose and configured to provide additional turbulent stimulus. The average measured bioluminescent intensity increased by only 22% when the hose length was decreased from 120 to 6 m. The bioluminescent color spectra showed little change. It was concluded that the longer hose caused little additional bioluminescent degradation. Later measurements (Lieberman et al., 1987) showed that further shortening of the hose, from 6 to 1 m, resulted in an additional increase in bioluminescence of up to 30%. It is anticipated, based on the present investigation, that an even greater (possibly as much as a factor of two to three) increase in bioluminescence would be observed at the hose inlet. The initial stimulation associated with the pipe inlet is impossible to avoid. However, it appears that in the region of fully-developed turbulent flow studied here, where the flow field stimuli is well characterized, some quasi-steady state evolves in which the bioluminescent response is not strongly dependant on downstream position. It is in this region that the present study is principally concerned. It is assumed that what is learned here about the fundamental nature of the response of luminous organisms to hydrodynamic stimuli will be relevant to all flows in general.

[10] Because of the high Reynolds number and the abruptness of the entrance, it is reasonable to assume (via Eq. 2) that fully-developed turbulent flow was established within the first few meters of hose.

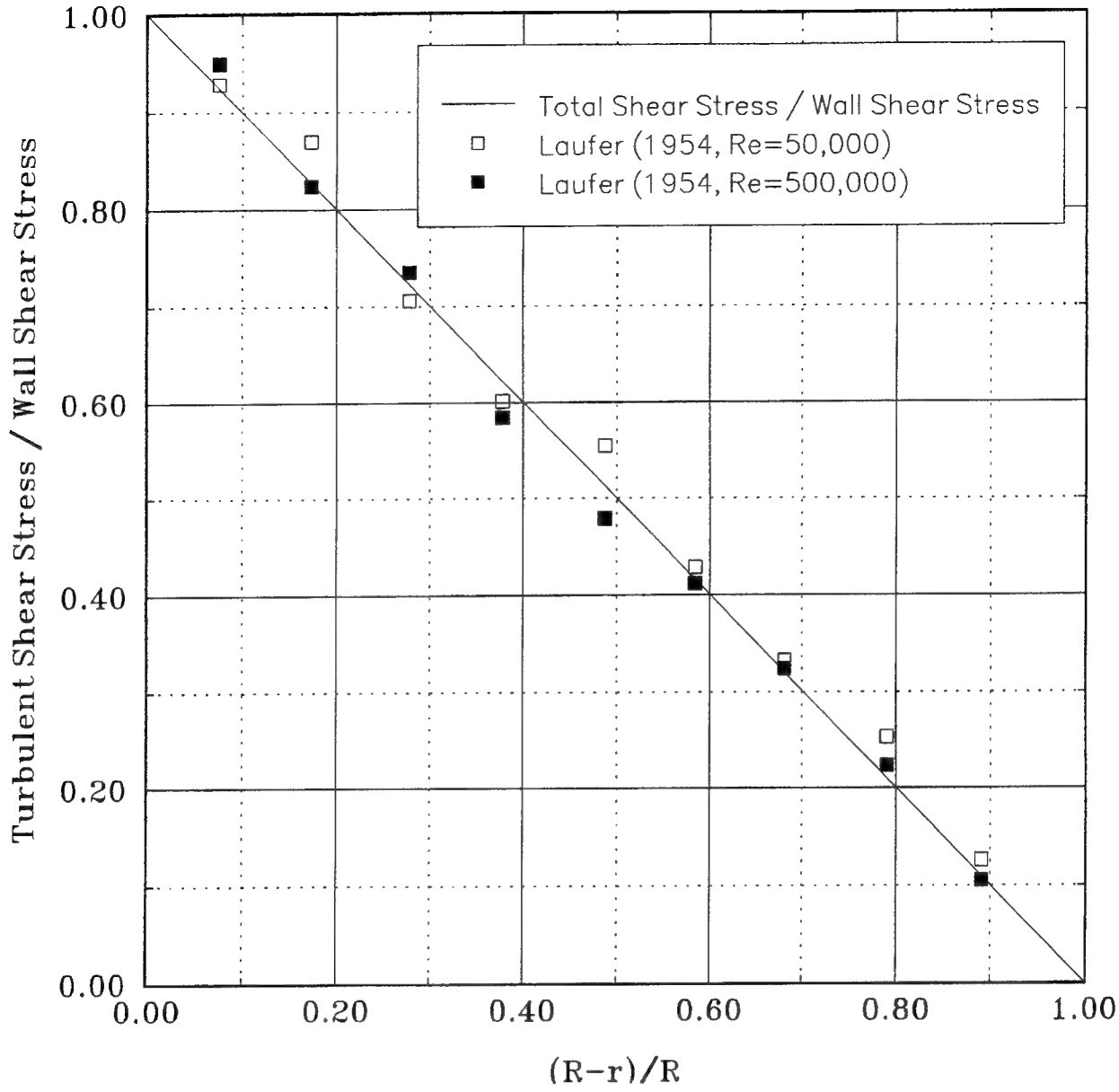

Figure 2.1. Experimentally observed (■ , □ ; Laufer, 1954) distribution of the normalized turbulent shear stress, $\frac{(\rho\overline{u'v'})}{\tau_{wall}}$, across a pipe in fully developed flow. Turbulent shear stress levels have been normalized by the wall shear stress, τ_{wall}, allowing different Reynolds number experiments to be compared. The solid line shows the distribution of the theoretical values of the total shear stress across the pipe. Except near the pipe wall ($r \rightarrow R$, $\rho\overline{u'v'} \rightarrow 0$; not shown) the total shear stress is essentially entirely turbulent in nature.

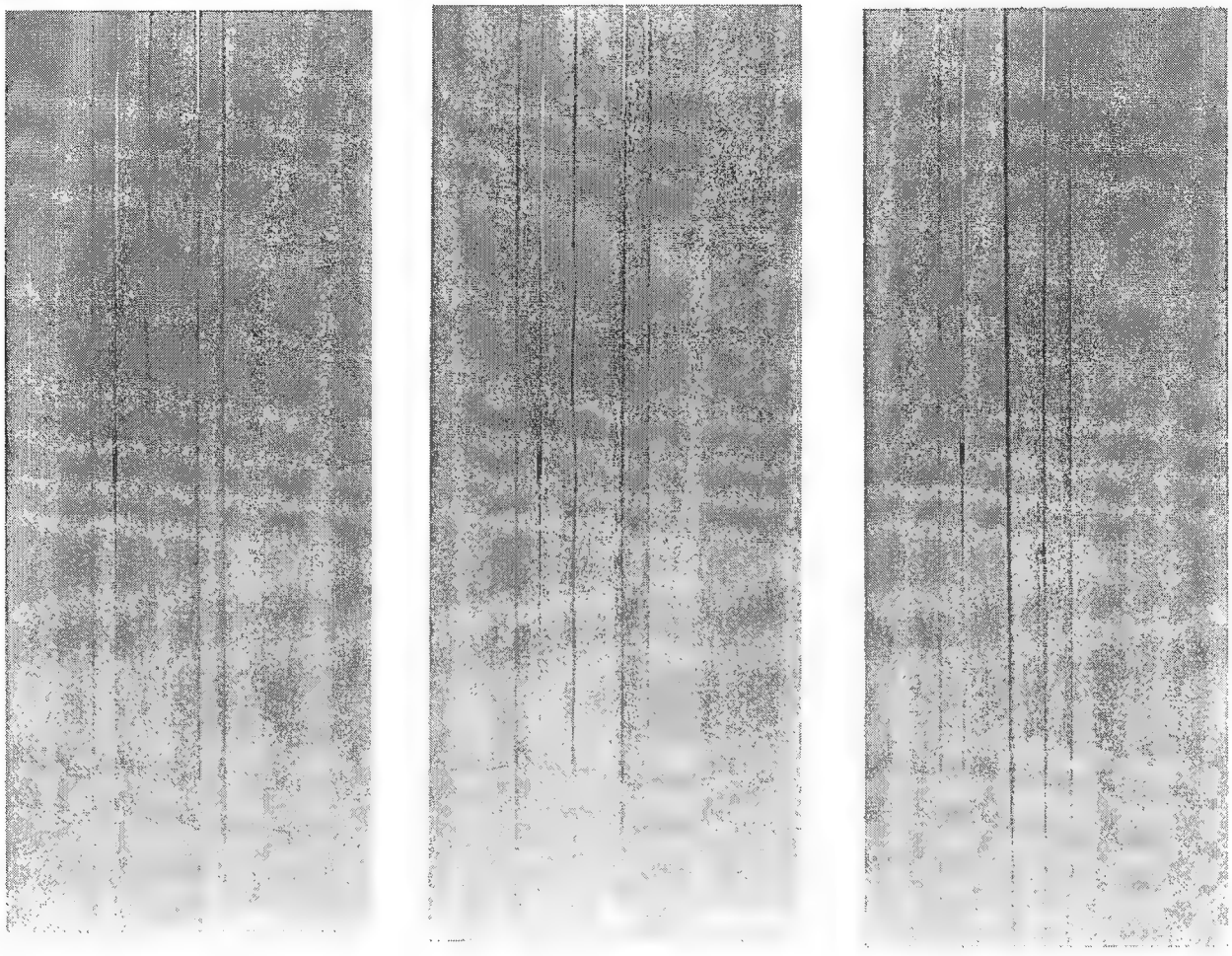

(a) Re = 13500, beginning of turbulent flow.

(b) Re = 10500, beginning of transitional flow.

(c) Re = 3200, laminar flow.

Figure 2.2. Photographs of dye streaks taken in the 0.635-cm i.d. pipe.

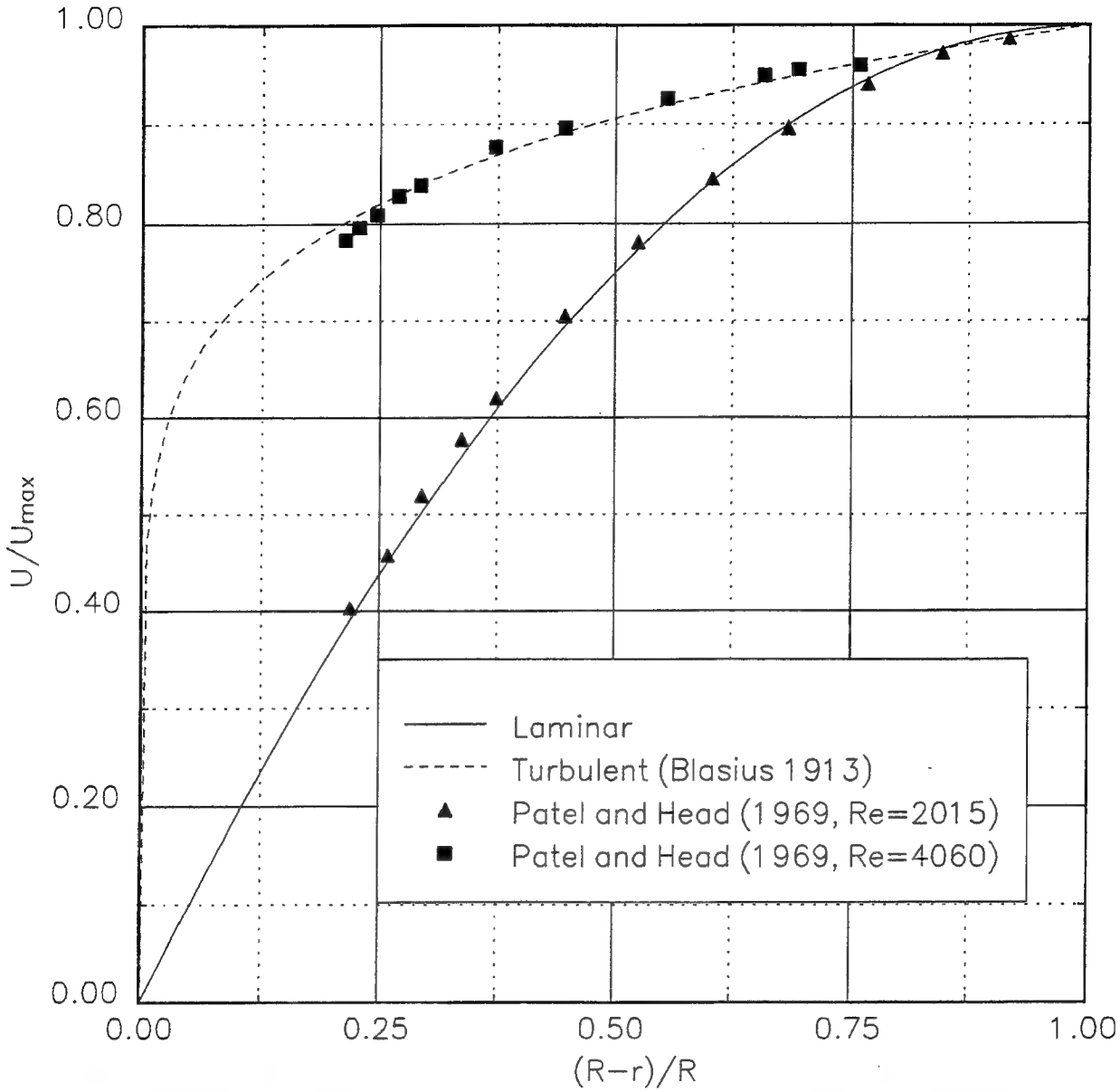

Figure 2.3a. Normalized velocity profiles in fully developed pipe flow. Data from Patel and Head (1969) for Re = 2015 (laminar) and Re = 4060 (turbulent). Solid line is the theoretical laminar velocity profile. Dashed line is the empirically derived (1/7 power law; Blasius, 1913) velocity profile.

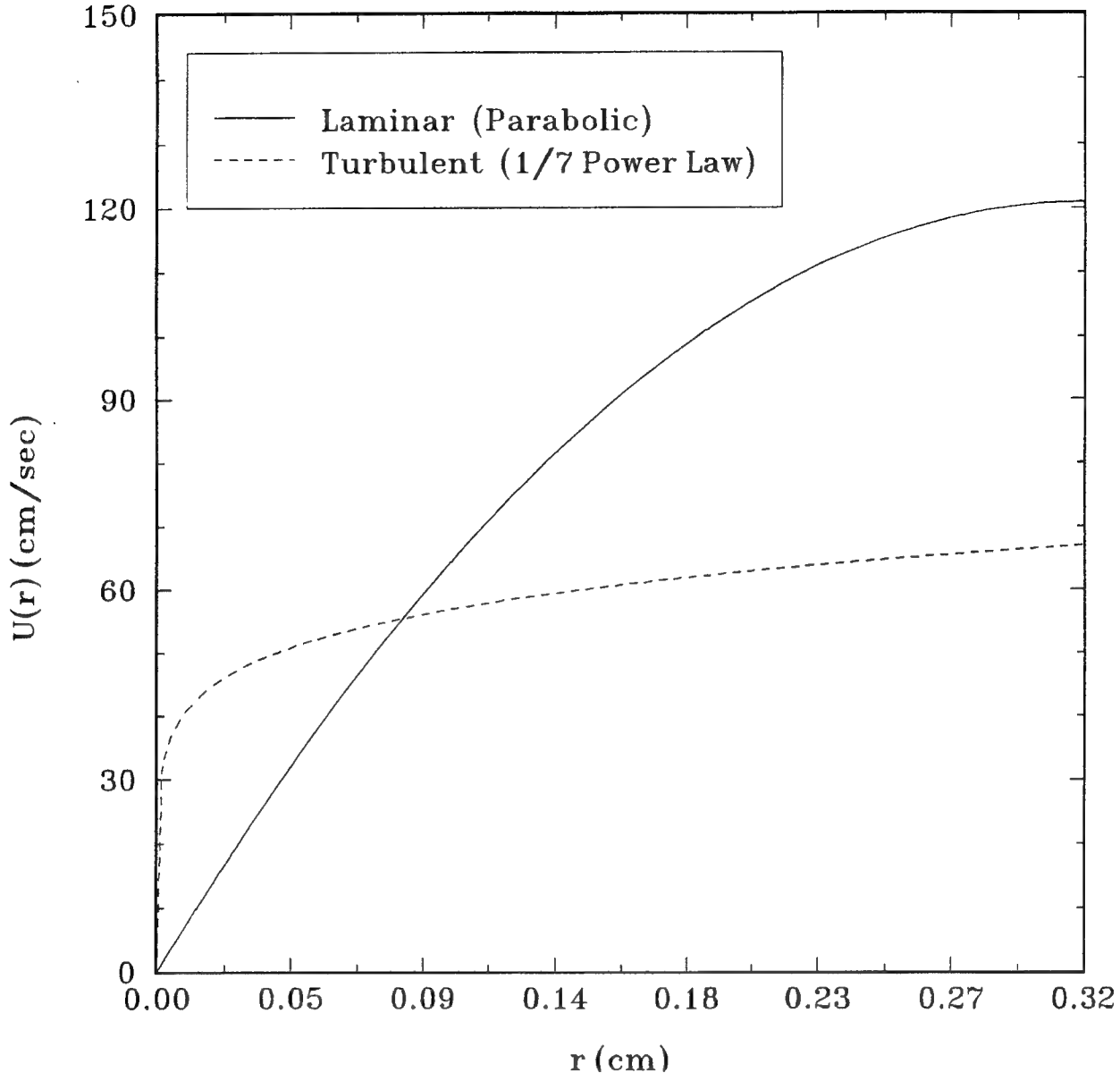

Figure 2.3b. Laminar (solid line) and turbulent (dashed line) velocity profiles in fully developed pipe (0.635-cm i.d.) flow with seawater at 25°C, for Re = 4060.

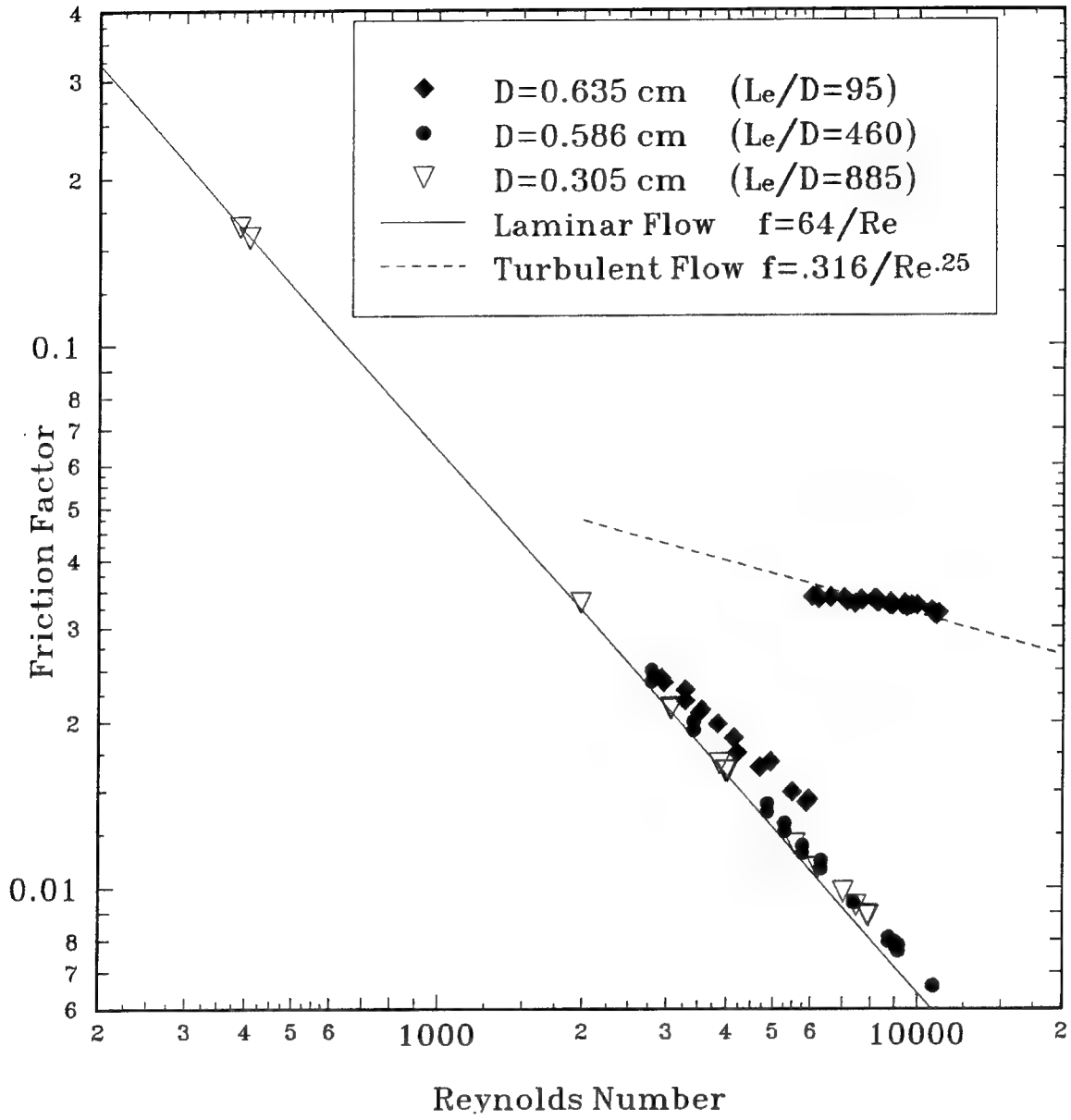

Figure 2.4a. Representative fresh water friction factor *vs* Reynolds number data. As expected for high Reynolds number laminar flow (equation 2a), with increasing L_e/D the discrepancy between measurements and theory (solid line) decreases. Comparison with similar seawater data in figure 4 is excellent.

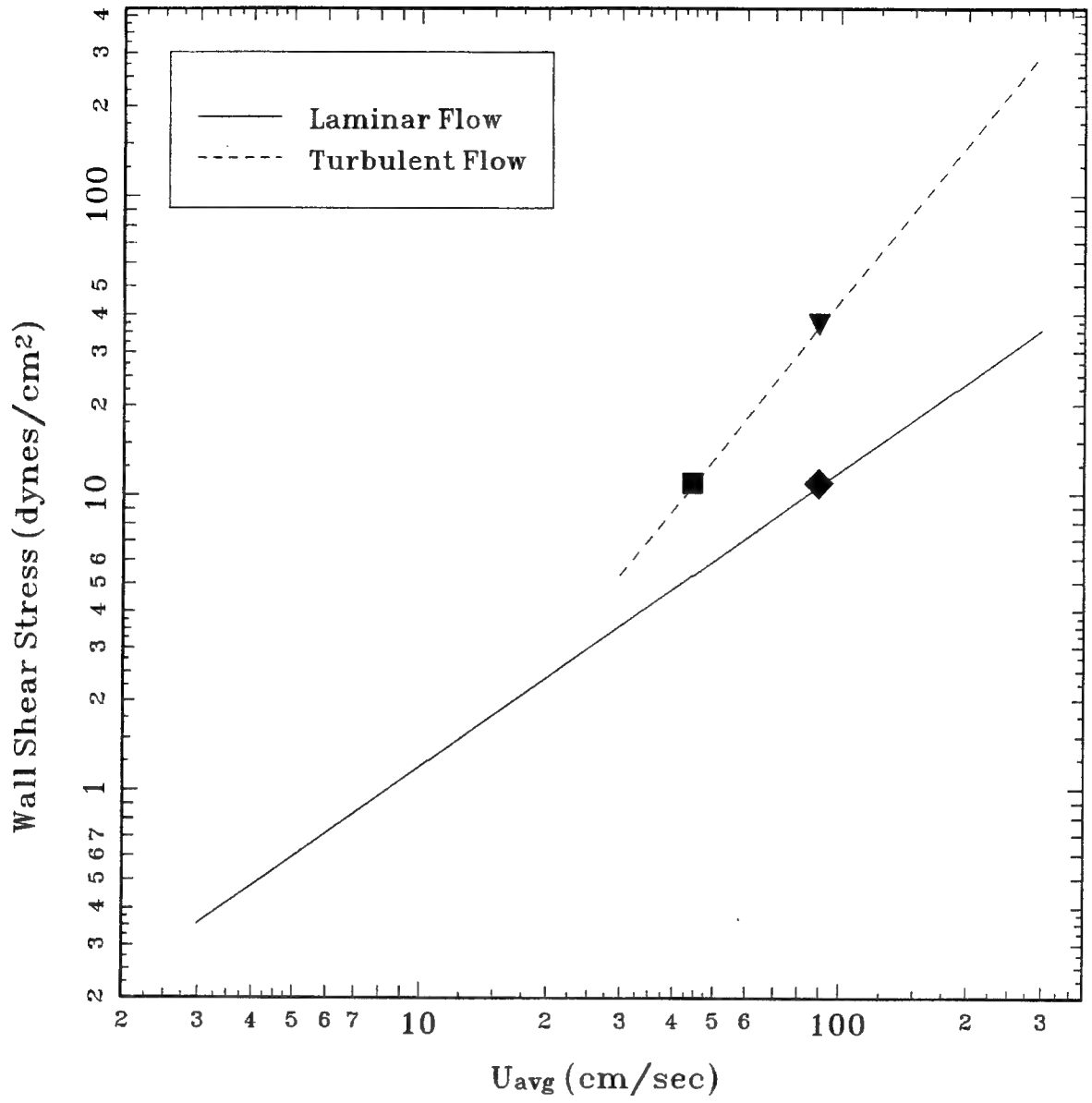

Figure 2.4b. Wall shear stress (τ_{wall}) *vs* average velocity (U_{avg}) for fully developed pipe (0.635-cm i.d.) flow (sea-water at 25°C). For U_{avg} = 89.3 cm/sec, $\tau_{wall\ laminar}$ = 10.9 dynes/cm^2 (◆) and $\tau_{wall\ turbulent}$ = 37.2 dynes/cm^2 (▼). For τ_{wall} = 10.9 dynes/cm^2, $U_{avg\ turbulent}$ = 44.3 cm/sec (■) and $U_{avg\ laminar}$ = 89.3 cm/sec (◆).

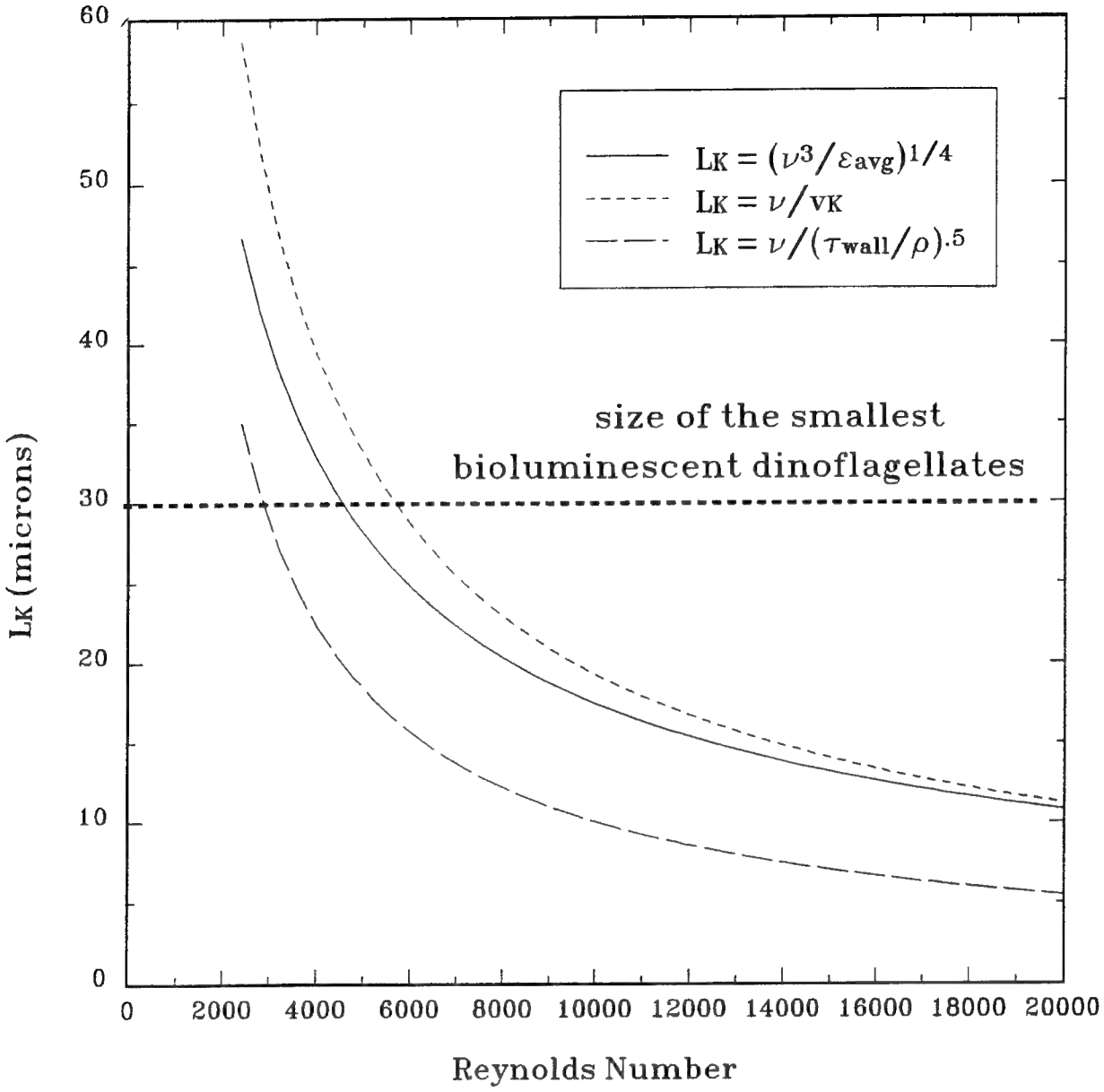

Figure 2.5. Estimated Kolmogorov length scales (L_K) as a function of Reynolds number for turbulent flow of 21°C seawater through a 0.635-cm i.d. pipe. The difference between curves result from using different dissipation values, i.e., average dissipation (solid line; equation 2.14), dissipation at the wall (long dash; equation 2.16), and dissipation throughout the central core of the pipe (short dash; Davies, 1972). A cutoff for the size of the smallest bioluminescent organisms anticipated to be present is included for comparison (dashed line).

REFERENCES FOR APPENDIX 2

Bakhmeteff, B. 1936. *The mechanics of turbulent flow.* p. 4, Princeton University Press, Princeton, New Jersey.

Blasius, H. 1913. Das Ahnlichkeitsgesetz bei Reibungsvorgangen in Flussigkeiten. Forschg. Arb.Ing.–Wes. No. 134, Berlin.

Cajori, F. 1946. *Sir Isaac Newton's Mathematical Principles.* Berkeley.

Childress, S. 1981. *Mechanics of swimming and flying.* p. 5, Cambridge University Press, Cambridge, England.

Davies, J.T. 1972. *Turbulence Phenomenon.* p. 54, Academic Press, London, England.

Hinze, J.O. 1975. *Turbulence,* 2nd ed. McGraw–Hill, New York.

Jayesh and Z. Warhaft. 1992. "Probability distribution, conditional dissipation, and transport of passive temperature fluctuations in grid-generated turbulence," *Phys. Fluids A,* 4:(10).

Kamykowski, D., R.E. Reed, and G.J. Kirkpatrick. 1992. "Comparison of sinking velocity, swimming velocity, rotation and path characteristics among six marine dinoflagellate species," *Mar. Biol.*, 113:319–328.

Kessler, J.O. 1985. "Co–operative and concentrative phenomena of swimming microorganisms," *Contemp. Phys.*, 26:2, 147–166.

Latz, M.I., J.F. Case, and R.L. Gran. 1994. "Excitation of bioluminescence by laminar shear associated with simple Couette flow," *Limnol. Oceanogr.,* 39(6), 1994, 1424–1439.

Laufer, J. 1954. "The structure of turbulence in fully developed pipe flow," Natl. Advisory Comm. Aeronaut. Tech. Repts. No. 1174.

Lieberman, S., D. Lapota, J. Losee, and A. Zirino. "Planktonic Bioluminescence in the Surface Waters of the Gulf of California," *Biological Oceanography,* vol. 4, no. 1, 1987.

Losee, J., and D. Lapota, 1981. "Bioluminescence measurements in the Atlantic and Pacific." In *Bioluminescence: Current Perspectives,* pp. 143–152, K. Nealson, Ed.

Morin, J.G. 1983. "Coastal bioluminescence: patterns and functions," *Bulletin of Marine Science,* 33:(4), 787–817.

Morita, M., and R. Johnson. 1974. "Field induced luminescence," TRW Report AT–SVD–TR–74–5.

Patel, V.C., and M.R. Head. 1969. "Some observations on skin friction and velocity profiles in fully developed profiles in fully developed pipe and channel flows," *J. Fluid Mech.* 38:(part 1), 181–201.

Pfenninger, W. 1961. In *Boundary layer and flow control.* 2 vols. G. V. Lachmann, Ed. Pergamon, Oxford.

Prandtl, L., and O.G. Tietjens, 1934. *Applied hydro- and aeromechanics.* p. 33, Dover Publications Inc., New York, NY.

Reynolds, O. 1883. "An experimental investigation of the circumstances which determine whether the motion of water will be direct or sinuous, and the law of resistance in parallel channels," *Philosophic Transactions of the Royal Society of London*, 174:935–982.

Rizk, M.A. and S. E. Elghobashi. 1984. "The motion of a spherical particle suspended in a turbulent flow near a plane wall," *Phys. Fluids* 28:(3) 806–817.

Rohr, J., J. Losee, and J. Hoyt. 1990. "Stimulation of bioluminescence by turbulent pipe flow," *Deep Sea Research,* 37:(10) 1639–1646.

Rouse, H. 1938. "Fluid mechanics for hydraulic engineers," pp. 171–172. Dover Publications, Inc. New York.

Schlichting, H. 1979. *Boundary-layer theory,* p. 599, 7th ed., McGraw–Hill Inc., NY.

Schonberg, J. A., and E. J. Hinch. 1989. "Inertial migration of a sphere in Poiseuille flow," *J. Fluid Mech.* 203:517–524.

Segre G., and A. Silberberg. 1962. "Behavior of macroscopic rigid spheres in Poiseuille flow: Part 1. Determination of local concentration by statistical analysis of particle passage through crossed light beams," *J. Fluid Mech.* 13:115–135.

Tennekes, H., and J.L. Lumley. 1972. *A first course in turbulence,* p. 19, MIT Press, Cambridge, MA.

Van Atta, C.W., and W.Y. Chen. 1968. "Correlation measurements in grid turbulence using digital harmonic analysis," *J. Fluid Mech.*, 34:(3)497–515.

Van Dyke, M. 1982. *An album of fluid motion,* p. 61. The Parabolic Press, Stanford, California.

Vogel, S. 1981. *Life in moving fluids*, p. 67. Willard Grant Press, Boston Massachusetts.

Wells, M.R., and D.E. Stock. 1983. "The effects of crossing trajectories on the dispersion of particles in a turbulent flow," *J. Fluid Mech.* 136:31–62.

White, F.M. 1974. *Viscous fluid flow,* p. 206. McGraw–Hill, Inc. New York, NY.

White, F.M. 1979. *Fluid mechanics*, p. 312. McGraw–Hill, Inc. New York, NY.

Yates, G.T. 1986. "How microorganisms move through water." *American Scientist*, July–August, Vol. 74, pp. 358–365.

Young, J. B., and T. J. Hanratty. 1991. "Optical studies on the turbulent motion of solid particles in a pipe flow," *J. Fluid Mech.*, 231:665–688.

APPENDIX 3: INTERPRETING PMT MEASUREMENTS IN FULLY DEVELOPED PIPE FLOW – THE ROLE OF THE MEAN VELOCITY

An increase in PMT levels with greater flow through the pipe may result from both increasing hydrodynamic stimulus and/or increasing mean velocity, U_{avg}. The explicit PMT dependence on mean velocity refers here to the convective effect of the flow on the flux of luminescent organisms, and excludes the flow's stimulatory aspects. Individual flash measurements of bioluminescent dinoflagellates have been represented as $I_0e^{t/\gamma}$, where Io is the peak intensity expressed as counts per second, and γ is the decay rate of the flash (Seliger et al., 1969; Widder et al., 1993). Modeled as such, the direct contribution of the mean velocity towards increasing PMT levels will depend on the ratio of the organism's residency time, L/U_{avg} (where L is the length of pipe within the PMT's field of view), to the organism's flash decay rate.

Bathyphotometers. – The relationship between an organism's flash kinetics and its PMT residency time has been previously derived for bathyphotometers (Widder et al., 1993) and are included here for the sake of comparison. Each flash in the bathyphotometer is assumed to be initiated at the beginning of the PMT's aperture. The time integrated flash fraction, I_F (counts), measured by the PMT of a single organism is the following:

$$I_F = \int_0^{L/U_{avg}} I_0 e^{-t/\gamma} dt = I_0\gamma(1 - e^{(-L/U_{avg})/\gamma}). \quad (3.1)$$

If $(L/U_{avg})/\gamma << 1$, then equation (3.1) reduces to

$$I_F \approx I_0(L/U_{avg}). \quad (3.2)$$

The mean intensity, I_{mean}, is proportional[1] to the product of the average signal each organism contributes and the number of organisms passing through the PMT's aperture per second. Thus for $(L/U_{avg})/\gamma << 1$,

$$I_{mean} \propto I_0(L/U_{avg})nU_{avg}A \propto nI_0LA, \quad (3.3)$$

where n is the concentration of luminous organisms, and A is the pipe area. No explicit dependence between I_{mean} and U_{avg} appears in equation (3.3). This results because while doubling U_{avg} doubles the flux of potential flashes, the duration of each flash within the PMT aperture is reduced by one half. An implicit dependence remains however, since the probability of stimulating an organism (and possibly the intensity and duration of its flash) will depend on the level of flow agitation which is a function of U_{avg}.

If $(L/U_{avg})/\gamma >> 1$, equation (3.1) reduces to

$$I_F \approx I_0\gamma, \quad (3.4)$$

[1] Not necessarily equal because not every organism passing the PMT is excited.

and I_{mean} becomes

$$I_{mean} \propto I_0 \gamma n U_{avg} A. \qquad (3.5)$$

There is now an explicit linear dependence between I_{mean} and U_{avg}. This results because each flash under the present conditions is recorded essentially in its entirety.

Fully developed pipe flow. – Where the flow is fully developed, hydrodynamic stimulation remains constant (in a statistical sense) along the flow direction. Hence, flash initiation is equally likely to occur anywhere along the pipe. Note, hydrodynamic stimulation is not the same across the pipe, as larger shear stresses are found in the slower flow near the pipe walls. Nevertheless, it is convenient to choose U_{avg} as a representative velocity of the stimulated organism, and discuss the consequences of this assumption later.

The delay time, τ, is introduced, so that the product $(U_{avg})(\tau)$ determines the location along the pipe where the flash begins. The integrated flash fraction of organisms stimulated within (I_{F1}) and upstream (I_{F2}) of the PMT's aperture are respectively

$$I_{F1} = \int_{\tau}^{L_2/U_{avg}} I_0 e^{-(t-\tau)/\gamma} dt = I_0 \gamma (1 - e^{\tau/\gamma} e^{(-L_2/U_{avg})/\gamma}), \qquad (3.6)$$

and

$$I_{F2} = \int_{L_1/U_{avg}}^{L_2/U_{avg}} I_0 e^{-(t-\tau)/\gamma} dt = I_0 \gamma e^{\tau/\gamma} (e^{(-L_1/U_{avg})/\gamma} - e^{(-L_2/U_{avg})/\gamma}). \qquad (3.7)$$

The average intensity per flash, I_{Favg}, is calculated by integrating τ from 0 to L_2/U_{avg}, and then dividing by L_2/U_{avg}. Thus,

$$I_{Favg} = [\int_0^{L_1/U_{avg}} I_{F2} d\tau + \int_{L_1/U_{avg}}^{L_2/U_{avg}} I_{F1} d\tau]/(L_2/U_{avg}) \qquad (3.8)$$

which after integration becomes

$$I_{Favg} = \gamma I_0 [(L_2 - L_1)/L_2 - \gamma (U_{avg}/L_2)(e^{-(L_1/U_{avg})/\gamma} - e^{(-L_2/U_{avg})/\gamma})]. \qquad (3.9)$$

If $(L_2/U_{avg})/\gamma$ and $(L_1/U_{avg})/\gamma << 1$, then

$$I_{Favg} \approx I_0 (L_2^2 - L_1^2)/(2U_{avg} L_2), \qquad (3.10)$$

and

$$I_{mean} \propto I_0 (L_2^2 - L_1^2)/(2U_{avg} L_2) n U_{avg} A \propto n A I_0 (L_2^2 - L_1^2)/(2L_2). \qquad (3.11)$$

Note that equation (3.11) contains no explicit dependence on the convective velocity. Comparison with the corresponding ($L_1 = 0$, $L_2 = L$, and $(L/Uavg)/\gamma << 1$) bathyphotometer results

shows that I_{mean} defined by equation (3.11) for fully developed pipe flow, is 1/2 of I_{mean} defined by equation (3.3) for the bathyphotometer. The factor of 1/2 arises because the organisms in fully developed pipe flow are equally likely to flash anywhere within the PMT aperture.

If $(L_2/U_{avg})/\gamma$ and $(L_1/U_{avg})/\gamma >> 1$, then

$$I_{Favg} \approx \gamma I_0(L_2 - L_1)/L_2, \tag{3.12}$$

and

$$I_{mean} \propto \gamma I_0((L_2 - L_1)/L_2)nU_{avg}A. \tag{3.13}$$

An explicit linear dependence between PMT levels and the convective velocity now appears. Comparing again to the corresponding (i.e., $(L/U_{avg})/\gamma >> 1$) bathyphotometer results, it is found that equation (3.13) reduces to equation (3.5). Here the agreement is exact because in both cases essentially the full flash is recorded regardless of where it is initiated within the PMT's field of view.

For the 0.635-cm i.d. pipe flow experiments described earlier, and assuming L_1 = 65 cm, L_2 = 70 cm and γ = 0.1 s, the PMT dependence on the convective velocity is found (figure 3.1) to be nearly linear throughout the entire flow regime of interest (Re < 20,000). Note under these conditions, $L_1/U_{avg}/\gamma >> 1$ and $L_2/U_{avg}/\gamma >> 1$. In regards to using U_{avg} as the average convective velocity of stimulated organisms, note that a smaller value which would be more appropriate for the highly stimulatory flow occurring near the wall, only makes the approximation, $(L_{1,2}/U_{avg})/\gamma >> 1$, better.

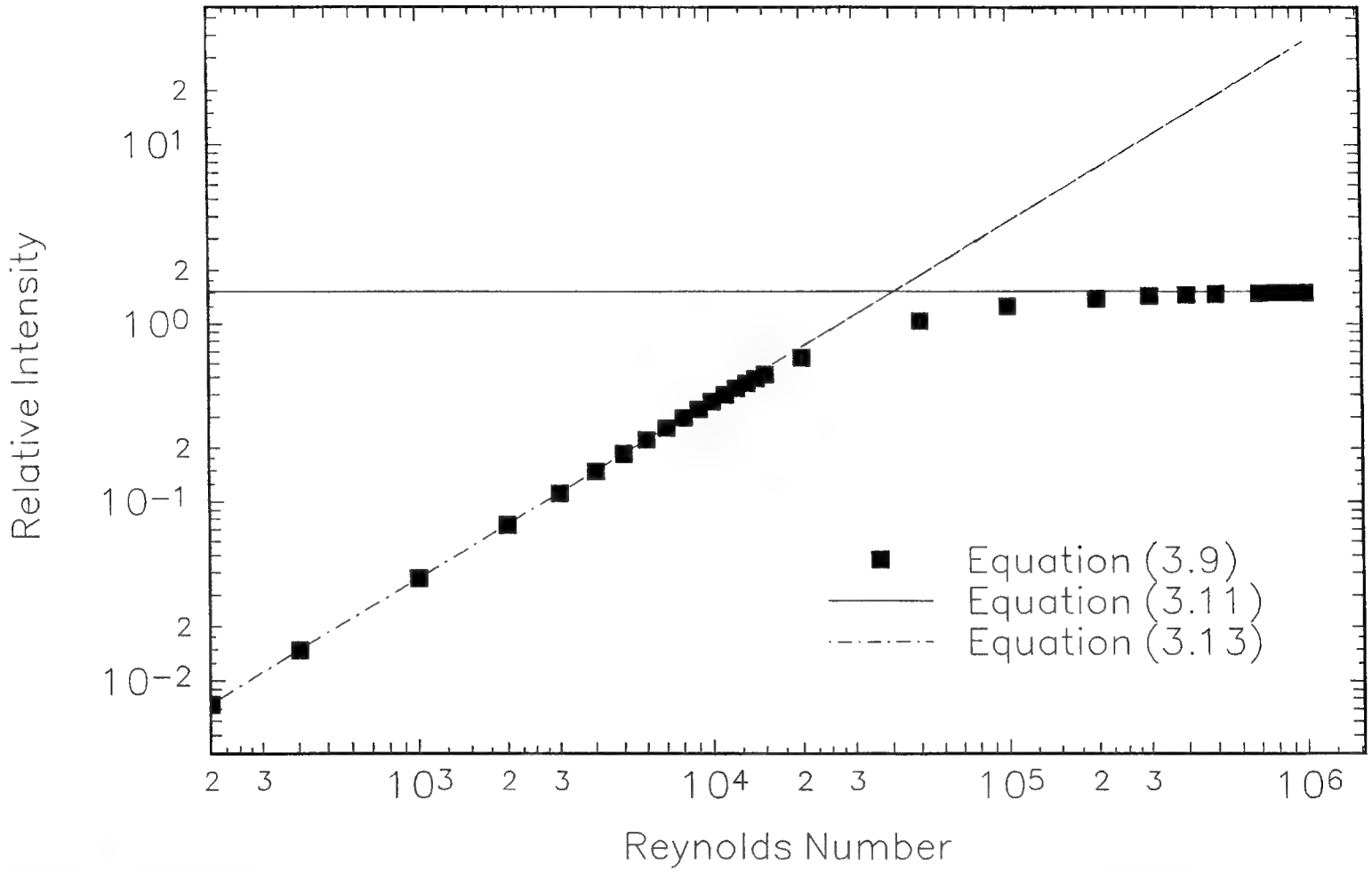

Figure 3.1. Relative PMT level ($I_{mean}/(I_o n)$) *vs* Reynolds number as predicted by equation (3.9). Pipe flow parameters are: D = 0.635 cm, L_1 = 65 cm, L_2 = 70 cm, ν = 0.0104 cm²/sec (25.6°C). Decay rate of flash (γ) is assumed to be 0.1 sec. Limiting behavior for $(L_{1,2}/Uavg)/\gamma << 1$ (equation 3.11, solid line) and $(L_{1,2}/Uavg)/\gamma >> 1$ (equation 3.13, dashed line) are included.

REFERENCES FOR APPENDIX 3

Seliger, H.H., W.G. Fastie, and W.D. McElroy. 1969. "Towable photometer for rapid area mapping of concentrations of bioluminescent marine dinoflagellates," *Limnol. Oceanogr.*, 14:(5) 806–813.

Widder, E.A., J.F. Case, S.A. Bernstein, S. MacIntyre, M.R. Lowenstine, M.R. Bowlby, and D.P. Cook. 1993. "A new large volume bioluminescence bathyphotometer with defined turbulence excitation," *Deep-Sea Research*, 40:607–627.

REPORT DOCUMENTATION PAGE

Form Approved
OMB No. 0704-0188

1. AGENCY USE ONLY *(Leave blank)*	2. REPORT DATE	3. REPORT TYPE AND DATES COVERED
	August 1994	Final

4. TITLE AND SUBTITLE

THE RESPONSE OF BIOLUMINESCENT ORGANISMS TO FULLY DEVELOPED PIPE FLOW

5. FUNDING NUMBERS

PR: ZW77
PE: 0601152N
WU: DN303010

6. EDITORS

J. Rohr, J. Losee, and G. Anderson

7. PERFORMING ORGANIZATION NAME(S) AND ADDRESS(ES)

Naval Command, Control and Ocean Surveillance Center (NCCOSC),
RDT&E Division
San Diego, CA 92152–5001

8. PERFORMING ORGANIZATION REPORT NUMBER

TR 1360

9. SPONSORING/MONITORING AGENCY NAME(S) AND ADDRESS(ES)

Office of Chief of Naval Research
Independent Research Program (IR)
Arlington, VA 22217–5000

10. SPONSORING/MONITORING AGENCY REPORT NUMBER

11. SUPPLEMENTARY NOTES

12a. DISTRIBUTION/AVAILABILITY STATEMENT

Approved for public release; distribution is unlimited.

12b. DISTRIBUTION CODE

13. ABSTRACT *(Maximum 200 words)*

This report records the study and response of *in situ* luminescent organisms to hydrodynamic stimuli in a well characterized flow field. In particular, using fully developed pipe flow: (1) the bioluminescent response of freshly collected organisms are compared in laminar and turbulent flow, (2) threshold values of wall shear stress, τ_{wall}, are determined, and (3) the flash level of individual organisms as a function of τ_{wall} are examined. Several trends describing the response of *in situ* luminescent organisms to fully developed pipe flow stimuli are reported. Further work with a greater range of τ_{wall} and Re_{trans} values is necessary to corroborate this initial study. Also the reaction of these luminescent organisms to varying shear stress (transitional flows) and acceleration (developing flows) needs to be investigated.

14. SUBJECT TERMS	15. NUMBER OF PAGES
Bioluminescence Pipe Flow	85
	16. PRICE CODE

17. SECURITY CLASSIFICATION OF REPORT	18. SECURITY CLASSIFICATION OF THIS PAGE	19. SECURITY CLASSIFICATION OF ABSTRACT	20. LIMITATION OF ABSTRACT
UNCLASSIFIED	UNCLASSIFIED	UNCLASSIFIED	SAME AS REPORT

21a. NAME OF RESPONSIBLE INDIVIDUAL	21b. TELEPHONE *(include Area Code)*	21c. OFFICE SYMBOL
J. Rohr	(619) 553–1604	Code 574

INITIAL DISTRIBUTION

Code 0012	Patent Counsel	(1)
Code 0271	Archive/Stock	(6)
Code 0274	Library	(2)
Code 574	J. J. Rohr	(50)

Defense Technical Information Center
Alexandria, VA 22304–6145 (4)

NCCOSC Washington Liaison Office
Washington, DC 20363–5100

Center for Naval Analyses
Alexandria, VA 22302–0268

Navy Acquisition, Research and Development
Information Center (NARDIC)
Arlington, VA 22244–5114

GIDEP Operations Center
Corona, CA 91718–8000

Office of Naval Research
Arlington, VA 22217–5000 (6)

Naval Surface Warfare Center
Bethesda, MD 20084–5000 (3)

Naval Oceanographic Office
Stennis Space Center, MS 39522–5001

ARPA/MSTO
Arlington, VA 22203–1714

California Lutheran University
Thousand Oaks, CA 91360

Harbor Branch Oceanographic Institute
Fort Pierce, FL 34946

University of California, Los Angeles
Los Angeles, CA 90024–1606

Scripps Institution of Oceanography
La Jolla, CA 92093–0230

The Kildare Corporation
New London, CT 06320–5594